Dynamic Subchondral Bone Changes in Murine Models of Osteoarthritis

Sander Martijn Botter

The research described in this thesis was performed at the departments of Orthopaedics and Internal Medicine, Erasmus MC, University Medical Centre, Rotterdam, The Netherlands.

Cover: Meltwater ponds along Greenland's West Coast, an area as dynamic as subchondral bone itself. Image taken by NASA's TERRA satellite (2004). Courtesy Dr. Konrad Steffen, Cooperative Institute for Research in Environmental Sciences at the University of Colorado.

ISBN: 978-90-8559-148-1

Layout and printing: Optima Grafische Communicatie, Rotterdam, The Netherlands

Dynamic Subchondral Bone Changes in Murine Models of Osteoarthritis

Dynamische subchondrale botveranderingen in muis modellen van artrose

Proefschrift

ter verkrijging van de graad van doctor aan de
Erasmus Universiteit Rotterdam
op gezag van de
rector magnificus

Prof.dr. H.G. Schmidt

en volgens besluit van het College voor Promoties.

De openbare verdediging zal plaatsvinden op
dinsdag 21 december 2010 om 13.30 uur

door

Sander Martijn Botter

geboren te Driebergen-Rijsenburg

Promotiecommissie

Promotoren:	Prof.dr. J.P.T.M. van Leeuwen
	Prof.dr.ir. H. Weinans
Overige leden:	Prof.dr. S.M.A. Bierma-Zeinstra
	Dr. E. Lubberts
	Prof.dr. F.P.J.G. Lafeber
Copromotor:	Dr. G.J.V.M. van Osch

"Als ik één ding heb ontdekt in mijn leven, dan is het wel dit: als je heel diep over iets nadenkt, dan kom je altijd bij iets uit dat niet klopt. Probeer maar eens — klopt altijd! "

Herman Finkers, uit: Geen spatader veranderd (1997)

TABLE OF CONTENTS

List of abbrevations

ACLX, ACLT	anterior cruciate ligament transection
ADAMTS	a disintegrin and metalloproteinase with thrombospondin-like motifs
ANOVA	analysis of variance
BMD	bone mineral density
BML, BME	bone marrow edema-like lesion
BV	bone volume
CC	calcified cartilage
CD	connectivity density
CKO	conditional knockout
CT	computed tomography
Ct.Th.	cortical thickness
Ctrl	control
DNA	deoxyribonucleic acid
ECM	extracellular matrix
EDTA	ethylenediaminetetraacetic acid
GAG	glycosaminoglycan
IGF-1	insulin-like growth factor 1
IL-1	interleukin 1
IVC	individually ventilated cage
K&L	Kellgren/Lawrence
MIA	mono-iodoacetate
MMA	methyl methacrylate
MMP	matrix metalloproteinase
MMX	medical meniscus transection
MRI	magnetic resonance imaging
NCC	non-calcified cartilage
NER	nucleotide excision repair
NGF	nerve growth factor
OA	osteoarthritis
OARSI	osteoarthritis research society international
Oc.N./BS	osteoclast number/bone surface
Oc.S./BS	osteoclast surface/bone surface
PCR	polymerase chain reaction
PET	positron emission tomography
pQCT	peripheral quantitative computed tomography

RIVM	Rijksinstituut voor volksgezondheid en milieu
ROS	reactive oxygen species
Sb	subchondral
Sb.Pl.Th.	subchondral bone plate thickness
SEM	standard error of the mean
SMI	structure model index
SPECT	single photon emission computed tomography
Tb.N.	trabecular number
Tb.Sp.	trabecular spacing
Tb.Th.	trabecular thickness
TC	transcription-coupled
TGFβ	transforming growth factor beta
TNFα	tumor necrosis factor alpha
Trab	trabecular
TRAP	tartrate resistant alkaline phosphatase
TTD	trichothiodystrophy
TV	tissue volume
VEGF	vascular endothelial growth factor
VOI	volume of interest
WT	wild type
XPD	xeroderma pigmentosum D

Chapter 1

General introduction

THE JOINT: NORMAL ANATOMY VERSUS OSTEOARTHRITIC PATHOLOGY

'Arthritis' is a generic term which includes many different rheumatic disease types, all of which are connected with impaired functioning of joints. Osteoarthritis (OA) is the most common form of arthritis, and the leading cause of chronic disability in the Western world. In OA normal functioning of a joint becomes impaired. Movement of the joint is painful and limited, and in advanced disease stages patients may complain of nocturnal or permanent pain.

In a diarthrodial joint, the ends of two bones meet, marked by a bony end plate called the subchondral bone plate. To provide frictionless movement, the subchondral bone plate is covered with a smooth surface of articular cartilage. Cartilage also acts as a shock absorber of mechanical forces and distributes the stresses more evenly on the underlying tissues. For joint lubrication, lubricin and hyaluronic acid are produced by the synovium and by the superficial layer of the articular cartilage. Menisci, tendons and ligaments firmly hold the two bones in place, and the surrounding musculature ensures that the bones are able to move with respect to each other. These latter structures also play an important role in shock absorption to protect the joint from excessive mechanical forces.

In OA, these joints structures are altered so that proper joint functioning is no longer possible. The most striking disease characteristic is the loss of articular cartilage, eventually leading to exposure of the subchondral bone plate, but also other joint components undergo pathological changes. The synovium can become inflamed, although inflammation in itself is not so much a typical OA hallmark. Still, low-level inflammation can lead to increased production of synovial fluid (joint effusion), which may be noticed by the patient as swelling of the joint and can restrict the range of motion of the joint. On top of that, various inflammatory cytokines are produced, which can damage the articular cartilage and lead to disease progression (1). Some joints contain a fat pad which may act as a potential source of inflammatory cytokines (2). Finally, muscles and ligaments surrounding the joint can become affected as well (3,4). The image of OA being a 'whole-organ' disease is now becoming widely accepted (5,6). Some authors even propose to distinguish several forms of OA, by looking at the joint component at which OA can first be discerned (7). As such, a distinction between cartilage-, ligament-, bone-, meniscal- and synovial-derived OA, or a combination, may be made.

The term 'osteo' in osteoarthritis points to the involvement of bone in the disease. In fact, one of the most obvious signs of OA is the development of bony outgrowths called osteophytes, arising at the margins of the joint. In addition, a pathological remodeling process takes place in the subchondral bone, which leads to sclerotic bone tissue, although the quality of this added bone is bad (8). For decades, these changes in the bone structure of a joint have been recognized as hallmarks of OA, although it was long

thought that these alterations were merely secondary manifestations developing in the course of the disease. However, many studies suggest that bone, and more specifically, subchondral bone, could also have an etiological role and therefore may hold disease modifying potential (9,10).

To summarize, OA is a disease affecting all structures of the joint. Not only do these alterations inhibit the joint's normal functioning, some of them also cause pain and thereby further decrease the quality of life of patients.

RISK FACTORS AND CLASSIFICATIONS

Because OA is most often observed in load-bearing joints such as hips and knees, it is thought to be initiated in part by excessive mechanical stress, hence the term 'wear and tear' disease. Although (excessive) mechanical stress undoubtedly plays a role in the disease process, it is not the sole reason for developing OA, since non-weight bearing joints such as the hands also become affected. Most likely, combinations of several risk factors play a role. Often risk factors are (somewhat arbitrarily) classified in those that cause idiopathic or primary OA, such as age or gender, and those that cause secondary OA, such as aberrant joint posture, trauma and excessive joint loads due to obesity or in sports (11). It is important to note that although these risk factors play a role in incident (new-onset) OA, they may not play a role in progression of disease (12). Key issue however remains that the etiology of OA is most likely multifactorial, with inflammatory, metabolic, as well as mechanical causes.

Since more and more people are at risk for developing OA (e.g. due to increases in obesity and average age of the population), it is expected that the number of individuals suffering from OA will rise with 52% between present day and 2040 (13). At present knee OA patients represent the majority of cases: At the age of 55, 30% of the population has (radiographic) OA, and this percentage increases to 50% at the age of 80 (14). In the Netherlands more than 300.000 patients are suffering from knee OA (13).

For determining OA severity, a radiograph of the joint is made to determine the absence or presence of osteophytes, as well as to measure the joint space width, from which the amount of articular cartilage can be estimated. A generally used grading system that features these joint characteristics is the Kellgren/Lawrence (K&L) scale (15), ranging from 'none' (K&L=0) to 'severe' (K&L=4). In addition, this scale takes into account changes in the structure of the subchondral bone, with subchondral sclerosis present in K&L=3. Next to the K&L assessment, which only considers anatomical changes in the joint, pain perception can be used to further define OA severity. Importantly, anatomical changes and pain perception can be mutually exclusive, as symptoms of joint pain are often found to be independent of radiographic severity (16).

Next to radiographic assessment and pain perception, OA severity can be scored histologically by the Mankin histopathology grading system (17). In this system, the severity of cartilage damage is estimated with a 14-point scale based on a combination of cellular changes, histochemical presence of matrix staining and architectural changes (erosion and vessel penetration through the tidemark). Because this scoring system was originally developed for human cartilage samples, its use is limited for preclinical studies. Therefore, a simpler modified version of the Mankin is often applied and more recently, a workgroup founded by the Osteoarthritis Research Society International (OARSI) proposed an alternative scoring system (18). This last system employs a separate grading and staging system, where grade reflects severity and stage reflects extent of damage. By multiplying the grade and stage score, a damage score can be derived with a maximum of 24 points. Importantly, this system is easy to use both in clinical and preclinical studies.

THE OSTEOCHONDRAL INTERFACE

The area where articular cartilage and subchondral bone are located is termed the osteochondral interface. Articular cartilage consists of chondrocytes embedded in an extracellular matrix (ECM). The ECM is made of collagen type II, providing structural strength, and hydrophilic proteoglycans, which retain water and provide resilience when the tissue becomes compressed during weight-bearing movement. In fact, water represents 70-75% of the cartilage wet weight. The ECM contains no vascular, neuronal or lymphatic tissue. Because of the absence of blood vessels, nutrients must reach the chondrocytes via diffusion from the synovial fluid and the underlying subchondral bone. In addition, the absence of blood vessels mean that chondrocytes produce their energy under relative anoxic conditions, with oxygen tensions varying from around 6% at the joint surface to 1% in the deep layers of healthy articular cartilage (19). Chondrocytes in adult cartilage almost never divide, but their mitotic cellular program can become reactivated when the ECM becomes damaged, as is the case in OA.

The constituents of articular cartilage (cellular as well as acellular) are not uniformly distributed, but instead can be ordered into several layers (figure 1). First of all, a distinction can be made between the upper noncalcified cartilage, and the lower mineralized or calcified cartilage. The noncalcified cartilage can be further divided in a superficial tangential zone, middle zone and deep zone. In each of these layers the alignment of the collagen molecules is different, allowing the cartilage to withstand stresses from different directions. Also, the morphology of the chondrocytes differs, with small flattened cells in the superficial zone, and larger, hypertrophic cells in the deep zone and calcified cartilage.

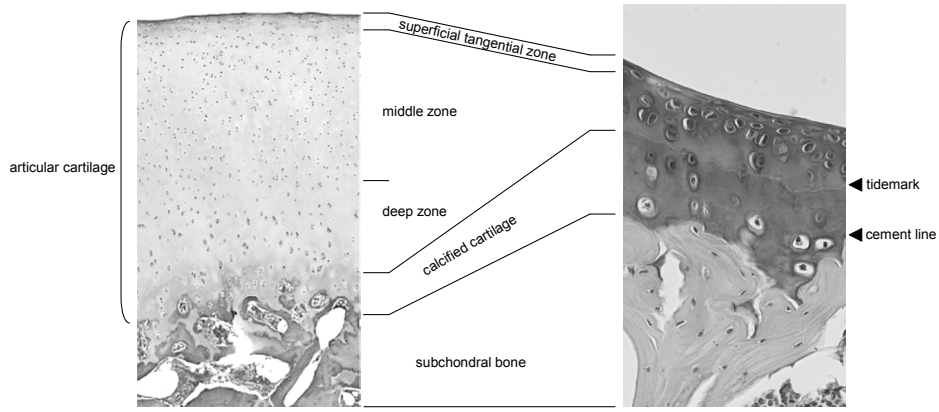

Figure 1. The osteochondral interface in humans (left) and mice (right). In mice, the middle and deep zones of the articular cartilage are more difficult to discern. The tidemark delineates the boundary between the non-calcified (superficial, middle and deep zones) and the calcified cartilage. The cement line demarcates the boundary between calcified cartilage and the subchondral bone plate.

On the top side the calcified cartilage is bordered by the deep zone of the noncalcified cartilage, delineated by the so-called tidemark, and on its bottom side by the subchondral bone, delineated by the cement line. Located as an intermediate layer between the soft, non-calcified cartilage and the rigid underlying subchondral bone, some studies showed that the calcified cartilage contains more mineral and is actually stiffer compared to the latter (20,21). Because of many curvatures at its base, the calcified cartilage, and thereby the whole articular cartilage layer, remains securely anchored to the subchondral bone (22).

The subchondral bone encompasses the subchondral bone plate and the underlying trabecular bone and bone marrow space (21,23). The subchondral bone plate, also called endplate, is a sheet-like part of dense bone directly at the bottom of the calcified cartilage. It forms the main supporting structure for the articular cartilage and transmits loads from the cartilage onto the trabecular bone beneath. Direct contact between articular cartilage and subchondral bone is possible via perforations inside the subchondral bone plate (24,25). In literature, the subchondral bone plate sometimes includes the calcified cartilage (25,26), whereas others prefer to use the term 'subchondral plate' instead (27). In this thesis, the term 'subchondral bone' refers to the subchondral bone plate (excluding the calcified cartilage layer) and the subchondral trabeculae of the epiphysis, whereas 'subchondral bone plate' refers to the bony plate underneath the calcified cartilage. Importantly, all of the abovementioned structures can be identified in other species as well, such as in knee joints of mice. This is of great use for conducting preclinical studies (also see paragraph 'Animal models of OA' below).

CHANGES IN OSTEOARTHRITIC SUBCHONDRAL BONE

In OA the subchondral bone undergoes substantial alterations in the course of the disease (figure 2). One of the most obvious visible alterations on a standard anterior-posterior X-ray photograph of an osteoarthritic (knee) joint is subchondral sclerosis, which results from a period of increased subchondral bone remodeling, eventually leading to a net increase in bone. This bone was shown to be of inferior quality (8), probably due to a fast bone remodeling process.

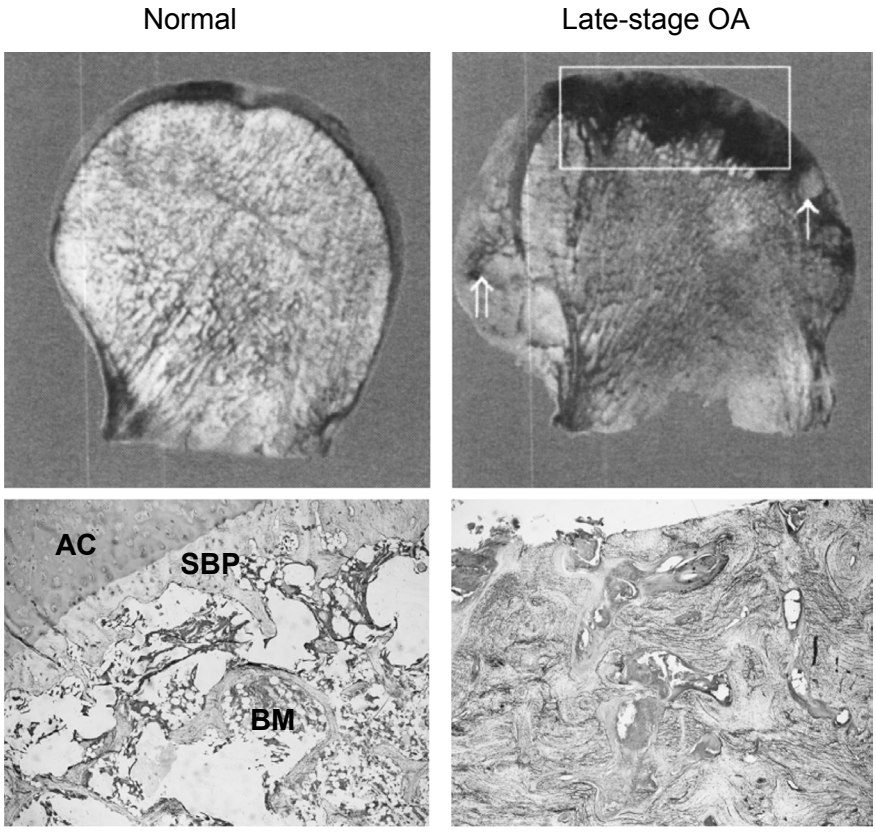

Figure 2. A normal healthy (left) and advanced osteoarthritic femoral head (right). Macroscopically, osteophyte formation (top right, left arrow), subchondral edema (right arrow) and subchondral sclerosis (rectangle) can be readily identified. Below, histological images of the subchondral bone plate (SBP) area show changes at the microscopic level. Note the increase in subchondral bone, resulting in smaller bone marrow (BM) cavities, and the absence of articular cartilage (AC). Modified from Day *et al*. (8).

Although it was long thought that changes in subchondral bone structure were merely a consequence of cartilage damage, it is now known that changes in cartilage and subchondral bone occur simultaneously and some studies even suggest that sub-

chondral changes precede changes in cartilage (28-32). This opens the possibility for subchondral bone as a target to influence the disease process.

Next to subchondral sclerosis, X-ray photographs of advanced OA joints often also show mineralized osteophytes at the joint margins. Starting as cartilaginous precursors that mineralize in the course of the disease, these bony outgrowths are thought to act as a protective countermeasure, stabilizing the joint (33). In addition, by enlarging the surface area of the joint, some of the excess load may be redistributed to the osteophyte (34). The sites at which they develop are often located at the insertion sites of tendons or from the periost covering the bone. Unfortunately, by doing so, osteophytes deform the joint which in turn often leads to movement inhibition and pain sensation, as they can press on neighboring tissues as well.

Also in the subchondral bone marrow changes take place, in the form of bone marrow edema-like lesions (BMLs or BMEs), which can be identified using MRI (35-37). Histologically, BMLs are mainly represented by bone marrow necrosis, fibrosis, and trabecular and vascular abnormalities (35,38). Importantly, correlations between BMLs and disease progression and/or pain have been found in osteoarthritic knees (39-41), which opens the possibility for BMLs to function as a biomarker tool.

Subchondral BMLs are highly associated with yet another common subchondral bone alteration: bone attrition (42,43). This bone adaptation is thought to represent remodeling of the subchondral bone in weight bearing surface from a curved to a more flattened appearance, and can already be identified in mild OA cases (44). Not much is known about the origin of this adaptation, although some studies suggest a link between bone attrition and malalignment of the joint (45).

IMAGING TECHNIQUES TO VISUALIZE AND QUANTIFY CHANGES IN SUBCHONDRAL BONE

To monitor changes in the osteoarthritic subchondral bone, several techniques can be applied. In preclinical models, histological analysis is often used. Osteoarthritic (knee) joints embedded in paraffin or the plastic compound methyl methacrylate (MMA) can be sectioned and stained with e.g. Safranin O to visualize proteoglycans surrounding chondrocytes or e.g. Goldner to visualize changes in osteoblast activity. Osteoclasts can be visualized because of their specific tartrate resistant alkaline phosphatase (TRAP) activity. However, the procedure of embedding, sectioning and staining is laborious, and hardly suitable for larger amounts of samples. In addition, histology only allows quantification in two dimensions, although serial sectioning partly compensates this disadvantage.

Alternatively, a fast and reliable technique which can also be used to visualize and quantify bone changes is X-ray computed tomography (CT) scanning. This technique was first used in the clinic in the mid-1970s, and since then has been used as a standard technique to visualize both soft tissue and bone. The technique uses X-rays to generate a three-dimensional image of an object from a large series of two-dimensional X-ray images taken around a single axis of rotation. In the beginning of 1990, this technique has been refined for very small samples which can be scanned with very high spatial resolution (i.e., <1 µm), and today micro-computed tomography (micro-CT) has become a standard tool in bone imaging research. In this thesis, micro-CT imaging was frequently used. Bone samples from mice were scanned and with the aid of several software programs the subchondral bone plate and subchondral trabeculae were selected and analyzed (see figure 3). Using micro-CT, changes in subchondral bone can be measured both fast and accurate. In addition, the samples are left intact, and can be used to perform histology afterwards. A downside however is that, similar to radiographs, the articular cartilage is not visible, although this disadvantage can be overcome with the help of contrast agents (46). In the last decade, micro-CT has also been applied longitudinally (47-49). Changes in subchondral bone structure in the same laboratory animal, as large as a rabbit, can thus be quantified over time. Not only does this approach minimize the amount of laboratory animals needed for the experiment, the statistical evaluation of the data also becomes more powerful since the animal is compared with itself at an earlier time point, which reduces biological variation. An important issue however is to minimize the amount of radiation applied to the animal, since X-rays are known to interfere in cellular processes.

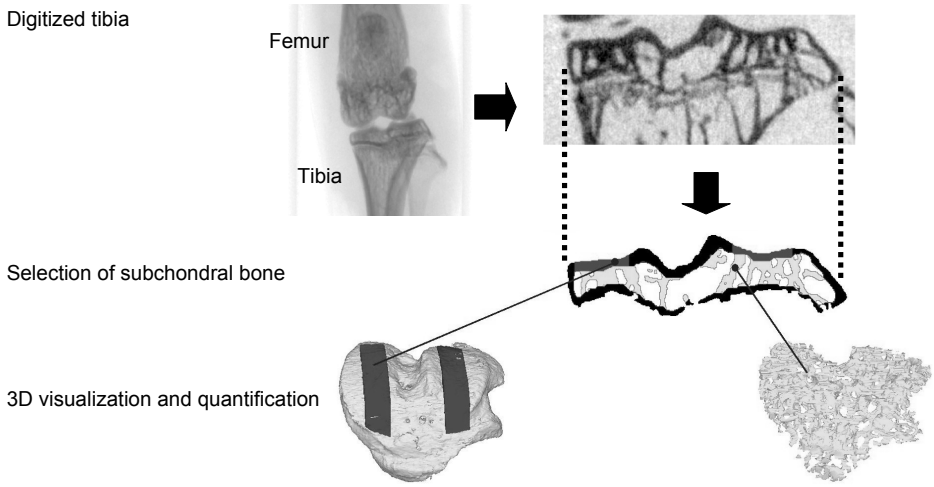

Figure 3. A technique that was used in every study in this thesis was micro computed tomography (micro-CT). Here, a bone specimen (a murine knee joint is shown here) is digitized, the raw grey-scale images are binarized and separated into several anatomical components (red: subchondral bone plate, yellow: subchondral trabeculae) that can be analyzed separately.

ANIMAL MODELS OF OA

The development of OA is not restricted to humans: rodents such as rats and mice, but also rabbits, guinea pigs, dogs, sheep and horses are known to develop OA. In a laboratory setting, these animals offer the possibility to study OA in greater detail. Some specific species are increasingly susceptible for spontaneous OA development, such as STR/ORT mice and Dunkin Hartley guinea pigs, which both develop OA within a couple of months. The C57Bl/6 mouse also develops OA spontaneously, although only later in life (50). To speed up the disease process, genetic modification can be employed, or a specific joint, usually the knee joint, can be destabilized by surgical or chemical means (51). An often-used approach is to transect the anterior cruciate ligament (ACLX), the medical meniscus (MMX), or to combine both procedures (30,52,53). Alternatively, intra-articular injection of bacterial collagenase weakens the collagen-containing ligaments, while keeping the healthy collageneous cartilage matrix intact (54,55). Other interventions are aimed at directly damaging the articular cartilage, by intra-articular injection of metabolic inhibitors such as mono-iodoacetate (MIA) (56) or by making a groove in the surface of the articular cartilage (57).

Animals OA models allow the study of the earliest processes in the joint at the molecular level, which is often difficult or (ethically) impossible in humans. Inducing OA ensures a well-defined starting point of the disease process, minimizing experimental variability. Classical histological techniques, but also modern imaging approaches such as micro-CT, micro-MRI, SPECT and PET, are able to unravel the molecular mechanisms in OA. In model species such as the mouse, joint anatomy shows great resemblance to the human situation, and the key components of the osteochondral interface are all represented (see figure 2). Also, the molecular players in the disease process itself (e.g. cytokines) are largely similar. This way, animal models are of great use to study both early and late stages of OA. However, important limitations should be kept in mind: although the joints of animals and humans look much alike, anatomical, mechanical as well as metabolic differences do exist (58-62). Therefore, although animal models of OA can give important clues in understanding the disease process and testing intervention strategies, one should be cautious for over interpretation of experimental findings to the human situation.

AIM AND OUTLINE OF THIS THESIS

Currently, OA is still a progressive disease without a cure and until now no disease modifying agents are available. Before such agents can be developed, it is first important to understand the biology of the disease: which changes occur inside the diseased joint

and how do these changes contribute to the disease process? With respect to subchondral bone, it is known that in an osteoarthritic joint, the subchondral bone architecture is altered compared to a healthy joint, but how did these changes occur in the first place? The general aim of this thesis was therefore to answer the following question: *How do the skeletal alterations develop in the subchondral bone of the murine knee joint during the osteoarthritis disease process?* To answer this question, we made use of several different mouse models of OA. Since knee joints are commonly affected, we specifically looked at changes in the tibial subchondral bone structure in osteoarthritic knee joints of mice.

First of all, Chapter 2 describes if micro-CT is capable of capturing early changes in the subchondral bone structure of murine knee joints. More specifically, changes in the subchondral bone plate and subchondral trabeculae of the tibial epiphysis were quantified. The next two chapters deal with one of the most important questions to answer when studying bone-cartilage interactions in OA: 'do subchondral bone changes lead to cartilage changes or *vice versa*?', a genuine 'chicken or the egg' dilemma. Since some studies have indicated that increased bone mass is related to an increased risk for osteoarthritis development, we wanted to know if a high bone mass phenotype influences the disease outcome of which the results are described in Chapter 3. Next, to approach our dilemma from a different perspective, we describe in Chapter 4 whether differences in cartilage biology had an effect on subchondral bone changes. For this we made use of a knockout mouse that lacked a specific enzyme important in cartilage turnover, A Disintegrin And Metalloproteinase with ThromboSpondin-like motifs type 5 (ADAMTS5), which was already shown to have less OA development after surgical destabilization (63).

In Chapter 5, we focused on one of the key risk factors for developing OA: aging. Since OA mainly develops in the elderly, it is also important to know the spontaneous age-related dynamics in subchondral bone remodeling and cartilage damage, and to see if these changes are similar to induced (secondary) OA. Another important risk factor is gender: women are known to be more at risk for developing OA, and gender also contributes to the variation seen in various OA mouse models (64,65). We therefore studied the spontaneous OA development both in male and female mice. Besides wild type animals, we also made use of a mutant mouse with a prematurely aging phenotype, and asked if these mice would develop more spontaneous OA and which subchondral bone changes were involved.

So far, we have utilized cross sectional approaches where different groups of mice are compared, without knowledge of the changes preceding those time points. Therefore, to truly know how subchondral bone changes occur over time, in Chapter 6 we deal with the temporal dynamics of subchondral bone changes in instability-induced OA by using *in vivo* micro-CT. Finally, in Chapter 7 of this thesis the findings of the different studies are discussed and a hypothesis is generated on how subchondral bone changes may contribute to the development of OA, which can be used as a direction for future research.

Chapter 2

Quantification of subchondral bone changes in a murine osteoarthritis model using micro-CT

S.M. Botter, G.J.V.M. van Osch, J.H. Waarsing, J.S. Day, J.A.N. Verhaar, H.A.P. Pols, J.P.T.M. van Leeuwen, H. Weinans

Biorheology 2006;43:379–388

ABSTRACT

In the past few years there has been a considerable interest in the role of bone in osteoarthritis. Despite the increasing evidence of the involvement of bone in osteoarthritis, it remains very difficult to attribute the cause or effect of changes in subchondral bone to the process of osteoarthritis.

Although osteoarthritis in mice provides a useful model to study changes in the subchondral bone, detailed quantification of these changes is lacking. Therefore, the goal of this study was to quantify subchondral bone changes in a murine osteoarthritis model by use of micro-computed tomography (micro-CT). We induced osteoarthritis-like characteristics in the knee joints of mice using collagenase injections, and after four weeks we calculated various 3D morphometric parameters in the epiphysis of the proximal tibia.

The collagenase injections caused cartilage damage, visible in histological sections, particularly on the medial tibial plateau. Micro-CT analysis revealed that the thickness of the subchondral bone plate was decreased both at the lateral and the medial side. The trabecular compartment demonstrated a small but significant reduction in bone volume fraction compared to the contralateral control joints. Trabeculae in the collagenase-injected joints were thinner but their shape remained rod-like. Furthermore, the connectivity between trabeculae was reduced and the trabecular spacing was increased.

In conclusion, four weeks after induction of osteoarthritis in the murine knee subtle but significant changes in subchondral bone architecture could be detected and quantified in 3D with micro-CT analysis.

INTRODUCTION

In osteoarthritis cartilage becomes progressively damaged and many of the other joint tissues, such as synovium, ligaments and bone, are altered as well. The bone changes consist of the formation of osteophytes and sclerosis of the subchondral bone, which are both considered radiological hallmarks of osteoarthritis. In the past few years there has been a considerable interest in the role of the subchondral bone in the disease process of osteoarthritis. Despite the rising evidence of the involvement of bone in osteoarthritis (reviewed in 21,29,31,66,67, examples of experimental data in 68-70), it remains very difficult to attribute the cause or effect of subchondral bone changes to the process of osteoarthritis.

The subchondral bone presumably has an important role in evenly distributing the forces resulting from joint loading, thereby protecting the cartilage from high peak stresses and damage. A change in subchondral bone architecture could in this view lead to altered loading patterns, which may play a role in osteoarthritis initiation and progression. Among the first to recognize the role of bone in the disease process were Radin and co-workers (71): They stated that initiation of cartilage lesions probably required local stiffening of the subchondral bone, creating transverse stresses at the base of the articular cartilage, which would eventually lead to formation of cartilage lesions. These lesions would then progress as a result of stiffer subchondral bone (72). Although this concept of osteoarthritis progression was never confirmed by experiments (73), this hypothesis led to an increasing interest in the role of subchondral bone changes in osteoarthritis (73-78). In the laboratory, animal models are useful to further deepen our insights in the etiology of the disease. Various rodent models exist that simulate some of the osteoarthritic changes, either developing spontaneously (79,80) or post-traumatically (54,81,82). In one of these models osteoarthritis-like characteristics can be induced by an intra-articular injection of collagenase in the knee joints of mice, creating instability by weakening the joint ligaments (54,83). This instability eventually leads to cartilage damage and bone changes and is likely to reflect a post-traumatic osteoarthritic situation (64).

Micro-computed tomography (micro-CT) is currently applied to study bone changes in various animal models of osteoarthritis, such as dogs (84), cats (85) and guinea pigs (86). Furthermore, it is known that micro-CT can be of use for disease monitoring in mice (87) but until now detailed quantification of the changes occurring in the subchondral bone of mice remains obscure. Therefore, the goal of this study was to quantify subchondral bone changes in a murine osteoarthritis model. To achieve this, we induced osteoarthritis-like changes in the knee joints of mice using collagenase injections and after four weeks we evaluated whether, and if so which, changes in the subchondral bone architecture could be detected. By calculating various 3D morphometric parameters we

quantified changes of the subchondral bone plate and the subchondral trabeculae in the epiphysis of the proximal tibia.

MATERIALS AND METHODS

Following the approval of the local animal ethics committee, 16-week old male C3H/HeJ mice (*n*=13) were used. The animals were housed in Individually Ventilated Cages (IVC's) with three brother littermates per cage and were fed ad libitum. Animals were anesthetized with a 5% isoflurane/N_2O/O_2 mixture, and a small incision was made in the skin on the frontal side of the knee joint. Six µl containing 10U of highly purified bacterial type VII collagenase (Sigma, St Louis, MO) was injected into the right knee intra-articular space whereas the left knee was injected with 6 µl saline (54). As an analgesic, the animals also received a subcutaneous injection of buprenorphine (Temgesic, 0.01 mg/kg body weight). After four weeks the mice were euthanized and their knee joints were excised. After fixation in 4% formalin for two days, the knee joints were scanned using a micro-computed tomography (micro-CT) scanner (Skyscan 1072, Skyscan, Aartselaar, Belgium) with a voxelsize of 8 µm. In order to distinguish bone tissue from non-bone tissue, the reconstructed greyscale images were segmented, using an automated tresholding algorithm (88). Using 3D data analysis software (CTAnalyzer, Skyscan) the epiphysis of the tibia was selected as region of interest (ROI) for further analysis. Since we were only interested in bone changes occurring underneath the articular cartilage layer, care was taken not to include any outgrowing osteophytes. Furthermore, to verify whether changes in bone only occurred in the epiphysis or also at remote sites of the joint, a sample of the distal metaphyseal cortex was analyzed as well. The epiphysis was further divided in a cortical part (i.e., the subchondral bone plate) and a trabecular part, which were analyzed separately for differences in bone structure using the freely available software package 3D-Calculator (*http://www.erasmusmc.nl/47460/386156/Downloads*). The following 3D morphometric parameters were calculated to describe the bone structure of the trabecular compartment: bone volume fraction, which describes the ratio of bone volume over tissue volume (BV/TV), structure model index (SMI), describing whether a bone structure is rod-like or plate-like (89), connectivity density (CD), which calculates the number of trabecular connections in a given volume (90), and bone thickness (91), which could be applied for trabeculae (trabecular thickness, Tb.Th.), the cortex of the distal metaphysis, and the medial and lateral subchondral bone plate (both expressed as Ct.Th.). Furthermore, the bone thickness algorithm could also be used to calculate the size of the marrow cavities, reflecting trabecular spacing (Tb.Sp.). The above-described procedure for the analysis of the epiphysis is depicted schematically in figure 1. The differences found between collagenase-injected joints and controls were expressed as

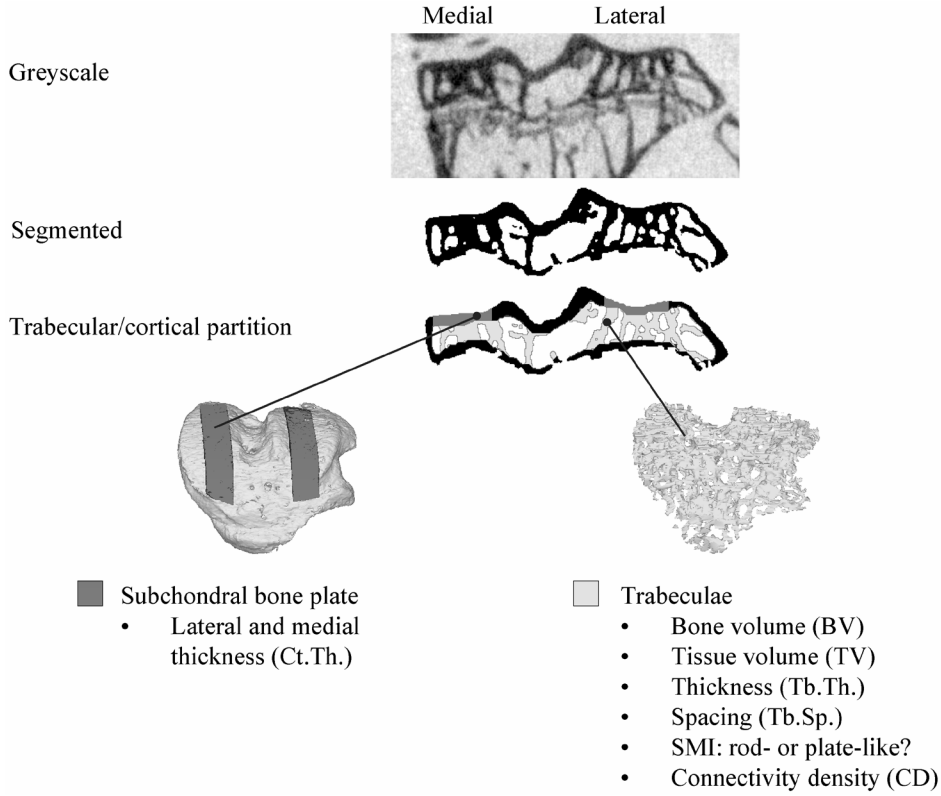

Figure 1. Stepwise display of the methods used to analyze subchondral bone architecture with micro-CT. The micro-CT scans of the knee joints were reconstructed into greyscale images and segmented, i.e., binarized, to discriminate bone from non-bone. Following segmentation, the epiphysis of the proximal tibia was selected and the trabecular and cortical compartment were isolated. Each compartment was analyzed separately for the 3D morphometric parameters shown in the lower part of the scheme. BV = bone volume, TV = tissue volume, SMI = structure model index, CD = connectivity density, Tb.Th. = trabecular thickness, Tb.Sp. = trabecular spacing, Ct.Th. = cortical thickness.

percentage changes from controls and Student's paired t-test was applied for statistical analysis, where $p<0.05$ was considered significantly different.

Following the scanning procedure, knee joints were embedded in methyl methacrylate (MMA) and sectioned in coronal orientation to verify the presence of osteoarthritis characteristics such as cartilage damage and osteophytes. Per knee joint 8-14 undecalcified sections of 6 µm thickness were obtained, with 100 µm interspacing. Goldner staining was performed and all sections were scored for cartilage damage on the medial and lateral side of the tibia. A semi-quantitative scoring system was applied as follows: 0) no damage, 1) mild disruption of the cartilage surface, 2) moderate disruption of the cartilage surface accompanied by fissures, and 3) exposure of the calcified zone or subchondral bone. The average cartilage damage score was calculated, ranging from 0 (no

damage) to 3 (maximal damage in medial or lateral side of the joint, in every section). In this case, the non-parametric Mann-Whitney test was applied for statistical analysis, where $p<0.05$ was considered significantly different.

RESULTS

The animals resumed normal activity within a few hours after surgery and limping of the collagenase-treated limb was observed only in the first few days after the operation. There was no significant decline in body weight during the experiment.

After four weeks typical osteoarthritis characteristics were found, such as osteophytes and cartilage damage (figure 2). The cartilage damage score in the collagenase-injected knees was 1.2 at the medial side vs. 0.2 at the lateral side, whereas in the contralateral control joints virtually no damage was observed (figure 3).

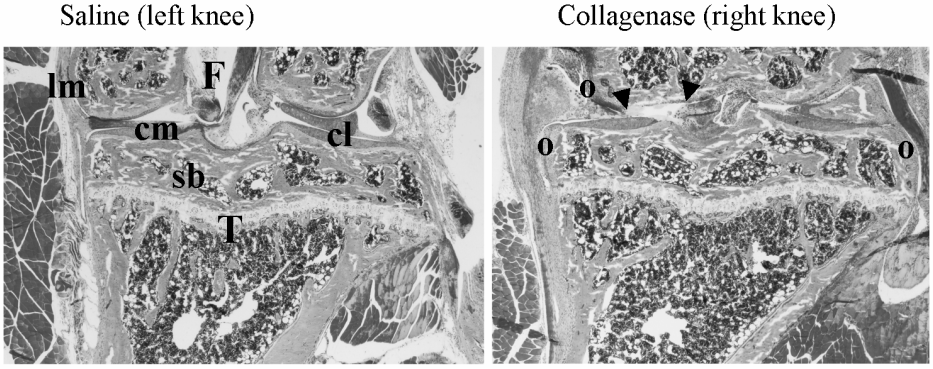

Figure 2. Histology of a saline-injected and collagenase-injected murine knee joint. Knee joints were fixed in formalin, embedded in MMA, sectioned and Goldner staining was performed. Both cartilage damage (on medial femur between arrowheads) and osteophytes (o) were observed. The cartilage damage in the tibia was scored and is presented in Figure 3. Original magnification×40. F = femur, T = tibia, cm = cartilage medial, cl = cartilage lateral, lm = ligament, sb= subchondral bone in the epiphysis.

The collagenase-injection changed the bone architecture of the epiphysis. The bone volume fraction (BV/TV) of the epiphyseal trabecular bone was consistently lower in all osteoarthritic knees compared to the contralateral controls (figure 4). On average a decrease of 11% was found, mainly as a result of increased TV (i.e., trabecular bone volume + marrow cavity volume). Although the general shape of the trabeculae remained rod-like as indicated by the unchanged SMI, a small decrease in trabecular thickness (Tb.Th.) was observed, accompanied by a corresponding increase in trabecular spacing (Tb.Sp.). Furthermore, the number of trabecular connections (CD) was found to be lower in collagenase-injected knee joints than in controls (figure 5). These bone changes

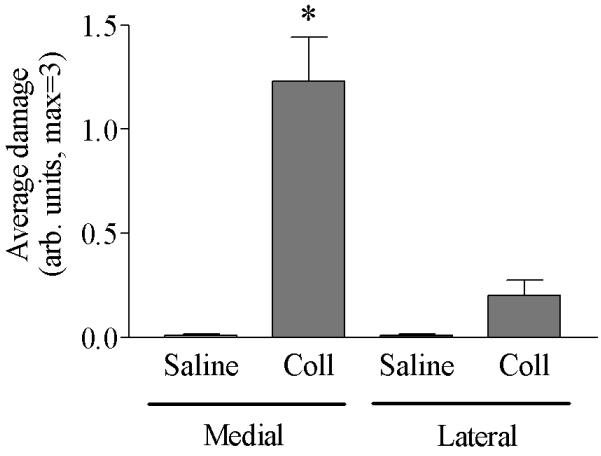

Figure 3. Cartilage damage in the tibia at the lateral and medial side. For each collagenase or saline-injected contralateral joint (both n = 13), microscopic scoring of cartilage damage in the tibia was performed, using a semi-quantitative scale. This resulted in an average lateral or medial damage value with a maximum value of 3 (i.e., maximum damage observed in every analyzed section, on both the medial and lateral side). Values are mean ± SEM, $*p < 0.05$. Coll = collagenase.

were apparently restricted to the epiphyseal area close to the joint, since the cortical thicknesses of the distal metaphysis remained unchanged (mean ± standard deviation saline-injected: 272.7 ± 13.6 µm, collagenase-injected: 268.8 µm ± 13.6, p=0.312).

The cortex of the epiphysis also changed in osteoarthritic joints: The subchondral bone plate was thinner both at the lateral and the medial side (figure 6A). This finding, derived from micro-CT analysis, was qualitatively confirmed by histology (figure 6B).

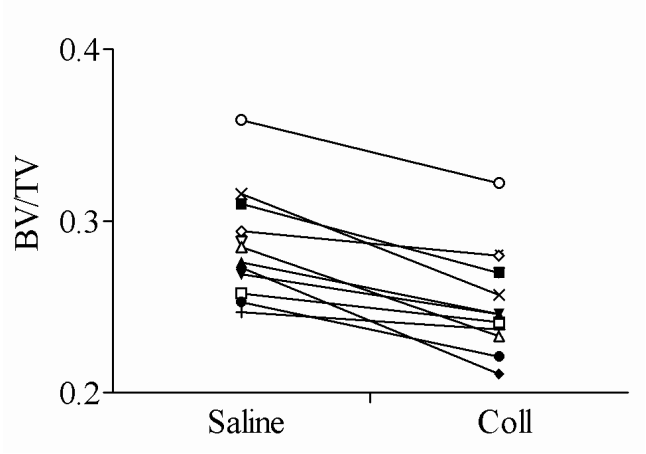

Figure 4. Consistently lower bone volume fraction in the epiphysis. The crude BV/TV value of each individual knee joint is shown, and a connection is made between the joints of one animal to indicate the direction of change. In all cases, the value was lowering the collagenase-injected knee joint (average decrease: 11%, see Figure 5).

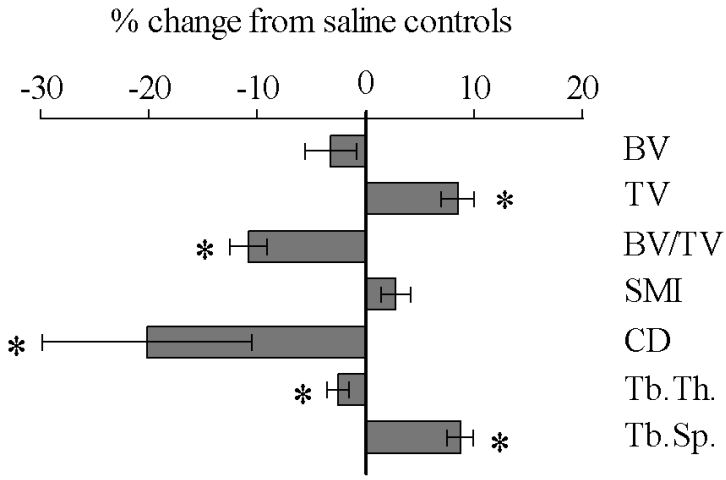

Figure 5. Changes in 3D bone morphometric parameters. The isolated trabeculae (see Figure 1) were analyzed separately for the indicated morphometric parameters. Of each parameter, the percentage change from the saline-injected control knee joints was calculated. Values are mean ± SEM, $*p < 0.05$. BV = bone volume, TV = tissue volume, SMI = structure model index, CD = connectivity density, Tb.Th. = trabecular thickness, Tb.Sp. = trabecular spacing, Ct.Th. = cortical thickness.

DISCUSSION

This study showed that micro-CT can be used to detect subtle changes in subchondral bone in a murine model at a relatively early stage of osteoarthritis. Since the most prominent bone changes were to be expected in close vicinity of the diseased joint, we concentrated on the epiphysis of murine tibiae, and analyzed both the subchondral bone plate as well as the subchondral trabecular compartment. Opposite to what has been reported in studies using clinical samples with late-stage osteoarthritis (21,68,92), our results show that the subchondral bone plate became thinner. As a result, the volume of the trabecular compartment became slightly larger, leading to a decrease in bone volume fraction (BV/TV). The trabecular architecture also changed: We measured a reduction in trabecular thickness contributing to the observed increase in trabecular spacing. Furthermore, connections between trabeculae were lost as indicated by the decrease in connectivity density.

The fact that instead of sclerosis, subchondral bone loss occurred might reflect that in our model the osteoarthritic process is still in a relatively early stage, and that sclerosis might occur afterwards. Other animal models confirm this hypothesis: In 1993, Dedrick *et al.* reported on subchondral bone changes in a canine model in which the anterior cruciate ligament was transected (ACLT). At three time points (3, 18 and 54 months) after ACLT, they found loss of subchondral trabecular bone (84). More recently, the same model was used by Boyd *et al.*, who also found loss of trabecular bone 12 weeks

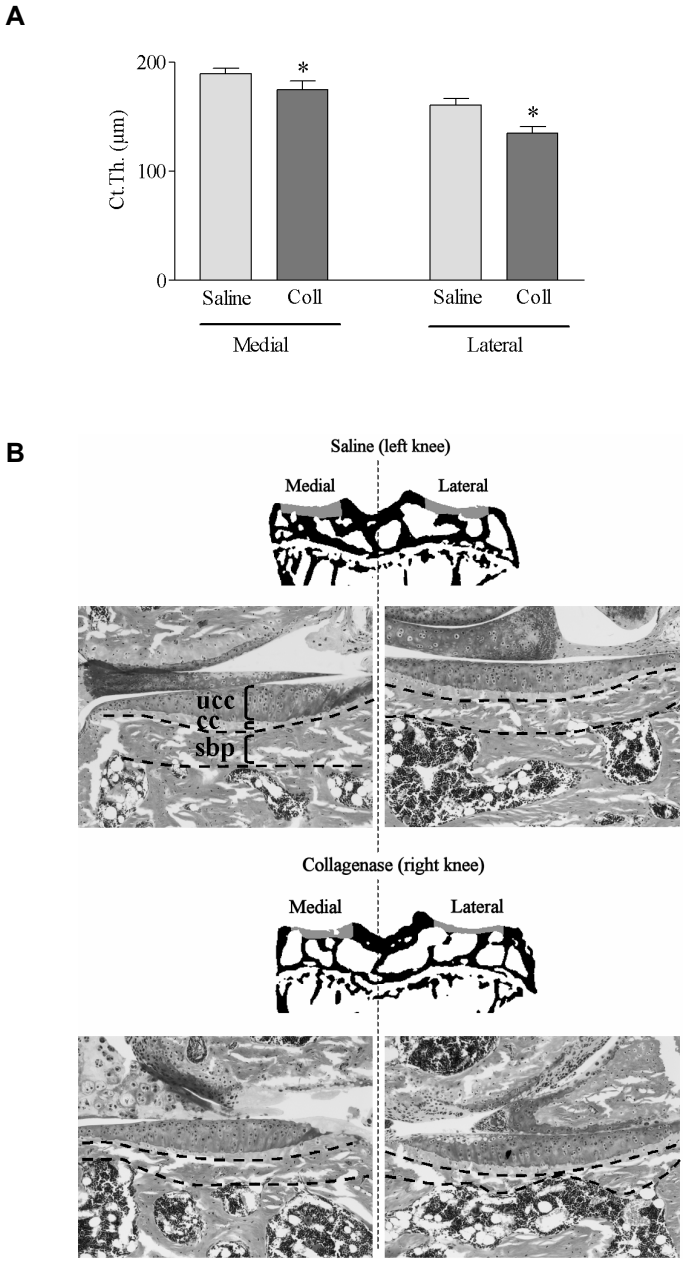

Figure 6. Decreased thickness of the subchondral bone plate. A, the thickness of the subchondral plate at the medial and lateral side was calculated from the segmented images, values are mean ± SEM, $*p < 0.05$. B, segmented image from a saline and collagenase-injected joint, with the subchondral bone plate shown in grey. Note the decrease in thickness on both the medial and lateral side. Below each segmented image are the corresponding histological sections, with the thickness of the subchondral bone plate indicated between dotted lines. Original magnification ×200. ucc = uncalcified cartilage, cc = calcified cartilage, sbp = subchondral bone plate.

post-ACLT (93). The latter group also applied the ACLT model in cats and reported both a decrease in trabecular bone as thinning of the subchondral bone plate (85). In the long-term though a discrepancy existed between cats (85), where the subchondral bone plate remained thin, and dogs, where the bone plate became almost twice as thick (84). Recovery of bone loss was also observed in a rabbit (94) and rat (81) ACLT model and in a guinea pig meniscectomy model (95). So, recovery of bone loss, as well as high turnover and anabolic effects on osteoblasts (69,96-98) seem to be a normal trend in a later phase of osteoarthritis.

Whether the observed bone loss might be due to unloading of the treated (collagenase-injected or ACLT) limb remains subject of discussion. Gait alterations and unloading of the osteoarthritic limb have been reported in dogs (99) and rats (100). Although we have not quantified the degree of unloading, we did observe some limping in the first few days after the injection procedure but after this initial period normal usage of the limb was observed. Indeed, the cortical thickness of the distal metaphysis was not changed after four weeks, indicating that the observed bone loss was localized in the subchondral region of the diseased knee only.

The current study indicates that in this murine osteoarthritis model subtle subchondral bone changes occur at a relative early stage in the disease process. When these bone changes are compared to the observed cartilage damage, another interesting finding was that the decrease in subchondral bone plate thickness at the medial and lateral sides was comparable despite the fact that the lateral side had only little cartilage damage. This finding is suggestive for the fact that the changes found in the subchondral bone run parallel to or maybe even precede the cartilage degeneration. However, to confirm this hypothesis, a longitudinal study is necessary. Thus, our future plans are aimed at analyzing the process in time using *in vivo* micro-CT scanning, which has already been proven useful in both a rat osteoarthritis (48) and osteoporosis model (49). By scanning the joints of the same animal at successive time points in the disease process, we hope to further elucidate the relation between bone and cartilage changes in osteoarthritis.

ACKNOWLEDGMENTS

The authors would like to thank Nicole Kops for help with histology, Jan Floris de Graaf for computing a large part of the morphometric data and the Erasmus Animal Laboratory for taking care of the animals.

Chapter 3

Cartilage damage pattern in relation to subchondral plate thickness in a collagenase-induced model of osteoarthritis

S.M. Botter, G.J.V.M. van Osch, J.H. Waarsing, J.C. van der Linden, J.A.N. Verhaar, H.A.P. Pols, J.P.T.M. van Leeuwen, H. Weinans

Osteoarthritis and Cartilage 2008;16(4):506-514

ABSTRACT

Objective: To see how initial differences in subchondral bone phenotype influence the development of cartilage damage and changes in subchondral bone architecture in an osteoarthritis-induced mouse model.

Method: Intra-articular collagenase injections (right knee joint) and saline controls (left knee joint) were applied in the knees of two mouse strains known to have either a low or a high bone mass phenotype: The low bone mass C57Bl/6 mice with a thin subchondral bone plate and high bone mass C3H/HeJ mice with a thick subchondral bone plate. The age of the mice was 16 and 30 weeks, with *n*=8 per group. The collagenase injection induced an osteoarthritic phenotype that was evaluated four weeks later in the tibia using histological analyses and micro-computed tomography (micro-CT).

Results: Both strains developed cartilage damage in the collagenase-injected right knee joints to a comparable extent, however the spatial distribution of cartilage damage differed significantly: C57Bl/6 mice had most damage at the postero-lateral side, whereas in C3H/HeJ mice the postero-medial region was affected the most. Spontaneous cartilage damage was found in the saline-injected left control knees of C57Bl/6 mice, but in C3H/HeJ mice spontaneous cartilage damage was virtually absent. In both strains the subchondral bone plate of collagenase-injected joints became thinner, independent of the site of cartilage damage. TRAP-positive osteoclasts were observed underneath the subchondral bone plate, in line with the observed decreased thickness. No link was found between subchondral bone plate thickness and cartilage damage in the collagenase-injected joints. The subchondral trabecular architecture only changed in the high bone mass C3H/HeJ mice, with thinning of trabeculae and increased trabecular spacing.

Conclusion: Thinning of the subchondral bone plate was found as a common observation four weeks after osteoarthritis had been induced in two strains of mice having either a high or low bone phenotype, but no relation was found with the amount of cartilage damage. In addition, this study shows that different strains of mice can react differently to instability-induced OA with respect to the spatial arrangement of cartilage damage and changes in subchondral trabecular structure.

INTRODUCTION

Osteoarthritis (OA) is among the leading causes of disability in the elderly and forms a major burden to health care. About 30% of persons aged 65 and over are affected with knee or hip OA (101). A disease modifying treatment is not yet available and treatment is focused on reduction of symptoms. Therefore, more basal knowledge about its possible cause(s) is needed.

Located directly underneath the cartilage, the subchondral bone plate was initially thought to play a role in osteoarthritis initiation and progression (72). The proposed idea was that stiffness variations in the subchondral bone plate would lead to the initiation of cartilage fibrillation. During the disease process the bone plate would then become stiffer, causing a reduced shock-absorbing capacity and leading to progression of these lesions. However, more recent work shows that the stiffness of subchondral bone in OA is actually decreased, because of an increased porosity and a reduced mineral content (68,78,92,102,103).

Apart from changes in composition, the amount of subchondral bone also changes and subchondral sclerosis is universally recognized as being a typical OA characteristic. This is also seen in animals, for instance in macaques who develop OA spontaneously (104). Specifically, thickening of the subchondral bone plate has been observed in guinea pigs (80,105), rabbits (106), and mice (87). Besides having more bone at the location of disease, OA patients also seem to have a higher bone mass at other sites of the skeleton (107-110). A study by Bergink *et al.* even suggests that a high systemic bone mineral density (BMD) before disease initiation is associated with increased incidence and progression of knee OA (111).

From these studies it is clear that changes in the subchondral bone play a role in OA, and that bone phenotype may influence disease onset and/or progression. However, the relation between subchondral bone architecture, subchondral bone plate thickness and the resulting pattern of cartilage damage during OA development is not clear. The aim of the current study was therefore to study these issues in a murine model of collagenase-induced OA (54,64). Specifically, to investigate the relation between subchondral bone phenotype and development of OA, we compared two mouse strains: the C57Bl/6 strain that has a low bone mass and a thin subchondral bone plate and the C3H/HeJ strain that has a high bone mass as well as a thicker bone plate, at two different ages.

METHODS

Animals

Following the approval of the local animal ethics committee, male C3H/HeJCrlBR mice (Charles River, Sulzfeld, Germany) and C57Bl/6 mice (Harlan, Zeist, The Netherlands) aged 16 and 30 weeks were used with 8 mice per group. The animals were maintained on a 12:12 h light-dark cycle, housed in individually ventilated cages with three brother littermates per cage and were fed *ad libitum*.

For induction of osteoarthritis, we used the collagenase OA model as described previously (54,64). This model utilizes bacterial collagenase injected into the knee joint space, thereby inducing damage to joint structures containing type I collagen such as tendons, ligaments and menisci, and causes an increase in knee joint laxity resulting in cartilage damage (83,112). The enzyme has minimal direct effect on articular cartilage, which contains type II collagen that is resistant to digestion by the bacterial enzyme (55). Test-injections in cadavric mice using the dye toluidine blue confirmed the injected fluid to be present in the knee joint space only. At 16 or 30 weeks of age, the animals were anesthetized with a 5% isoflurane/N_2O/O_2 mixture. A small incision was made in the skin at the anterior side of the knee joint such that the patellar tendon was exposed and an accurate injection could be applied. Six µl containing 10U of highly purified bacterial type VII collagenase (Sigma, St Louis, MO) was injected into the right knee intra-articular space, the left knee was injected with 6 µl saline.

As an analgesic the animals received one subcutaneous injection of buprenorphine (Temgesic, 0.01 mg/kg body weight) directly after the collagenase injection. After four weeks the mice were euthanized and their knee joints were excised and fixed in 4% formalin for two days.

Micro-computed tomographic scanning and quantification of bone morphometric parameters

The knee joints were scanned with a voxelsize of 9 µm using the Skyscan 1072 micro-CT scanner (Skyscan, Aartselaar, Belgium). In order to distinguish calcified tissue from non-calcified tissue, the reconstructed greyscale images were segmented by an automated algorithm using local thresholds (88). The epiphysis of the tibia was chosen as the region of interest to study subchondral bone. The outline of the epiphysis was manually selected using 3D data analysis software (CTAnalyzer, Skyscan) and care was taken not to select outgrowing osteophytes (Fig. 1a). Also, 1.0 mm of the proximal metaphyseal bone directly underneath the growth plate was selected, as well as 0.3 mm of diaphyseal cortical bone (Fig. 1b).

The subchondral bone plate and trabeculae of the epiphysis, and cortex and trabeculae of the metaphysis were separated using in-house developed automated software. Bone morphometric parameters of the thus obtained bone structures were determined

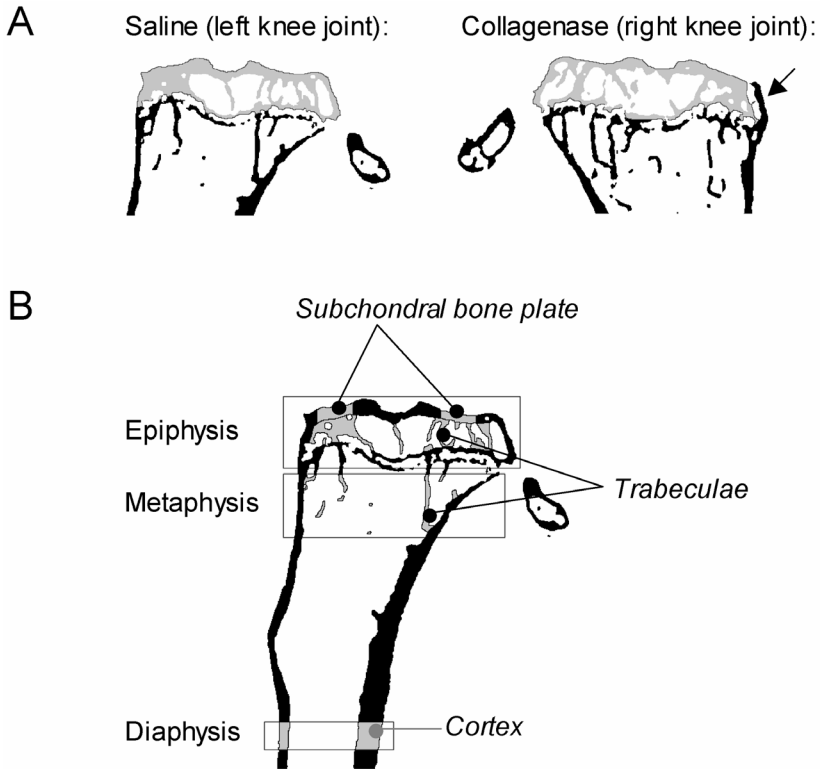

Figure 1. Selection procedure of the epiphysis, metaphysis and diaphysis of the tibia for 3D morphometric analysis. A, first, the epiphysis (left, grey) was manually selected as representative of subchondral bone, outgrowing osteophytes were excluded (right, arrow). B, epiphyseal and metaphyseal trabeculae were separated from the subchondral bone plate and cortex, respectively. Each of the thus obtained bone regions was analyzed separately.

using the freely available software package 3D-Calculator (*http://www.erasmusmc.nl/47460/386156/Downloads*). The following 3D morphometric parameters were calculated for the trabecular compartments: bone volume fraction (Trab BV/TV), which is the ratio of trabecular bone volume (Trab BV) over endocortical total volume (TV), trabecular thickness (Tb.Th.), trabecular spacing (Tb.Sp.), trabecular number (Tb.N.), connectivity density (CD), which calculates the number of trabecular connections per unit volume (90) and structure model index (SMI), indicating whether trabeculae have a rod-like or plate-like shape (89). The thickness of the medial and lateral subchondral bone plate, as well as the diaphyseal cortex was measured using the same algorithm as used for determining Tb.Th. A subset (0.5 mm medio-lateral width, 1.0 mm ventro-dorsal length) of the weight-bearing region at the medial and lateral side of the tibial plateau was taken as region of interest.

Histological analysis

Following the scanning procedure, knee joints were embedded in methyl methacrylate and frontal sections were made to verify the presence of OA characteristics such as cartilage damage and osteophytes. Per knee joint 8-10 undecalcified sections of 6 μm thickness were obtained, with 100 μm interspacing. Of the obtained sections six were analyzed per joint, three in the anterior region and three in the posterior region in the load-bearing region of the joint. Goldner staining was performed which gave excellent discrimination between noncalcified cartilage, calcified cartilage and subchondral bone. Thicknesses of noncalcified and calcified cartilage were measured in one anterior and one posterior section using Bioquant Osteo v7.20 (Bioquant, Nashville, TN). This programme measures the thickness every 5 μm over a distance of 400 μm, producing roughly 80 measurements, which were then averaged.

Cartilage damage was quantified in the antero-medial, postero-medial, antero-lateral and postero-lateral regions of the tibial plateau using the semi-quantitative grading and staging system devised by the OARSI Working Group (18). In this system the grade-score, reflecting the severity of the damage, ranges from 0 (no cartilage damage) to 6 (all cartilage lost, complete disorganization and deformation of the joint). A separately assigned stage-score, reflecting the extent of damage, ranges from 0 (whole cartilage surface intact) to 4 (>50% of cartilage surface affected). Grade and stage scores are then multiplied, giving a maximum cartilage damage score of 24 for each of the four analyzed regions of the tibial plateau. We summed the damage scores of the four regions to reflect the total cartilage degeneration in the tibia, with a maximum obtainable summed damage score of 96.

Osteophyte presence was scored as follows: Each of the 6 sections analyzed for cartilage damage was also analyzed for the presence of osteophytes at the medial and lateral side of the tibia. In case an osteophyte was observed in any of these 6 sections, the knee joint was considered osteophyte-bearing. The percentage of osteophyte-positive knee joints was calculated for each group.

TRAP stainings were performed to visualize osteoclastic activity. Bone sections were deacrylated and stained using 1.1 mM Naphtol AS-BI phosphate (Sigma, St Louis, MO) as substrate, 5.2 mM pararosanilin as coupler, and 46.5 mM sodium L-tartrate as inhibitor according to Scheven *et al.* (113). Nuclei were stained with methylene green.

Data-analysis

Differences between left and right knee joints within strains were analyzed with the Wilcoxon matched paired test. The Mann-Whitney U test was applied for differences between age groups, both within strains and between strains. In all cases, $P<0.05$ was considered statistically significant. In all graphs, the error bars depict standard error of the mean (SEM).

RESULTS

Effect of the operation

Twelve hours after the operation, which corresponds to the therapeutic effective time span of the used analgesic, the animals were observed closely. Cage activity was normal apart from slight limping of the right leg and no further analgesia was applied. After a few days normal walking patterns returned. Although weight loss (2-6% of the original body weight) was measured in the first week after the operation, all animals had normal weight gain thereafter.

Basal tibial bone morphometry

All basal tibial bone morphometric parameters were derived from the control knee joints four weeks after the saline injection. As reported previously, C3H/HeJ mice had a thicker metaphyseal and diaphyseal cortex than C57Bl/6 mice confirming the high bone mass phenotype of the C3H/HeJ mice (table 1, metaphysis C3H/HeJ approx. 155 vs 130 μm C57Bl/6, diaphysis 260 vs 190 μm). In accordance, the subchondral bone plate of the epiphysis was significantly thicker in C3H/HeJ than in C57Bl/6 mice, both at the medial (C3H/HeJ: approx. 180 μm, C57Bl/6: 150 μm) and at the lateral side (C3H/HeJ: approx. 150 μm, C57Bl/6: 110 μm). In both mouse strains and at both ages the medial side of the subchondral bone plate was thicker than the lateral side. The morphometric parameters between the ages of 16 and 30 weeks confirmed aging effects in trabecular bone architecture in C57Bl/6 mice only. At 16 weeks of age the amount of trabecular bone (Trab BV/TV) in either epiphysis (30%) or metaphysis (15%) was not different between strains, but at 30 weeks C57BL/6 mice had lost trabecular bone at both anatomical sites. This was paralleled by a decrease in trabecular connectivity and an increase in trabecular spacing, although Tb.Th. remained the same. In contrast, C3H/HeJ mice did not show a change in trabecular bone architecture between 16 and 30 weeks, neither in the epiphysis nor in the metaphysis. However, in this strain the lateral side of the subchondral bone plate became significantly thinner with age from 16 weeks (168 μm) to 30 weeks (149 μm) whereas the thickness at the medial side remained unchanged. C57Bl/6 mice did not show such a decrease in bone plate thickness. Finally, the thickness of both the metaphyseal and diaphyseal cortex did not change due to aging in either strain. Table 1 summarizes the examined bone morphometric parameters.

Histological changes

Quantification of total cartilage thickness (i.e., calcified plus noncalcified) on histology revealed no significant difference between the two strains at both ages, neither at the medial nor at the lateral side of the tibial plateau (data not shown). However, a difference in the ratio between calcified and noncalcified cartilage thickness was noted: C57Bl/6 mice

Table 1. Basal tibial bone morphometry in male C57Bl/6 and C3H/HeJ mice. All parameters were derived from the saline-injected left knee joints, four weeks after injection. Values shown are averages ± SEM. Trab BV/TV= trabecular bone volume fraction, Tb.Th.= trabecular thickness, Tb.Sp.= trabecular spacing, CD= connectivity density, Ct.Th.= cortical thickness, Sb.Pl.Th.= subchondral plate thickness, med= medial, lat= lateral, #P<0.05 age within strain, &P<0.05 med vs lat within strain, ns= not significant.

Location	*Parameter*	*Age*	*C57Bl/6*		*C3H/HeJ*		*Strain difference*
Epiphysis	Trab BV/TV (%)	16wks (+4)	30.3 ± 0.6		30.7 ± 1.1		ns
		30wks (+4)	27.1 ± 0.5	#	30.5 ± 0.9		P<0.01
	Tb.Th. (μm)	16wks (+4)	66.2 ± 0.6		72.1 ± 1.8		P<0.01
		30wks (+4)	68.3 ± 0.6	#	74.4 ± 1.2		P<0.01
	Tb.Sp. (μm)	16wks (+4)	195.7 ± 3.6		205.9 ± 5.2		ns
		30wks (+4)	207.8 ± 3.1	#	210.1 ± 5.2		ns
	CD	16wks (+4)	189.6 ± 16.3		99.8 ± 21.0		P<0.01
		30wks (+4)	88.6 ± 6.8	#	104.7 ± 18.2		ns
	Sb.Pl.Th., med (μm)	16wks (+4)	144.0 ± 5.3		188.8 ± 6.5		P<0.01
		30wks (+4)	157.8± 6.3		179.2 ± 4.6		P<0.05
	Sb.Pl.Th., lat (μm)	16wks (+4)	113.6 ± 4.1	&	168.6 ± 5.5 &		P<0.01
		30wks (+4)	112.6 ± 3.0	&	150.9 ± 5.1 &	#	P<0.01
Metaphysis	Trab BV/TV (%)	16wks (+4)	14.0 ± 0.7		15.2 ± 1.6		ns
		30wks (+4)	10.0 ± 0.4	#	14.8 ± 0.8		P<0.01
	Tb.Th. (μm)	16wks (+4)	58.3 ± 1.2		63.7 ± 1.3		P<0.05
		30wks (+4)	59.9 ± 0.8		62.9 ± 1.3		ns
	Tb.Sp. (μm)	16wks (+4)	264.9 ± 8.6		329.3 ± 35.2		ns
		30wks (+4)	361.0 ± 7.9	#	315.3 ± 25.9		ns
	CD	16wks (+4)	45.5 ± 9.1		59.3 ± 16.7		ns
		30wks (+4)	16.2 ± 4.4	#	40.0 ± 5.2		P<0.01
	Ct.Th. (μm)	16wks (+4)	125.8 ± 2.9		157.8 ± 3.2		P<0.01
		30wks (+4)	133.2 ± 1.5		154.1 ± 3.5		P<0.01
Diaphysis	Ct.Th. (μm)	16wks (+4)	192.5 ± 2.4		263.2 ± 5.9		P<0.01
		30wks (+4)	188.3 ± 4.3		261.7 ± 3.2		P<0.01

had significantly thicker calcified cartilage, and significantly thinner noncalcified cartilage compared to C3H/HeJ mice, primarily at the medial side (Fig. 2). In collagenase-injected joints, no significant change was observed in the thickness of calcified cartilage compared to saline-injected joints, whereas the noncalcified layer became thicker at the lateral side, in both strains and at both ages (Fig. 2). At the medial side, no changes were observed.

All C57Bl/6 mice developed spontaneous cartilage damage in the saline-injected joints, with a summed damage score of approx. 10 out of a maximum of 96 at 16 weeks of age (Fig. 3a, top) that increased to approx. 15 at 30 weeks. In contrast, in C3H/HeJ mice spontaneous cartilage damage was virtually absent in all but one mouse at 30 weeks of age. We tested the possibility that the subchondral bone plate thickness of the

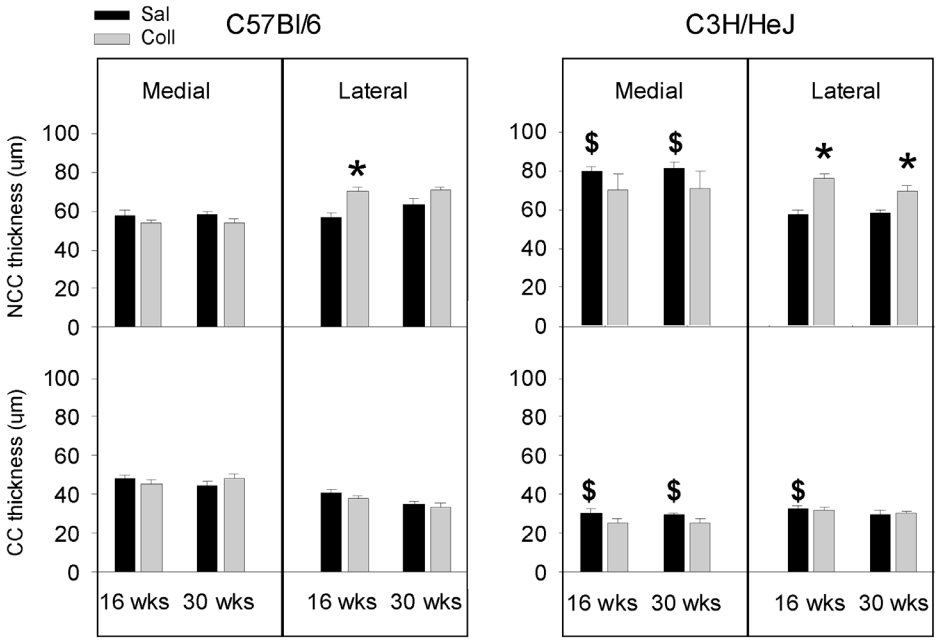

Figure 2. Thickness of the noncalcified and calcified layers of the articular cartilage at the medial and lateral side in saline-injected and collagenase-injected knee joints. Each bar represents the average (±SEM) of two measurements, one made in anterior region of the knee, and one in the posterior region. Please note the decreased values and increased standard error of the collagenase-injected joints of C3H/HeJ mice at the medial side. In these mice it was sometimes not possible to obtain a thickness value in the postero-medial region due to the severe amount of cartilage damage, in these cases '0' was used as value. Significant differences between saline-injected joints and collagenase-injected joints within strains are indicated by *, between strains of the same age by $. NCC= noncalcified cartilage, CC= calcified cartilage.

saline-injected joints was related to the amount of spontaneous cartilage damage, but no relation was found.

In collagenase-injected joints the summed cartilage damage of the whole tibial plateau did not differ significantly between the two strains at either 16 or 30 weeks of age. However, the damage scores of the four separate examined anatomical regions (antero-medial, antero-lateral, postero-medial and postero-lateral) revealed that C57Bl/6 mice had most damage at the lateral side, whereas in C3H/HeJ mice the medial side was the most degenerated (Fig. 3a, bottom). Besides these differences in spatial arrangement, we also observed a difference in the type of cartilage damage: in C57Bl/6 mice the top layer of the noncalcified cartilage became fibrillated and was loosened in some sections, whereas in C3H/HeJ mice vertical clefts were observed more often. Specifically for C3H/HeJ mice, the postero-medial region showed severe cartilage degeneration with damage scores of 20 or higher out of a maximum of 24. In this region the subchondral bone plate was worn away and the trabecular bone became exposed (Fig. 3b). This was not seen in any of the C57BL/6 mice.

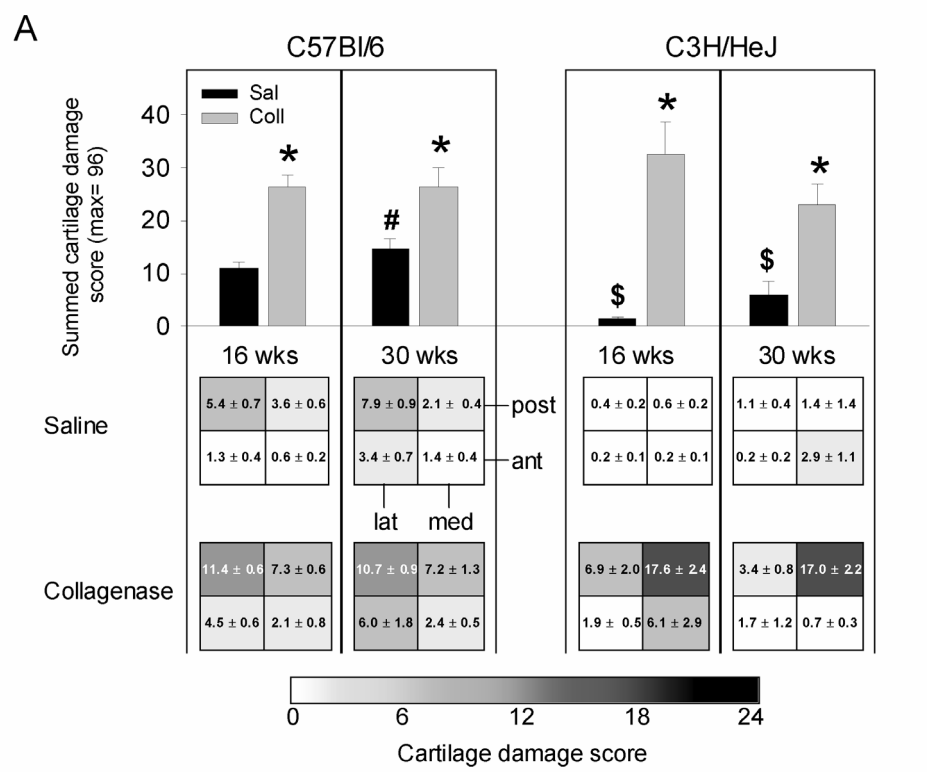

Figure 3. Cartilage damage in saline-injected knee joints and collagenase-injected knee joints. A, top: summed cartilage damage score of the antero-lateral, antero-medial, postero-lateral and postero-medial region of the tibial plateau. For each region a maximum score of 24 could be obtained, the maximum obtainable summed score was therefore 96. Significant differences between saline- and collagenase injected joints within strains are indicated by *, between ages within strains by #, between strains of the same age by $. A, bottom: schematic view of cartilage damage in the four separate regions. For each region the cartilage damage scores (average ±SEM) are depicted in colour-code. B, histology of the posterior region in knee joints of control and osteoarthritic knee joints. Note the exposure of the subchondral bone at the medial side in collagenase-injected joints of C3H/HeJ mice. The blue boxes indicate a magnification of the lateral (C57Bl/6) and medial (C3H/HeJ) sides, shown on the right.

In addition to cartilage damage, osteophytes were observed in all collagenase-injected joints of both mouse strains at both ages. Specifically, at the medial side of the tibia the incidence was 100%. At the lateral side of the tibia the incidence was the same, except for the 30-week-old C57Bl/6 mice in which only 5 out of 8 animals (62.5%) were osteophyte-bearing. In saline-injected joints osteophytes were observed as well, although its sizes were significantly smaller compared to the collagenase-injected joints (data not shown). At 16 weeks of age, these small osteophytes were seen in two out of eight (25%) C57Bl/6 mice at the medial tibia, whereas C3H/HeJ mice of the same age did not have any osteophytes. At the lateral tibia no osteophytes were seen in both strains. At 30 weeks of age, the incidence of small osteophytes became larger with five out of

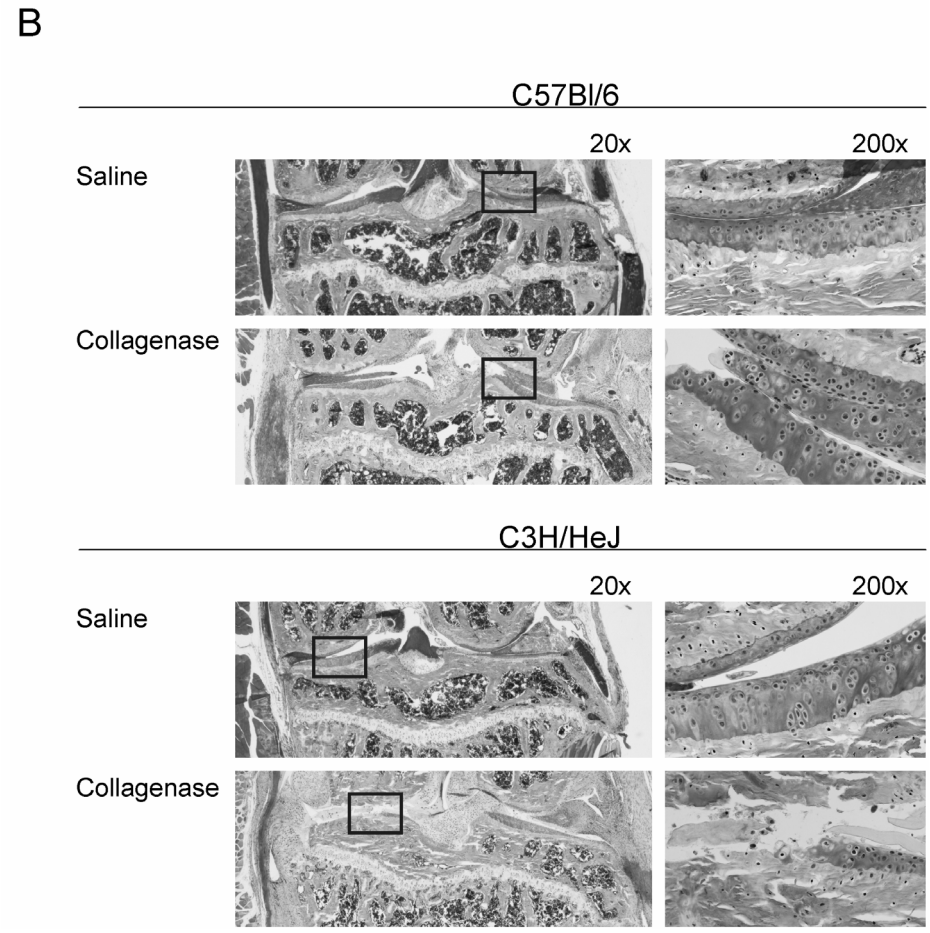

Figure 3. (continued)

eight (62.5%) C57Bl/6 mice and eight out of eight (100%) C3H/HeJ mice positive at the medial tibia, and one out eight C57Bl/6 (12.5%) vs two out of eight C3H/HeJ (25%) at the lateral tibia. The mineralized parts of these osteophytes became visible on the micro-CT images as bony outgrowths (see Fig. 1a, right).

Bone changes in the proximal tibia due to intra-articular collagenase-injection

The subchondral bone plate was significantly thinner in collagenase-injected joints compared to the contralateral saline-injected joints in both strains and at both ages (Fig. 4a). The lateral side of the bone plate seemed to be affected the most with a thickness reduction of 12% (16 weeks old) to 18% (30 weeks old) in C57Bl/6 and 20% (16

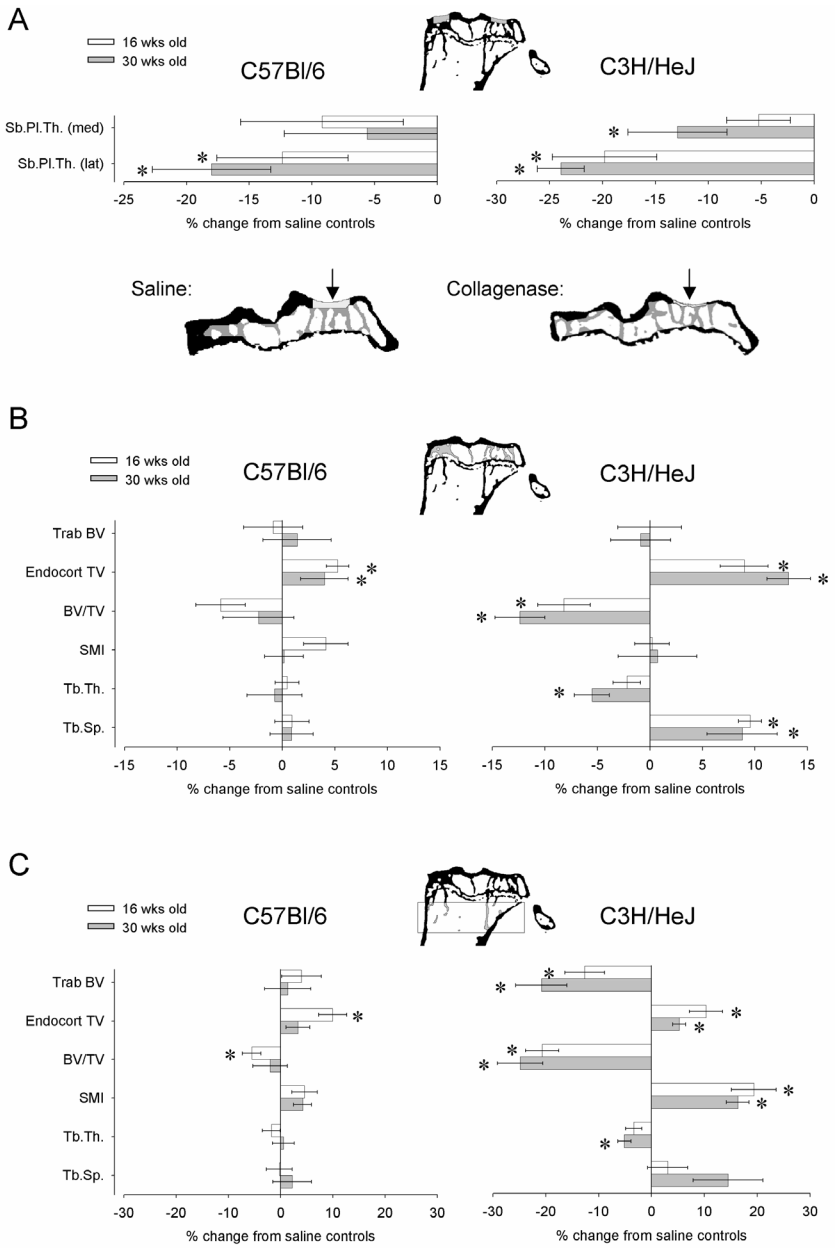

Figure 4. Bone changes in the proximal tibia expressed as percentage change from saline-injected contralateral joints. A, thickness changes of the medial and lateral subchondral bone plates (Sb.Pl.Th.), with below two examples of thinning of the lateral subchondral bone plate (indicated by arrow) in epiphyses of a saline-injected and collagenase-injected joint from a 30-week-old C57Bl/6 mouse. B, changes in the epiphyseal trabeculae, the following parameters were measured: trabecular BV (Trab BV), endocortical TV of which the ratio (Trab BV/TV) determines the volumetric amount of bone. Trabecular thickness (Tb.Th.), trabecular spacing (Tb.Sp.), and SMI, indicating the degree of rod-like structure, were also calculated. C, changes in metaphyseal trabeculae. *$P < 0.05$.

weeks old) to 24% (30 weeks old) in C3H/HeJ mice. In addition, in 30-week-old C3H/HeJ mice the medial side of the bone plate also became significantly thinner. Separate analysis at the antero-medial, antero-lateral, postero-medial and postero-lateral region as done for the assessment of cartilage damage revealed the bone plate thinning to be present throughout the tibial plateau (data not shown). Histological analysis showed TRAP-positive osteoclasts directly underneath the bone plate up until the calcified cartilage in collagenase-injected knee joints (Fig. 5). In epiphyses of saline-injected joints osteoclasts were only scarcely observed.

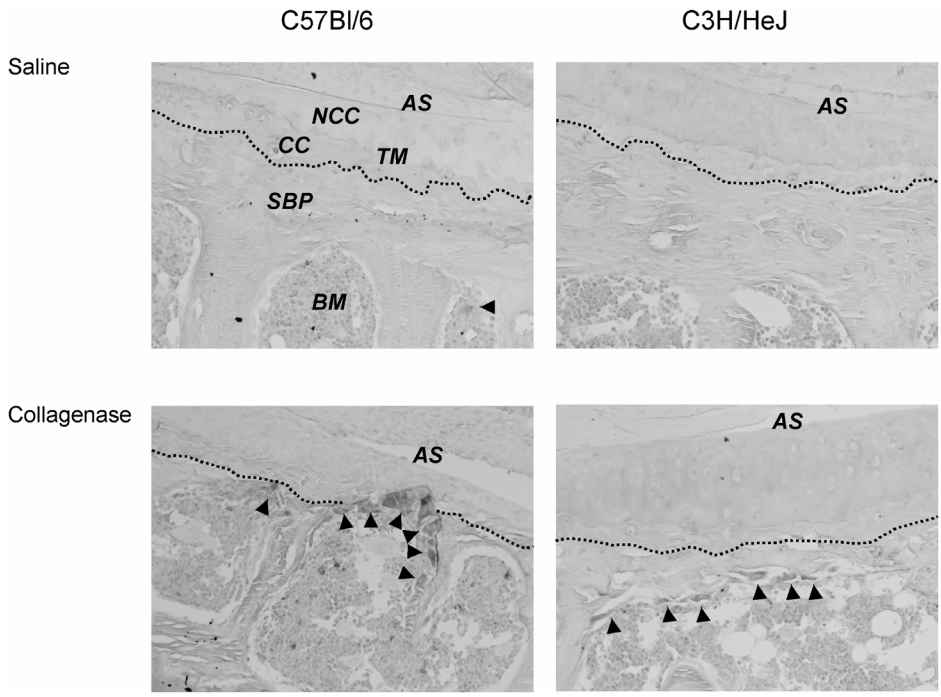

Figure 5. TRAP staining in histological sections of saline-injected and collagenase-injected knee joints. In saline-injected joints, osteoclasts (arrowheads) were observed occasionally. At some locations in collagenase-injected joints osteoclasts resorbed the subchondral bone plate up to the noncalcified cartilage. The division between the calcified cartilage and the subchondral bone plate is indicated by a dotted line. AS= articular surface, NCC= noncalcified cartilage, CC= calcified cartilage, SBP= subchondral bone plate, TM= tidemark. Original magnification 200x.

The epiphyseal trabecular architecture was not altered in C57Bl/6 mice after osteoarthritis induction, since trabecular bone volume, thickness, SMI and spacing did not change significantly in either age group (Fig. 4b, left). However, a small increase of about 5% in endocortical total volume (TV) was measured compared to the contralateral saline-injected joints, but this did not lead to lead to a significant decrease in Trab BV/TV. An increase in endocortical TV was also observed in collagenase-injected joints of C3H/HeJ mice,

lowering the Trab BV/TV ratio about 10% in both age groups (Fig. 4b, right). Furthermore, trabeculae in the epiphysis of collagenase-injected C3H/HeJ knee joints were thinner and had increased spacing. Despite these changes in trabecular structure, no significant changes were seen in either connectivity density or trabecular number (data not shown). Periosteal expansion of the epiphysis other than osteophyte formation was not observed.

In the metaphysis of C57BL/6 mice the only noticeable change was a small decrease in bone volume fraction in collagenase-injected joints of the 16-week-old mice caused by an increase in endocortical total volume (Endocort TV, Fig. 4c). In the metaphysis of C3H/HeJ mice the endocortical total volume was also increased in collagenase-injected joints, which together with a reduced trabecular bone volume (Trab BV) resulted in a decreased Trab BV/TV of about 20%. In addition, SMI increased, indicating that the metaphyseal trabeculae became more rod-like. In both strains and at both ages the metaphyseal cortex of collagenase-injected joints contained small cavities with TRAP-positive osteoclasts, which were not observed in saline-injected joints. However the presence of these cavities did not lead to a significant decrease in cortical thickness (data not shown).

Bone changes in the distal tibia due to intra-articular collagenase-injection

To verify whether changes in bone also occurred at more remote sites in the joint, e.g. due to differences in limb loading, we measured which changes had occurred in a more distal region of the tibia, the diaphyseal cortex. Although in 16-week-old C57Bl/6 mice the thickness of the diaphyseal cortex in collagenase-injected joints was lower compared to contralateral saline-injected joints (saline-injected: 192 ± 2.4 μm, collagenase-injected 184 ± 2.1 μm, P=0.02), in all other groups of mice cortical thickness did not differ between saline-injected and collagenase-injected joints. An increase in osteoclastic activity as seen in the subchondral bone plate and the metaphyseal cortex was not observed.

DISCUSSION

This study showed both common findings as well as specific and consistent differences in subchondral bone adaptation and spatial arrangement of cartilage damage between the C57Bl/6 mice having an initial thin subchondral bone plate and C3H/HeJ mice having an initial thick subchondral bone plate. In both strains at both ages thinning of the subchondral bone plate was found in collagenase-injected knee joints, but subchondral trabecular changes were only found in C3H/HeJ mice. Both strains developed cartilage damage to a comparable extent, but the spatial arrangement of cartilage damage differed significantly between the two strains: In C57Bl/6 mice the cartilage damage was

located mainly at the lateral side of the tibial plateau, both in saline-injected (spontaneous damage) as in collagenase-injected (instability-induced damage) knee joints. In contrast, in C3H/HeJ mice the damage was principally located at the medial side. In these mice spontaneous damage was virtually absent in the saline-injected left control knee joints, so compared to these saline-injected controls the additional damage in the collagenase-injected joints was higher in C3H/HeJ mice.

The reason why we have chosen these two mouse strain was because of their well-described phenotypic difference in bone and subsequent subchondral bone phenotype, a consequence of their different genetic backgrounds (114-118). Since we know bone to be involved in OA, our initial hypothesis was that a difference in subchondral bone phenotype, and specifically subchondral bone plate thickness, might have an influence on cartilage damage, thereby linking the two. However, when we tested whether the thickness of the subchondral bone plate was related to the amount of cartilage damage, neither in saline-injected nor in collagenase-injected knee joints a relation was found. Besides bone structure, the mice likely differ in other phenotypical aspects as well such as joint loading and joint alignment. We found a difference in the amount of spontaneous cartilage damage between the two mouse strains and it is tempting to speculate that this might be caused by a difference in joint loading. However, although intuitively logical, there is as yet no literature data available for each of the strains which would substantiate this theory. Furthermore, differences in joint alignment might explain why there was such a pronounced difference in medial and lateral cartilage damage development. In this view, C57Bl/6 mice place a relative large amount of mechanical load on their lateral tibial plateau, which would increase in the instable collagenase-injected knee joints. This is further supported by the fact that the spatial arrangement of cartilage damage in the saline-injected joints (i.e., spontaneous damage) was the same as in the collagenase-injected joints (i.e., instability-induced damage) within each strain. In C3H/HeJ mice the highest amount of load would be more focal and present on the postero-medial side, explaining the rather drastic amount of cartilage damage seen at the postero-medial region of the tibial plateau in the C3H/HeJ mice.

The composition of the cartilage layer and extracellular matrix might also differ between the two strains. Reports concerning cartilage biology or cartilage mechanical properties in C3H/HeJ mice are scarce and papers comparing these properties between C3H/HeJ and C57Bl/6 are, to our knowledge, non-existing. We demonstrate for the first time a difference in the calcified/noncalcified ratio of the articular cartilage between these two strains. This might influence the stresses in the cartilage resulting from load bearing. Finally, the mechanical properties of joint tendons between the two strains were also found to be different: A recent publication described that joint tendons of C3H/HeJ mice are of inferior quality, although a significant difference in joint laxity between C57Bl/6 and C3H/HeJ mice was not found (119).

In this study we observed that in both strains the subchondral bone plate became thinner in collagenase-injected joints. This was caused by osteoclastic resorption of the subchondral bone plate, at some locations even up to the noncalcified cartilage. Newly formed cavities were observed in the subchondral bone plate, occupied by invading osteoclasts. These cavities might be analogous to the subchondral resorption pits observed in human OA (120). Whether the mice were 16 or 30 weeks of age at the start of the experiment did not seem to be of influence in either strain, since the direction and magnitude of changes in both bone and cartilage were similar in both age groups. We measured calcified cartilage thickness which, because of its high mineral content (21), cannot be discriminated from bone in micro-CT analysis and found no thickness differences between saline-injected and collagenase-injected joints. Thus, the thickness changes we observed are caused solely by changes in the subchondral bone plate.

There are several explanations for the increased osteoclastic activity in the osteoarthritic joints. One possibility might be a regional acceleratory phenomenon (RAP) due to noxious stimuli such as the stress of surgery or increased amount of inflammation (121). However, the differences we observed were compared to the saline-injected joints that underwent the same surgical procedure. In addition, although after the collagenase-injection a small inflammatory response is known to occur, this response is only short-lived and is markedly reduced already 3 days after the injection (54). Therefore, it seems unlikely that RAP plays a role in this process.

Another possibility for increased osteoclastic activity is that the destabilized joint was unloaded, which is known to induce bone resorption (122). Male C3H/HeJ mice have been shown to lose epiphyseal trabecular bone in response to unloading (123), however in these models complete unloading is established by hind limb suspension whereas in our model the mice still had the ability to load their limbs. It is unlikely that a few days of lameness would induce extensive resorptive activity. In addition, the C57Bl/6 strain is known to be more responsive to unloading compared to C3H/HeJ mice (124,125), but in our study the amount of trabecular bone in both the epiphysis and the metaphysis of C57Bl/6 mice was not decreased, and no major changes were found in the thickness of the diaphyseal cortex. We therefore think that unloading does not play an important role and that the bone changes that we have observed are truly part of the disease process.

The fact that we observed subchondral bone plate thinning and increased osteoclastic activity in both strains might be contra-intuitive since subchondral sclerosis is considered as an OA hallmark, but is in fact observed in other animal models of OA as well. Bailey and Mansell identified the formation of subchondral cysts in an early disease stage in guinea pigs (28), which might indicate initial weakening of the subchondral bone. They stated that subchondral bone thickening might be a compensatory response observed later on in the disease process. This theory was confirmed in a rat model in

which anterior cruciate ligament transection (ACLT) was performed (30) and in a canine model using the same approach (84,126). Interestingly, these studies also found sclerosis of the subchondral bone to occur eventually. Recovery of initial loss of subchondral bone was seen in a post-traumatic OA model in rabbits as well (94), with initial bone loss followed by bone accrual and subsequent sclerosis later on. Lastly, a feline study also showed subchondral plate thinning (85) at 16 weeks following ACLT.

These beforementioned studies suggest that the OA disease process in our study is likely to be in an early phase, whereas in human studies the disease has already progressed further. Other lines of evidence from our study further confirm this hypothesis: first, even though the instability-induced cartilage damage was clearly present in both strains and C3H/HeJ mice had severe amounts of cartilage damage locally, the summed cartilage damage was still quite low, approximately 25 whereas a maximum score of 96 could be obtained. Second, the process of cartilage wear and tear was still in an early phase, as indicated by the swelling of the noncalcified cartilage layer in collagenase-injected joints (see Fig. 2), a known feature of early OA (127,128). Finally, the osteophytes that were formed in the collagenase-injected joints were not yet fully mineralized, indicating an immature stage of osteophyte development.

In summary, we evaluated changes in bone and cartilage 4 weeks after osteoarthritis induction in two strains of mice having a different subchondral bone phenotype. The subchondral bone plate was found to become thinner in both strains, but the spatial distribution of cartilage damage after OA induction was found to differ significantly. The observed thinning was not linked to the location and severity of cartilage damage in either strain, but seemed to be a diffuse event taking place across the whole tibial plateau.

ACKNOWLEDGMENTS

We acknowledge Jan-Floris de Graaf for assisting in the analysis of the bone morphometric data, Nicole Kops for helping with histology and the personnel of the Experimental Animal Facilty of the Erasmus MC for taking care of the animals during the experiment.

Chapter 4

ADAMTS5-/- mice have less subchondral bone changes after induction of osteoarthritis through surgical instability: implications for a link between cartilage and subchondral bone changes

S. M. Botter, S.S. Glasson, B. Hopkins, S. Clockaerts, H. Weinans, J.P.T.M. van Leeuwen, G.J.V.M. van Osch

Osteoarthritis and Cartilage 2009;17(5):636-645

ABSTRACT

Objective: Osteoarthritis (OA) is characterized by damaged articular cartilage and changes in subchondral bone. Previous work demonstrated aggrecanase-2 deficient (ADAMTS5-/-) mice to be protected from cartilage damage induced by joint instability. This study analyzed whether this protective effect on cartilage is also reflected in the subchondral bone structure.

Methods: Right knee joints from 10-week old male wild type (WT) and ADAMTS5-/- mice received transection of the medial meniscotibial ligament to induce OA, whereas left knees were left unoperated. After 8 weeks knee joints were scanned by micro-CT. The proximal tibia was selected for further analysis. Histology was performed to evaluate cartilage damage and osteoclast presence.

Results: ADAMTS5-/- joints had a significantly thinner subchondral plate and less epiphyseal trabecular bone compared to WT joints. Histology confirmed previous findings that ADAMTS5-/- mice have significantly less cartilage damage than WT in the instability-induced OA model. Although the subchondral bone plate became significantly thicker at the medial tibial plateau in operated joints of both genotypes, the percentage increase was significantly smaller in ADAMTS5-/- mice (WT: 20.7 +/- 4.7%, ADAMTS5-/-: 8.3 +/- 1.2% compared to the left unoperated control joint). In ADAMTS5-/- animals a significant decrease was found in both Oc.N./BS and Oc.S./BS. Finally, in WT but not in ADAMTS5-/- mice a significant correlation was found between medial subchondral bone plate thickness and cartilage damage at the medial tibial plateau.

Conclusion: ADAMTS5-/- joints that were protected from cartilage damage showed minor changes in the subchondral bone structure, in contrast to WT mice where substantial changes were found. This finding suggests links between the process of cartilage damage and subchondral bone changes in instability-induced OA.

INTRODUCTION

In the articulated joint, bone and cartilage are in close proximity. Although a sharp border exists between the two tissues there is evidence that they are in fact connected (24,74,129). Furthermore, there is evidence that osteoblasts and chondrocytes can influence each others metabolism (130,131), especially in a disease such as osteoarthritis (OA) (132-135). In OA, cartilage is damaged and apparent changes take place in the structure of the subchondral bone (8). Although the relation between cartilage damage and subchondral bone changes is still controversial, the subchondral bone is thought to play an important role in the progression and perhaps aetiology of the disease. In end-stage disease, the subchondral bone becomes sclerotic, which may be caused by, or might have an effect on, the overlying cartilage (31,136).

In cartilage the extracellular matrix (ECM) is composed of two main structural elements, collagen type II and aggrecan. The collagen fibrils confer strength and stiffness, whereas aggrecan's function is to retain water inside the ECM, thereby offering resistance to compressive forces and conferring the shock-absorptive capacity of cartilage. Aggrecan is a large proteoglycan consisting of a protein core backbone consisting of three globular domains, G1, G2 and G3. The G1 domain is responsible for the linkage to hyaluronic acid, thus making large aggregates containing up to 100 aggrecan monomers. Between domains G2 and G3, glycosaminoglycan (GAG) side chains (chondroitin sulphate and keratan sulphate) are attached to the protein core. In normal cartilage, there is a steady state between synthesis and degradation of aggrecan, but in OA accelerated proteolytic cleavage is observed (137-140). Fragments of aggrecan have been identified in the synovial fluid of patients with various forms of arthritis, including OA (141,142). When aggrecan is cleaved, the carboxy-terminal tail of the protein containing the GAGs diffuses out of the cartilage and water is no longer retained. The structural integrity of the cartilage matrix is thus affected (143).

A major cleavage site for specific enzymes including aggrecanases that are able to cleave aggrecan is located in the region between G1 and G2, termed the interglobular domain, between amino acids 373 and 374. To date, three of such aggrecanases, termed 'A Disintegrin And Metalloproteinase with ThromboSpondin-like motifs' or ADAMTS were found to be able to cleave aggrecan: ADAMTS1 (144,145), ADAMTS4 (146) and ADAMTS5 (147) (a useful overview of the currently available data on the latter can be found in 148). ADAMTS4 and –5 possess the greatest cleavage efficiency and inhibition of their activity is known to prevent aggrecan degradation in osteoarthritic cartilage (149,150). ADAMTS4 was initially thought to be more detrimental to cartilage health since its rate of aggrecan cleavage was approximately two-fold higher than ADAMTS5 (151). However since in articular cartilage of mice its aggrecanase activity was not detected, ADAMTS5 is now thought to be the main aggrecanase responsible for aggrecan degradation in

articular cartilage (152). Previously, deletion of ADAMTS5 in mice prevented cartilage degradation after induction of OA (63). Compared to WT mice, ADAMTS5 deficient, but not ADAMTS1 or –4 (153) deficient mice were protected from cartilage damage and aggrecan loss after OA induction through surgical instability of the medial meniscus.Since ADAMTS5 deficient mice are protected from cartilage damage, and since it is well known that changes in subchondral bone occur in OA, we questioned whether the differences found in cartilage damage between WT and ADAMTS5 deficient mice are also reflected in the subchondral bone structure of these mice.

Previously, we demonstrated that subtle changes in subchondral bone structure can be quantified using micro-computed tomography (micro-CT) analysis (154). Therefore, the aim of this study was to compare the changes in subchondral bone structure following destabilizing the medial meniscus in WT and ADAMTS5 deficient mice using micro-CT.

METHODS

Generation of ADAMTS5 knockout mice

ADAMTS5 deficient (ADAMTS5-/-) mice used in these studies were generated as described earlier (63) from inbred 129SvEv-Brd mice carrying a cre/loxP-type conditional KO (CKO) allele of the ADAMTS5 gene (Lexicon Genetics, The Woodlands, TX). The conditional allele contained loxP sites flanking exon 3 so that cre recombination resulted in deletion of 56 amino acids encoded by exon 3, including the majority of the enzyme active site. The ADAMTS5-/- mouse line was produced by crossing CKO mice with protamine-cre (prot-cre)-transgenic mice (Lexicon Genetics), which resulted in cre-mediated deletion of exon 3 in the sperm of male offspring carrying both the mutant ADAMTS5 and prot-cre alleles. The deletion was confirmed by polymerase chain reaction (PCR) from tail DNA (63).

Surgical induction of OA by destabilization of the medial meniscus (DMM)

All studies were performed with approval of the Wyeth Institutional Animal Care and Use Committee. Knee joint instability was induced surgically in age-matched male 129S6/SvEv mice. At 10 weeks of age, 10 ADAMTS5-/- and 10 WT mice were anesthetized with 250 mg/kg intraperitoneal tribromoethanol (Sigma Aldrich, Milwaukee, WI) and instability of the right knee joint was induced by transection of the anterior attachment of the medial meniscus to the tibial plateau (53). Left knee joints were left intact and are termed 'left unoperated control joints'. All mice were weight bearing following recovery from anaesthesia. Buprenorphine (Buprenex, Reckitt&Colman, Kingston-upon-Hill, UK) was administered pre- and postoperatively. A subset of age-matched 5 ADAMTS5-/- and

5 WT animals was not operated and was considered naïve. Body weight of all mice was measured three times during the experiment: at 8 weeks, 10 weeks (the time point of DMM) and 18 weeks of age. All animals were sacrificed at 8 weeks post surgery (18 weeks of age). In total, 30 mice were used. All research was done in accordance with all applicable federal guidelines and institutional policies.

Histological analyses

Coronal (frontal) histological sections were taken through the joint at 70 μm intervals, stained with Safranin-O and cartilage damage was scored by two blinded observers using a modification of a published mouse scoring system by Chambers *et al.* (155). A score of 0 represents normal cartilage; 0.5 = loss of Safranin-O without structural changes; 1 = roughened articular surface and small fibrillations; 2 = fibrillation down to the layer immediately below the superficial layer and some loss of surface lamina; and 3 = mild (<20%), 5 = moderate (20%–80%) and 6 = severe (>80%) loss of articular cartilage (153). Scores of 4 (erosion to bone) were not a feature of this model. Histological scores were assigned to four quadrants (medial tibial plateau, medial femoral condyle, lateral tibial plateau, and lateral femoral condyle) of the left and right knee joints at all sectioned levels to obtain a summed OA score for the whole knee joint, or for the medial and lateral tibial plateau separately.

Since micro-CT analysis (see next paragraph) cannot distinguish calcified cartilage from bone, the thickness of the calcified cartilage was measured separately by histological analyses. Microphotographs were taken of toluidine-blue stained medial and lateral tibial plateaus and the thickness of the calcified cartilage was measured using Bioquant Osteo v7.20 (Bioquant, Nashville, TN). This programme measures the thickness of an indicated area (i.e., the calcified cartilage) every 5 μm over a distance of 400 μm, producing roughly 80 measurements, which were averaged afterwards. Osteoclasts were visualized using histochemical staining for tartrate-resistant acid phosphatase (TRAP) activity as described previously (156), using Gill's haematoxylin as counter stain. Osteoclast quantification included osteoclast surface/bone surface (Oc.S./BS, in %) and osteoclast number/bone surface (Oc.N./BS), again using Bioquant Osteo v7.2.

Micro-computed tomographic scanning and quantification of bone morphometric parameters

Prior to sectioning, knee joints were scanned using the Skyscan 1072 micro-CT scanner (Skyscan, Kontich, Belgium) with a voxel size of 10 μm. In order to distinguish calcified tissue from non-calcified tissue, the reconstructed greyscale images were segmented by an automated algorithm using local thresholds (88). In order to study subchondral bone the epiphysis of the tibia was chosen as the region of interest. The outline of the epiphysis was manually selected using 3D data analysis software (CTAnalyser, Skyscan)

and care was taken not to select outgrowing mineralized osteophytes. The volume of the medial tibial osteophytes was determined separately using the same procedure.

The subchondral bone plate and trabeculae of the epiphysis were separated using in-house developed software. For each cross-section in the 3D dataset, a virtual mask of the total bone was created, which was used to identify the bone marrow regions in the original image. These marrow regions were then expanded into a mask of the total marrow cavity. Bone inside the total marrow cavity is considered trabecular bone, the remainder is cortex. The programme is available upon request, including help on how to use it. Bone morphometric parameters of the thus obtained bone structures were determined using the freely available software package 3D-Calculator (*http://www.erasmusmc.nl/47460/386156/Downloads*). The following 3D-morphometric parameters were calculated for the trabecular compartments: trabecular bone volume fraction (Trab BV/TV), which is the ratio of trabecular bone volume (Trab BV) over endocortical total volume (TV, i.e., Trab BV plus marrow cavity volume), trabecular thickness (Tb.Th., in μm), trabecular spacing (Tb.Sp., in μm), connectivity density (CD), which calculates the number of trabecular connections per unit volume (90) and structure model index (SMI), indicating whether trabeculae have a rod-like (value near 3) or plate-like (value near 0) shape (89).

The thickness of the medial and lateral side of the subchondral bone plate (in μm) was measured using the same algorithm as used for determining Tb.Th. A subset (0.5 mm mediolateral width, 1.0 mm ventrodorsal length) of the weight-bearing region at the medial and lateral side of the tibial plateau was taken as the region of interest.

The same location was used to measure the bone volume fraction of the underlying subchondral trabecular bone (Sb BV/TV). Figure 1 shows a schematic overview of the analyzed bone structures.

Data-analysis

Statistical analyses utilized a nonparametric Mann–Whitney U test (GraphPad Prism, San Diego, CA). Differences between medial and lateral parameters within the same joint or within the same animal were analyzed with the Wilcoxon matched paired test.

Pearson's coefficient of regression was used to calculate correlations between cartilage damage and subchondral bone plate thickness. In all cases, $P<0.05$ was considered statistically significant. In all graphs, the error bars depict standard error of the mean (S.E.M.).

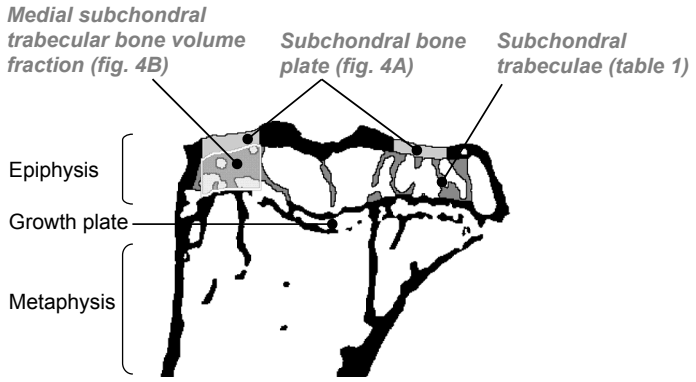

Figure 1. Selection procedure of tibial epiphysis for 3D-morphometric analysis. The epiphysis was manually selected as representative of subchondral bone, and outgrowing osteophytes were excluded. Epiphyseal trabeculae were separated from the subchondral bone plate and trabecular bone morphometric parameters were calculated (see Table I). A subset of the medial and lateral subchondral bone plate and underlying epiphyseal trabecular bone were analyzed separately, as indicated for the medial side.

RESULTS

The gross appearance of ADAMTS5-/- mice was not different from the WT mice, as reported previously (63). However, during the study the average bodyweight of the ADAMTS5-/- mice was less compared to the WT mice (at 18 weeks of age, WT: 27.6 ± 0.7 g; ADAMTS5-/-: 24.3 ± 1.0 g, P=0.01). In one ADAMTS5-/- mouse, osteomyelitis was diagnosed histologically in the right (DMM) knee joint. Another ADAMTS5-/- mouse had bone morphometric values and cartilage damage values more than three standard deviations below the group average. These mice were left out of all analyses.

Changes in cartilage in WT and ADAMTS5-/- mice

The summed OA score of the whole knee joint showed a significant increase in OA in right DMM knee joints compared to the left unoperated control knee joints in both genotypes (Fig. 2A). However, the amount of cartilage damage in ADAMTS5-/- mice was significantly lower compared to WT mice (WT: 19.3 ± 2.7, ADAMTS5-/-: 10.7 ± 1.5, P=0.02), in accordance with previously reported results (63).

When the OA scores of the medial and lateral tibial plateau were considered separately, WT mice showed a significant increase in cartilage damage at both the medial and lateral side, although the lateral increase was significantly lower (Fig. 2B). The same pattern was found in ADAMTS5-/- mice, but again lower damage scores compared to WT were observed, significantly at the lateral side. Similar to DMM joints of WT mice, in ADAMTS5-/- mice the damage at the lateral tibial plateau was significantly lower compared to the medial side.

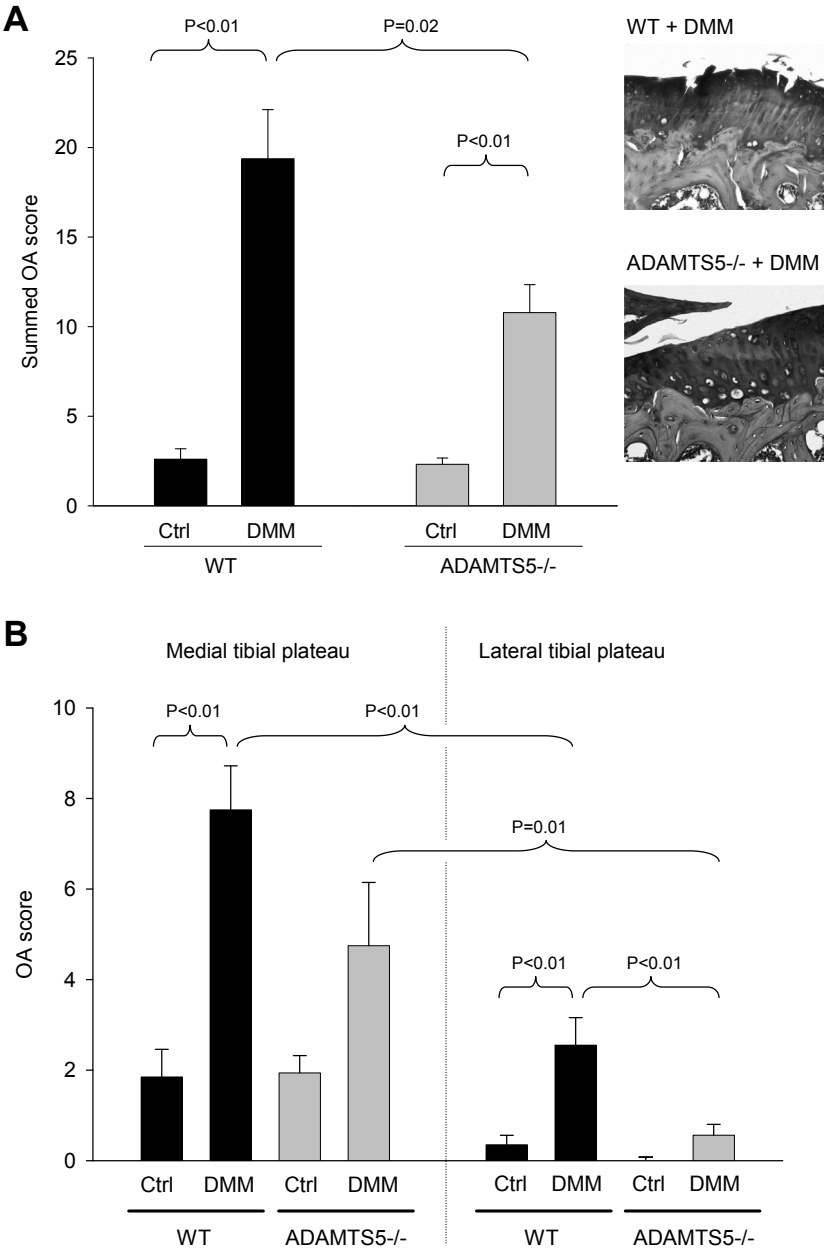

Figure 2. A, OA scores summed over the four analyzed quadrants (medial tibial plateau, medial femoral condyle, lateral tibial plateau, and lateral femoral condyle) from left unoperated control (Ctrl) knee joints and right knee joints that underwent dissection of the medial meniscus (DMM) of WT and ADAMTS5-/- animals at 18 weeks of age. Microphotographs on the right show examples of the amount of cartilage damage found in DMM joints of WT and ADAMTS5-/- mice (original magnification 200x). B, OA scores of the medial and lateral tibial plateau separately. Shown are averages ± S.E.M., $P < 0.05$ was considered significant.

Changes in bone in WT and ADAMTS5-/- mice

After DMM, mineralized osteophytes were observed at the medial side in all tibiae of both genotypes, but not at the lateral side (Fig. 3A). The average volume of these medial osteophytes was larger in WT mice, although the difference was not statistically significant (WT: 0.053 ± 0.004 mm^3, ADAMTS5-/-: 0.042 ± 0.004 mm^3, P=0.09). None of the unoperated Ctrl joints had osteophytes.

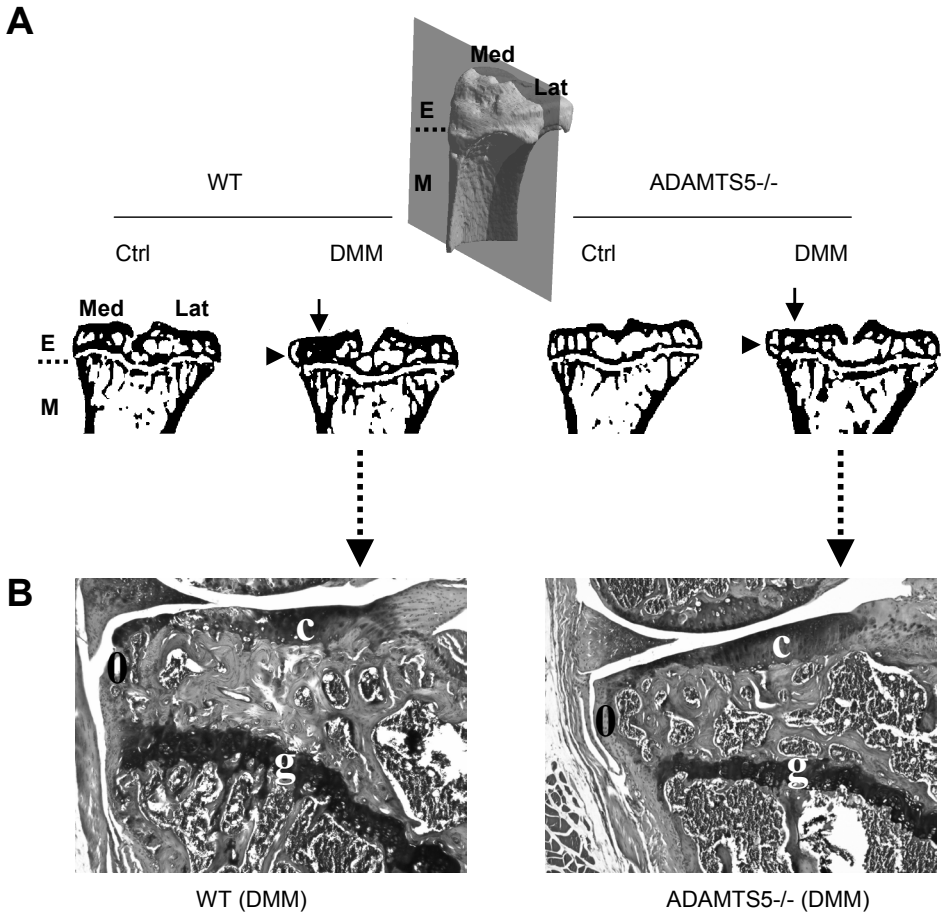

Figure 3. A, representative cross-sections of tibiae from WT and ADAMTS5-/- mice, both left unoperated control (Ctrl) and right DMM. The inset shows a 3D reconstruction of a proximal tibia with a plane indicating the location from which the cross-sections were taken. Epiphysis (E), metaphysis (M) and growth plate (dotted line) are indicated, as well as the medial (Med) and lateral (Lat) tibial plateau. Subchondral sclerosis was found in the medial region of the epiphysis (arrows), and medial osteophytes were observed as well (arrowheads). B, histological images of the medial tibia from DMM WT and ADAMTS5-/- mice, stained with toluidine-blue. Please note the pronounced sclerosis of the subchondral bone plate in the WT mice, whereas ADAMTS5-/- mice only showed mild sclerosis. Magnification 100x. C= cartilage, O= osteophyte, G= growth plate.

Pronounced sclerosis of the subchondral bone plate was found at the medial tibia in WT mice, on both micro-CT scans and histological images (Fig. 3A, 3B) whereas in ADAMTS5-/- mice sclerosis seemed to be less. These apparent differences were quantified further using micro-CT analysis. The bone morphometric data proved that in WT mice the thickness of the subchondral plate was increased at the medial side compared to the unoperated left knee joint (Fig. 4A). In ADAMTS5-/- mice this increase was observed as well, albeit significantly less compared to the increase seen in WT mice. Of note, the absolute subchondral bone plate thickness in the left unoperated control joints was already significantly higher in WT mice compared to ADAMTS5-/- mice, both at the medial and lateral side. This difference was observed in the group of naïve animals as well (data not shown). Therefore, we calculated the relative increase in plate thickness, expressed as a percentage. The percentage increase was also found to be significantly higher in WT mice (Fig. 4A, WT: 20.7 ± 4.7%, ADAMTS5-/-: 8.3 ± 1.2%, P=0.01). Neither WT nor ADAMTS5-/- mice showed an increase in plate thickness at the lateral side of the tibial plateau.

Contrary to these apparent changes, the DMM procedure did not affect the subchondral trabecular bone structure in either strain: the total Trab BV/TV of the epiphysis was not changed compared to left unoperated control joints, as well as Tb.Th., Tb.Sp., CD and SMI (table 1). However, ADAMTS5-/- mice had significantly lower Trab BV/TV and Tb.Th. compared to the WT animals.

Table 1. Trabecular bone parameters from male WT and ADAMTS5-/- mice. All parameters were derived from trabecular bone of the entire epiphysis of left unoperated control and right DMM tibiae, 10 weeks after the operation. Numbers shown are averages ± S.E.M. Trab BV/TV= trabecular bone volume fraction, Tb.Th. = trabecular thickness, Tb.Sp. = trabecular spacing, CD= connectivity density, SMI= structure model index. *P<0.05, **P<0.01 between genotypes and corresponding joints.

	WT		*ADAMTS5-/-*	
Parameter	*Ctrl*	*DMM*	*Ctrl*	*DMM*
Trab BV/TV (%)	36.3 ± 0.4	36.2 ± 0.4	33.8 ± 0.5**	33.3 ± 0.5**
Tb.Th. (μm)	75.0 ± 0.6	74.9 ± 0.7	69.2 ± 0.3**	69.2 ± 0.5**
Tb.Sp. (μm)	181.0 ± 2.7	180.1 ± 2.7	170.2 ± 2.6*	175.2 ± 4.1
CD	183.9 ± 6.8	182.6 ± 8.9	200.6 ± 11.2	187.8 ± 6.9
SMI	3.00 ± 0.02	3.00 ± 0.07	3.06 ± 0.03	3.09 ± 0.04

To examine whether Trab BV/TV might be changed locally, we measured the subchondral trabecular bone volume fraction (Sb BV/TV) directly underneath the medial and lateral regions of the subchondral bone plate in the weight-bearing region of the tibial plateau (Fig. 1, 4B). In WT mice no differences were found between the DMM joints and the left unoperated control joints, but in DMM joints of ADAMTS5-/- mice a significant decrease was measured at the medial, but not lateral side compared to unoperated

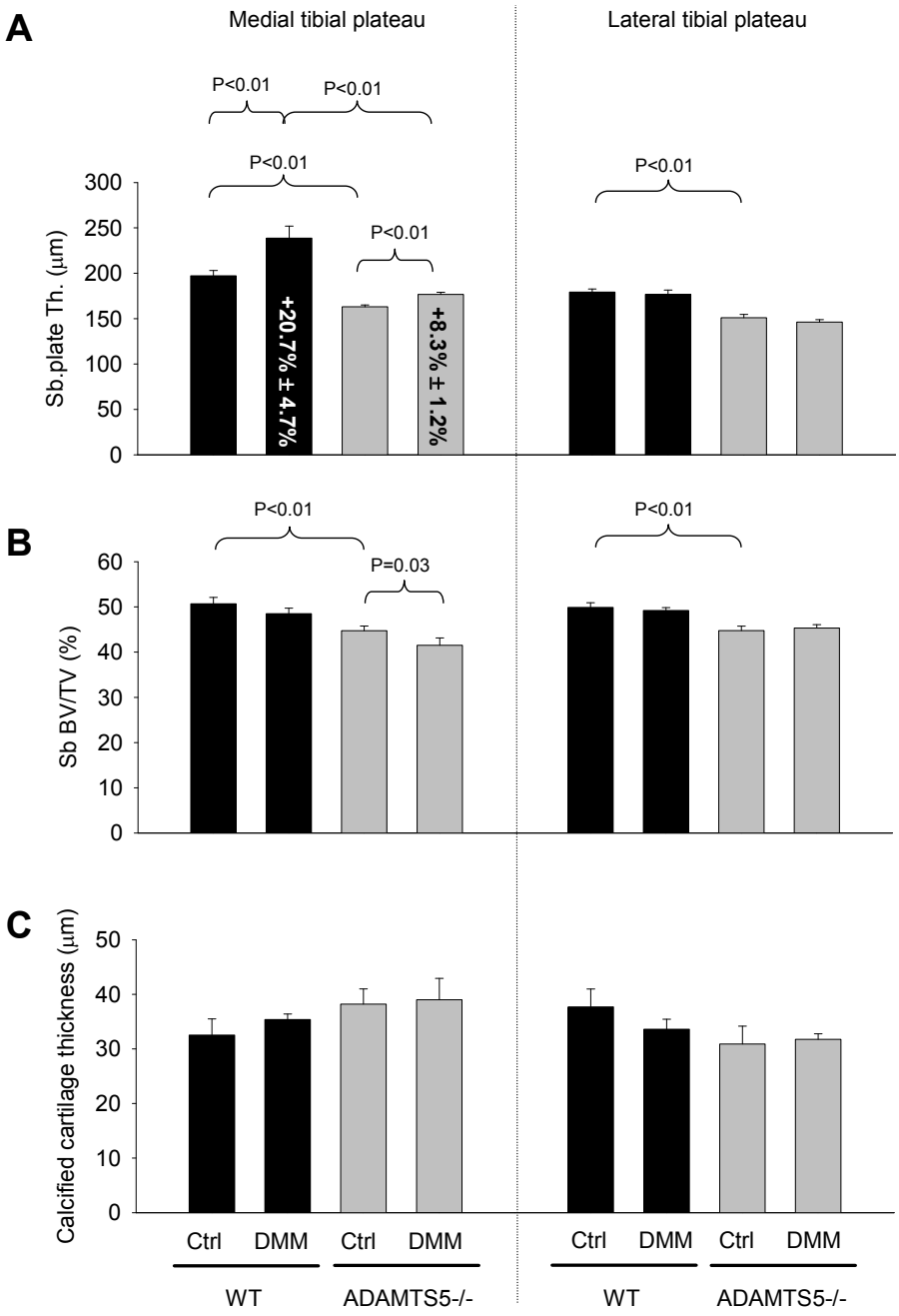

Figure 4. A, subchondral bone plate thickness (Sb. plate Th.) measured with micro-CT in left unoperated control (Ctrl) and right DMM knee joints, in WT and ADAMTS5-/- mice. The percentage increases in plate thickness in DMM joints as compared to the control joints are indicated inside the DMM bars. B, subchondral bone volume fraction (Sb BV/TV). C, calcified cartilage thickness, measured from histological images. Shown are averages ± S.E.M., $P < 0.05$ was considered significant.

joints. In addition, a significantly lower Sb BV/TV was noted in left unoperated control joints of ADAMTS5-/- mice compared to WT animals, as seen before for the whole Trab BV/TV of the epiphysis.

To specifically look further into the medial differences between genotypes, we quantified the presence of osteoclasts at the medial tibia in both WT and ADAMTS5-/- mice (Fig. 5). In WT animals, DMM did not have an effect on the amount or size of osteoclasts present in the medial tibia (Oc.N./BS: Ctrl 0.70 ± 0.24, DMM 0.71 ± 0.18, Oc.S./BS: Ctrl 4.30 ± 1.79, DMM 4.80 ± 1.05). Surprisingly, in ADAMTS5-/- mice we found a significant decrease in both Oc.N./BS as Oc.S./BS, indicating less osteoclasts (Oc.N./BS: Ctrl 0.70 ± 0.22, DMM 0.17 ± 0.10 $P<0.05$, Oc.S./BS: Ctrl 4.29 ± 1.43, DMM 0.96 ± 0.52 $P<0.05$).

Finally, no significant differences were found between thicknesses of calcified cartilage of left unoperated control and DMM joints in either strain, neither at the medial nor at the lateral side (Fig. 4C).

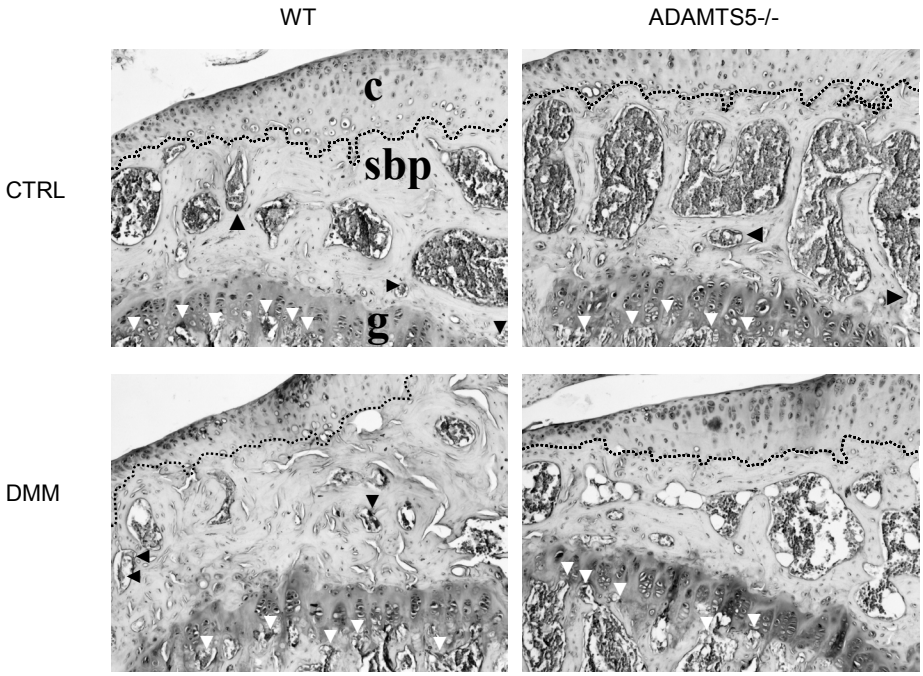

Figure 5. Examples of TRAP-stained osteoclasts in the medial tibia of WT and ADAMTS5-/- mice, both left unoperated control (Ctrl) and right DMM. Osteoclasts in the subchondral bone (black arrowheads) were observed in Ctrl and DMM joints of both genotypes, in addition to osteoclasts beneath the growth plate (white arrowheads). Please note that in DMM joints of ADAMTS5-/- mice, very few if any osteoclasts were observed despite the presence of osteoclasts beneath the growth plate. Also note the thinner subchondral bone plate in the ADAMTS5-/- joints and the subchondral sclerosis after DMM in the WT joint. Magnification 100x. C= cartilage, SBP= subchondral bone plate, G= growth plate.

Correlations between cartilage damage and subchondral bone plate thickness

When medial subchondral bone plate thicknesses were related to the amount of cartilage damage found at the medial tibial plateau a significant correlation was found in WT but not in ADAMTS5-/- mice (r^2=0.26, P=0.01). This correlation became more clear when the summed OA score was considered (r^2=0.42, P<0.01). Correlations between lateral subchondral bone plate thicknesses and lateral cartilage damage did not reach significance in either strain.

DISCUSSION

This study revealed that ADAMTS5-/- mice, next to being protected from cartilage damage, also show less changes in subchondral bone structure after induction of joint instability. Following instability, both WT and ADAMTS5-/- mice had an increase in subchondral plate thickness, although the increase was significantly less in ADAMTS5-/- mice. These findings were entirely attributed to the subchondral bone plate, since other calcified structures such as the calcified cartilage or the subchondral trabeculae were not changed. Furthermore, only at the site where the amount of cartilage damage was highest did the subchondral bone plate thickness change, since analysis of the bone plate thickness at the lateral side of the epiphysis showed no differences between left unoperated control and right DMM knee joints. Finally, since bone and cartilage changes were found to be specifically correlated at the medial side only, this provides a clear indication that changes in bone and cartilage are linked in this animal model.

Although it became clear from our results that changes in cartilage and bone took place in a synchronized fashion, the cross-sectional design of the study makes it difficult to conclude whether the changes in bone were a consequence or cause of the cartilage damage. Several explanations for the observed correlation might therefore be possible. First, via mechanical interactions, where cartilage damage leads to softening of the cartilage, thereby changing the loading of the underlying bone and bone metabolism. Second, via metabolic interactions in which chondrocytes in the articular cartilage might be able to influence bone turnover in the subchondral bone plate or *vice versa*. Several studies have shown direct means of contact between normal articular cartilage and normal bone (24,66,129,157) and chondrocytes and osteoblasts are able to influence each other's metabolism (130,131). In a pathological situation such as OA, the cross-talk between bone cells and chondrocytes might be disturbed leading to the observed effects. Possible cross-talk candidate molecules in this respect are prostaglandin E2 (158-160), IL-6 (135,161-163), and oncostatin M (164,165). In this respect, it is interesting that calcitonin, well known for its inhibitory effects on osteoclasts and therefore bone turnover (166), has been shown to be chondroprotective (167,168), although

there is still debate whether this protective effect is mediated directly on chondrocytes (169,170) or indirectly via the bone (171,172). In case calcitonin acts solely by inhibiting osteoclasts, this might also include osteoclasts at other locations in the knee joint, such as the synovium. Macrophages in OA synovial fluid and synovial fibroblasts have been shown to differentiate into osteoclasts as well (173-175). This way, calcitonin may directly inhibit the osteoclasts' collagen type II degradative abilities which play a role in the process of endochondral ossification (176).

In our mice, the absence of ADAMTS5 leads to impairment of aggrecan degradation and cartilage damage in a stressful environment, such as induced by DMM. Chondrocyte homeostasis might therefore be maintained for a longer period, and subchondral bone biology is not affected as much as seen in the WT mice. This argument is substantiated by the fact that the ADAMTS5-/- had significantly less OA through 6 months post-DMM (unpublished observations). The fact that the ADAMTS5-/- mice still had a detectable amount of cartilage damage is probably due to the possibility that ADAMTS5 is not solely responsible for joint destruction (177).

Finally, although the background of both mouse genotypes is the same and no obvious phenotypical differences were noted, we did observe subtle differences in the phenotype of the bones. Generally, ADAMTS5-/- mice had a thinner subchondral bone plate and less trabecular bone with thinner trabeculae. This could not be attributed to differences in osteoclast activity since the Ctrl (unoperated) values of Oc.N./BS and Oc.S./BS were virtually equal. Since ADAMTS5 is also expressed in bone (178,179) it may therefore play an important role in bone biology as well, possibly in the process of endochondral ossification, which may perhaps evolve less efficient, ending up with less bone. As such, these differences in bone architecture might affect joint mechanics and subsequently influence the stresses present in cartilage after DMM.

The relation between changes in subchondral bone plate thickness and cartilage damage was found for WT animals only. The reason for this was that in ADAMTS5-/- mice the data was too scattered to obtain a significant correlation, and although some of the mice having a relatively high cartilage damage score (but still lower compared to most WT animals) did seem to have a thicker subchondral bone plate this relation was not significant. Most probably, the changes in cartilage in ADAMTS5-/- mice were too small to have an effect on bone or vice versa. Furthermore, although the observed correlation is significant in WT animals, it is still quite low. Possibly, other factors besides cartilage damage may also contribute to the observed relation.

Currently, we do not have a suitable explanation as to why so few osteoclasts were found in DMM joints of the ADAMTS5-/- animals only. Although the results fit with the increase in subchondral bone plate thickness they do not fit with the observed medial decrease in Sb BV/TV in ADAMTS5-/- mice. We could exclude errors in the staining procedure since osteoclasts underneath in the growth plate were clearly visible (i.e., stained

bright red) in all of the sections analyzed. Possibly, at the time point of measurement (i.e., 8 weeks after DMM) bone turnover in the ADAMTS5-/- joints had already ceased and as a response to repair osteoclasts had already migrated to other areas. Another explanation might be that in DMM joints of ADAMTS5-/- mice the rate of osteoblastic activity might have been very low in trabeculae, unable to compensate for the osteoclastic activity present right after DMM. A clear limitation of this study was that due to our choice to perform histology on paraffin embedded (and therefore decalcified) knee joints we were also not able to perform Goldner trichome staining to visualize osteoid, or analyze any dynamic osteoblast activity using fluorescent markers.

In the current study, the weight of the ADAMTS5-/- mice was significantly lower than the WT. This difference in weight was not typical since all other studies have primarily shown no difference in weight, or occasionally, an increase in weight (unpublished results) and highlight the spurious results that can be observed in weight changes when knockout mice are utilized with group sizes of 10. However, to solely attribute the lower bone volume fraction to a lower body weight is highly unlikely since the lightest WT mouse still had more trabecular bone compared to the heaviest ADAMTS5-/- mouse (WT: 23,8 g, BV/TV 35.6%, ADAMTS5-/-: 28.8 g, BV/TV 31.1%).

Compared to other models of OA, our results are in line with spontaneous models such as the STR/ort and STR1N mice (87,180) and Dunkin-Hartley guinea pigs (86,105), which develop OA spontaneously, and in which subchondral sclerosis was observed as well. We previously published data in which an initial decrease in subchondral bone plate thickness was noted in mice (181) and dogs (182) after induction of OA. Other studies confirm these findings and in addition, report the amount of subchondral bone to increase later on (30,84,94,126). This biphasic pattern in bone turnover might reflect the disease status, where early stages are marked by bone loss, followed by an anabolic response resulting in bone sclerosis in more advanced stages of disease. In the present study we found sclerosis of the subchondral bone as well as fully mineralized osteophytes, arguing for a more advanced disease stage and indicating that OA, surgically induced by DMM, develops rather quickly.

In conclusion, in mice in which joint instability was surgically induced, we found an increase in subchondral bone plate thickness. However, in ADAMTS5-/- mice this increase was significantly lower, in accordance with a lower amount of cartilage damage. These findings again stress the importance of ADAMTS5 in OA biology and link the process of cartilage damage with changes in subchondral bone dynamics.

CONFLICT OF INTEREST

The authors declare that they have no conflict of interest.

ACKNOWLEDGMENTS

Thanks to Moisés Rivera-Bermúdez, Tracey Blanchet, Jennifer Tavares, Diane Peluso and Erwin Waarsing for technical expertise.

Chapter 5

Analysis of osteoarthritis in a mouse model of the progeroid human DNA repair syndrome trichothiodystrophy.

S.M. Botter, M. Zar, G.J.V.M van Osch, H. van Steeg, M.E.T. Dollé, J.H.J. Hoeijmakers, H. Weinans, J.P.T.M. van Leeuwen

Age (Dordr). 2010 Sep 7. [Epub ahead of print]

ABSTRACT

The increasing average age in developed societies is paralleled by an increase in the prevalence of many age-related diseases such as osteoarthritis (OA), which is characterized by deformation of the joint due to cartilage damage and increased turnover of subchondral bone. Consequently, deficiency in DNA repair, often associated with premature aging, may lead to increased pathology of these two tissues. To examine this possibility, we analyzed the bone and cartilage phenotype of male and female knee joints derived from 52- to 104-week-old WT C57Bl/6 and trichothiodystrophy (TTD) mice, which carry a defect in the nucleotide excision repair pathway and display many features of premature aging. Using micro-CT, we found bone loss in all groups of 104-week-old compared to 52-week-old mice. Cartilage damage was mild to moderate in all mice. Surprisingly, female TTD mice had less cartilage damage, proteoglycan depletion, and osteophytosis compared to WT controls. OA severity in males did not significantly differ between genotypes, although TTD males had less osteophytosis.

These results indicate that in premature aging TTD mice age-related changes in cartilage were not more severe compared to WT mice, in striking contrast with bone and many other tissues. This segmental aging character may be explained by a difference in vasculature and thereby oxygen load in cartilage and bone. Alternatively, a difference in impact of an anti-aging response, previously found to be triggered by accumulation of DNA damage, might help explain why female mice were protected from cartilage damage. These findings underline the exceptional segmental nature of progeroid conditions and provide an explanation for pro- and anti-aging features occurring in the same individual.

INTRODUCTION

During life our DNA is continuously damaged both from external (e.g., UV radiation and numerous chemicals) as well as internal (e.g., reactive oxygen species (ROS)) sources, resulting in numerous types of DNA lesions (e.g., strand interruptions). If left unrepaired, some of these lesions can cause mutations upon replication and consequently trigger carcinogenesis. Others can block transcription, thereby influencing cellular functionality and survival, which may affect lifespan of the organism as a whole (183,184).

To counteract this continuous genetic erosion, an intricate network of DNA repair systems has evolved that resolves both helix-distorting and non-helix-distorting types of DNA damage. A molecular pathway involved in counteracting helix-distorting types of DNA damage is the nucleotide excision repair (NER) pathway. NER consists of a complex multi-step 'cut and patch' reaction involving ~ 30 or more proteins that act genome wide, designated global genome NER, or specifically in actively transcribed genes, named transcription-coupled NER (TC-NER; (185)). TC-NER presumably is part of a broader transcription-coupled repair system that also eliminates non-helix-distorting type of transcription-blocking lesions. Since DNA lesions are thought to affect lifespan, a defective TC(-NE)R contributes to the process of aging (186,187). Indeed, human patients with an inborn defect in TC(-NE)R suffer from a so-called 'premature aging syndrome' and show numerous symptoms that normally develop much later in life, including sarcopenia, cachexia, progressive neurodegeneration, deafness, early infertility, and osteoporosis. Many patients die at early age.

An example of such a premature aging syndrome is trichothiodystrophy (TTD). Most patients suffering from this rare, autosomal recessive disease have a mutation in the helicase xeroderma pigmentosum D (XPD). This protein is a subunit of the transcription/repair complex TFIIH, which has a multi-functional role in both normal transcription and in NER. Previously, we mimicked the TTD phenotype by generating a knock in mouse carrying an XPD point mutation, found in several TTD patients (188). The resulting mice showed striking phenotypical similarities with human TTD patients, including characteristic brittle hair; scaly skin; early onset of osteoporosis, kyphosis, and cachexia; and a shortened lifespan (189-191). As such, they might present an ideal tool to study the process of aging and age-related diseases.

In the experiment described herein, TTD mice were used to study a common age-related disease: osteoarthritis (OA). In OA, the function of a joint (i.e., to provide frictionless movement) becomes radically disturbed due to drastic deformation of the joint components, which leads to severe mobility problems, pain, and reduction in quality of life. Currently, no curative treatment is available other than analgesia and eventually an operation, in which (part of) the joint is replaced by a prosthesis. Several joints can be affected but knee OA is a leading cause of OA-related impairments, affecting more than 4.3 million individuals in the general US population (192).

The knee joint is composed of several components, to ensure friction-less yet stable movement under loading conditions, and each of these components changes structure and/or becomes damaged in the OA disease process. The most well known is damage to the smooth joint surface that is provided by articular cartilage, but increased turnover of the subchondral bone, located directly underneath the articular cartilage, is of equal importance (9,31). An additional characteristic of OA is the development of bony outgrowths at the rims of the joint, named osteophytes.

Since TTD mice display many characteristics of age-related diseases which are found in the general human population, among which OA, we analyzed subchondral bone changes and cartilage damage in the knee joint of 52- and 104-week-old wild-type (WT) and DNA repair deficient, premature aging TTD mice.

MATERIALS AND METHODS

Generation of TTD knockout mice and selection of study samples

The generation of the mice used in this study has been described before (191,193,194). Briefly, gene-targeted mouse 129Ola ES cells, in which the *xpd* gene was mutated using a point mutation (R722W) found in a human TTD patient, were injected into C57Bl/6J blastocysts. Chimeric male mice were mated with C57Bl/6J females, and heterozygous offspring was bred into an isogenic C57Bl/6J genetic background for over 10 generations. In the second round of breeding, double heterozygous mice were intercrossed to obtain XPD^{TTD} homozygous mice (from now on termed TTD mice), which were then used in the third breeding round to generate the experimental animals analyzed in this study. The mice were compared to C57Bl/6J wild-type mice (from now on termed WT mice). WT mice are known to develop clear signs of OA from about 16 months (~70 weeks) of age (50,195).

An aging cohort was designed containing WT and TTD, both males and females (191). All mice were kept in animal facilities of the RIVM (Bilthoven, The Netherlands) under specific pathogen-free conditions in groups of four or less per cage after weaning. The room temperature was 20°C and the light/dark cycle was 12h/12h. Standard lab chow (Hope Farms, The Netherlands) and water were supplied *ad libitum*. Female TTD animals had a significantly reduced lifespan, with a median survival age of 103 weeks for WT and 93 weeks for TTD females (191). Mice were sacrificed at scheduled ages, including 52-week-old and 104-week-old mice. The physical condition of all animals used in the current study was assessed by a pathologist at sacrifice and only those animals that had no abnormal characteristics (e.g., tumor growth, infection) were used in this study. All procedures were performed in accordance with applicable federal guidelines and institutional policies.

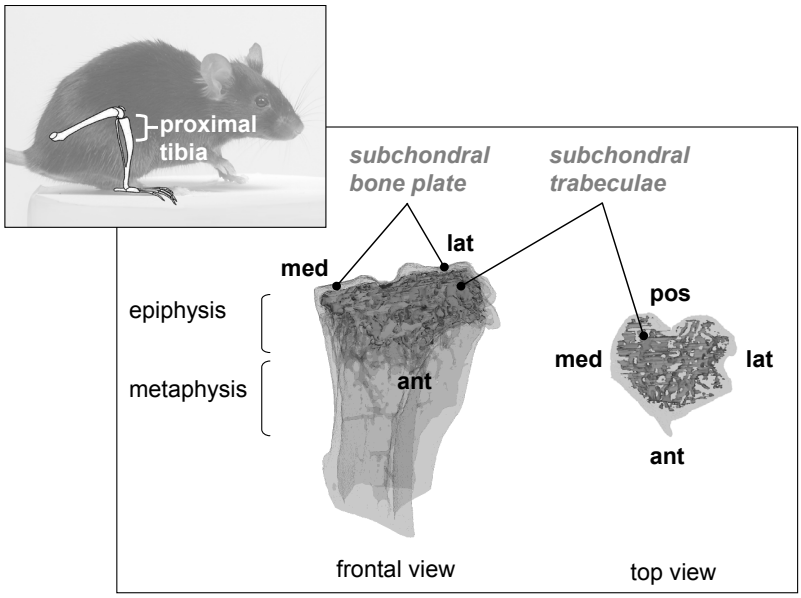

Figure 1 Analysis of bone phenotype of WT and TTD mice. Anatomical context with the analyzed region (proximal tibia) is indicated in the smaller panel. The larger panel shows a transparent 3D model of the proximal tibia. The subchondral (epiphyseal) trabecular bone structure is indicated in orange (left: frontal view, right: top view). The model was build from a transaxial stack of cross-sections of 10 μm thickness. Med= medial, lat= lateral, pos= posterior, ant= anterior.

Micro-computed tomographic scanning and quantification of bone morphometric parameters

Tibiae from male and female mice, both WT and TTD were selected for analysis, generating a total of eight groups of mice (*n*=6-7 per group). Methods used to scan and analyze the proximal portion of the tibiae (see Fig. 1) are described elsewhere (154). Briefly, tibiae were fixed in 4% formalin and scanned in the Skyscan 1072 micro-CT scanner (Skyscan, Kontich, Belgium) with a voxel size of 10 μm. To distinguish calcified tissue from non-calcified tissue and noise, the reconstructed greyscale images were segmented by an automated algorithm using local thresholds (88), resulting in a 3D dataset consisting of stacked black/white cross-sections. In order to study subchondral bone, the epiphysis of the tibia was chosen as the region of interest. The outline of the epiphysis was manually selected using 3D data analysis software (CTAnalyser, Skyscan) excluding any outgrowing mineralized osteophytes. Next, using in-house developed software (available upon request), the subchondral bone plate was separated from the subchondral trabeculae for each cross-section in the 3D dataset. For the epiphysis, the following 3D morphometric parameters were calculated using the freely available software package 3D-Calculator (*http://www.erasmusmc.nl/47460/386156/Downloads)*: Trabecular bone volume fraction (Trab BV/TV), which is the ratio of trabecular bone volume (Trab BV, in cubic millimeters) over endocortical tissue volume (TV, in cubic millimeters),

trabecular thickness (Tb.Th., in micrometers), trabecular spacing (in micrometers) and connectivity density (dimensionless), indicating the number of trabecular connections per unit volume (90). Subchondral bone plate thickness was measured in the weight-bearing region of the medial and lateral tibial plateau. At each location, a subset (0.5 mm mediolateral width, 1.0 mm ventrodorsal length) was taken as region of interest. We chose to present the thickness of the subchondral bone plate as an average of medial and lateral values, since changes in thickness were very similar for both anatomical locations, and for reasons of clarity. Thus, values presented here (Fig. 3c) represent average subchondral bone plate thickness (Sb.Pl.Th., in micrometers).

As a reference to other published work (especially with regard to the bone phenotype of WT mice), we also analyzed the amount of bone (i.e., Trab BV/TV) of the proximal metaphysis. For this, we selected a volume of interest located directly underneath the growth plate, of 1.0 mm height.

Histological analysis

Following decalcification in 10% EDTA for 14 days and embedding in paraffin, 6-μm thick coronal (frontal) histological sections were taken through the joint at 100 μm intervals. Sections were stained with Safranin O and Fast green and cartilage damage was scored using the semi-quantitative grading and staging system devised by the OARSI Working Group (18). In this semi-quantitative system, a *grade* score reflects severity of damage (0—no damage, 6—complete disorganization and deformation of the joint), and a *stage* score indicates extent of damage (0—cartilage surface intact, 4—>50% of cartilage surface affected). Grade and stage scores are then multiplied, resulting in a maximum obtainable cartilage damage score of 24 for each of the cartilage surfaces analyzed. Four locations were analyzed (medial tibial plateau, medial femoral condyle, lateral tibial plateau, and lateral femoral condyle) in three histological sections per joint. The cartilage damage scores thus obtained were averaged over the three sections and summed over the four locations, yielding a maximum obtainable summed cartilage damage score of 96.

Loss of proteoglycans (stained by Safranin O) was scored using a four-point scoring system from 0 to 3, where 0 represents no loss of proteoglycans and three indicates complete loss of staining for proteoglycans in more than half of the cartilage layer. Scores from the four anatomical locations were summed to reach a maximum obtainable score of 12.

As in mice osteophytes are most readily observed at the medial tibia (196), this location was taken to score osteophytosis according to the 4-point scoring system from Kamekura *et al.* (52), with 0—no osteophytes, 1—formation of cartilage-like tissues, 2—increase of cartilaginous matrix, and 3—endochondral ossification.

To measure cartilage thickness, microphotographs were taken of the medial tibial plateau and cartilage thickness was measured using Bioquant Osteo v7.20 (Bioquant, Nashville, TN). This program measures thickness of a selected area of interest (here the

cartilage layer) every 10 μm, producing roughly 80 measurements, which were then averaged. Thickness of the calcified cartilage (CC) was measured separately, after which thickness of the non-calcified cartilage (NCC) could be calculated.

Statistical analysis

Statistics were analyzed with GraphPad Prism v3.05 (San Diego, CA). When comparing group averages, non-parametric Mann-Whitney was applied. For correlations, non-parametric Spearman rank correlation was used. In all cases $p < 0.05$ was considered significantly different. In all graphs, data are presented as mean ± standard error of the mean (SEM).

RESULTS

Body weights

As noted before by Wijnhoven *et al.* (191), female and male WT mice reached a higher body weight than TTD mice, both at 52 and 104 weeks of age (Fig. 2a). No significant changes in weight between these time points were noted within the female and male genotypes. The weight differences were mainly due to the absence of adipose tissue, as became clear at autopsy during sacrifice. The reduction in fat also became clear from histological analysis of the bone marrow: in bone marrow of WT mice many fat vacuoles were present, in contrast to bone marrow of TTD mice, which contained almost no fat vacuoles (Fig. 2b). No differences were found in the length of either the tibia or the femur between WT and TTDs at either age (data not shown), indicating that the TTD animals were skeletally mature and excluding a developmental delay in growth of the animals.

Bone changes in knee joints of WT and TTD mice

In all groups of mice a significant amount of trabecular bone was lost at 104 weeks of age, as shown from the significant reductions in trabecular bone volume fraction (Trab BV/TV) in the epiphysis (Fig. 3a) and in the more distally located metaphysis (Fig. 3b). These findings are consistent with an aging-related bone decline in both WT and TTD mice (197-199). When comparing genotypes within each of the sexes we noticed that, especially in female mice, the amount of trabecular bone at 52 weeks of age was already lower in female TTDs compared to the age-matched WT mice, although this did not reach statistical significance (females, 52-week-old WT vs. TTD: p=0.06 for epiphyseal trabecular bone, p=0.07 for metaphyseal trabecular bone). It is important to note that at young age, the phenotype of TTD animals is not different from WT mice, but starts to deviate from about 13 weeks of age (191,199). The differences observed at 52 weeks are therefore in line with previous findings on accelerated bone loss in female TTD mice.

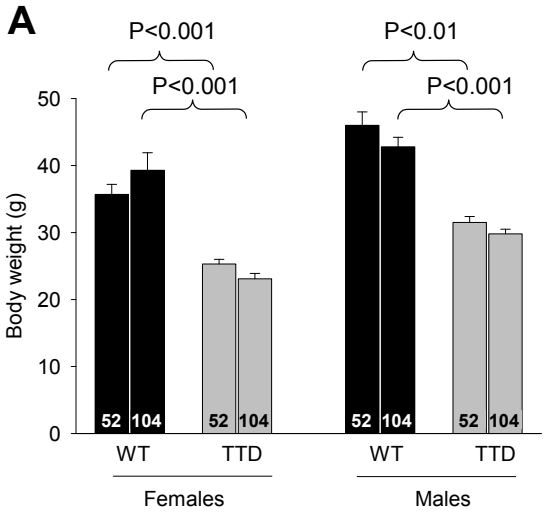

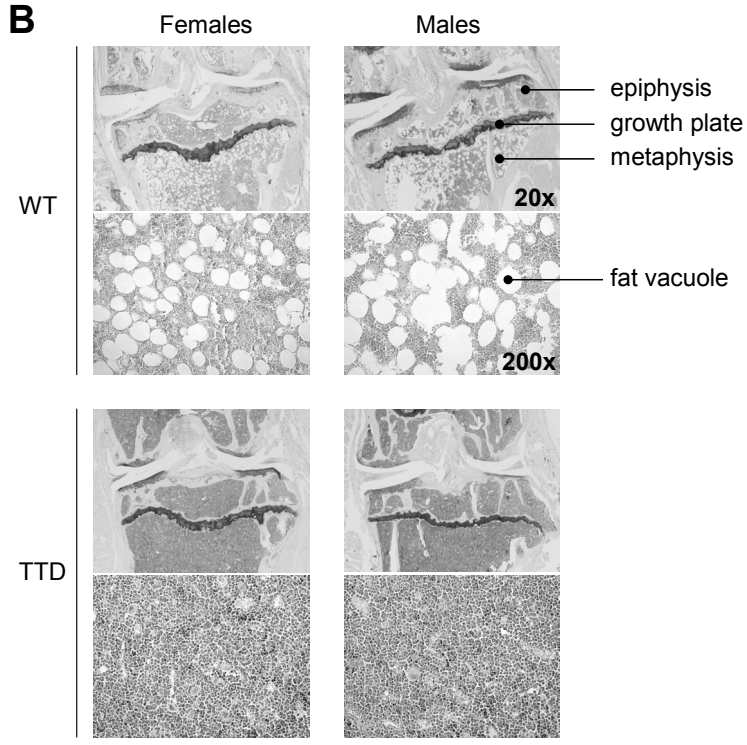

Figure 2. A, body weights of female and male WT and TTD, aged 52 and 104 weeks. B, gross histological overview of the proximal tibia of WT and TTD mice, aged 104 weeks. An enlargement (magnification x200) of the metaphyseal bone marrow is shown below each of the overview pictures (magnification x20). Please note the absence of fat vacuoles in the bone marrow of TTD mice. This difference was already visible at 52 weeks, albeit less clearly (images not shown).

Interestingly, at the age of 104 weeks TTD males displayed a further reduction to the same minimum as observed in TTD and WT females. This might indicate that the amount of trabecular bone reached a bottom value (around 15% in epiphysis, 3% in metaphysis) below which no further bone loss occurred. In WT males trabecular bone values were highest at 52 weeks and showed a significant reduction at the age of 104 weeks, but did not reach the low values observed in WT females and both TTD genders. Again, these findings are in agreement with accelerated bone loss in TTD mice.

Consistent with this interpretation, we found that the thickness of the subchondral bone plate (Sb.Pl.Th.) in both sexes of TTD mice decreased significantly between 52 and 104 weeks, whereas this decline was not observed in either female or male WT mice (Fig. 3c). This decrease was caused by thinning of bone tissue, since the thickness of the calcified portion of the cartilage layer (which is also detected by the X-rays used in micro-CT; SMB, personal observations) did not change in either gender or genotype (Fig. 3d). Also, no significant changes were found in the total thickness of the cartilage layer (Fig. 3d, NCC + CC).

Only small, but systematic reductions in average epiphyseal trabecular thickness (Tb. Th.) were measured in both sexes and in both genotypes (female WT: 52 weeks: 80.6 ± 1.7 μm; 104 weeks, 76.1 ± 1.3 μm; female TTD: 52 weeks, 78.6 ± 1.1 μm; 104 weeks, 75.0 ± 1.9 μm; male WT: 52 weeks, 77.9 ± 1.1 μm; 104 weeks, 75.1 ± 1.2 μm; male TTD: 52 weeks, 74.2 ± 1.5 μm; 104 weeks, 69.1 ± 0.5 μm) and this reduction was statistically significant for the 104-week-old TTD males ($p<0.01$ compared to 52-week-old TTD male, $p<0.01$ compared to 104-week-old WT male). The frequency distribution of the measured trabecular thicknesses (Fig. 4, upper panel) shows an approximate normal distribution. The area under the curve of each distribution is equal to the total amount of trabecular bone (Trab BV) inside the epiphysis. These areas are smaller in all groups of 104-week-old mice, indicating loss of trabecular bone. Thus, thinning of trabeculae does not fully explain the decreased amount of subchondral trabecular bone seen in all groups of mice. Equally important, trabeculae were lost, especially in the thickness range of 90 – 150 μm. This was further substantiated by the trabecular connectivity density, which dropped significantly in female WT mice (52 weeks, 58.8 ± 17.7; 104 weeks, 0.4 ± 0.4, $p<0.05$) and male TTD mice (52 weeks, 78.4 ± 14.4; 104 weeks, 26.7 ± 10.5, $p<0.05$), and also had a downward trend in female TTD mice (52 weeks, 39.2 ± 8.3; 104 weeks, 22.6 ± 9.1, $p=0.24$) and male WT mice (52 weeks, 78.8 ± 7.6; 104 weeks, 49.3 ± 9.4, $p=0.05$). In line with these findings, trabecular spacing was significantly increased in all 104-week-old groups of mice, except for the 104-week-old WT males (data not shown), who accordingly had the smallest decrease in subchondral trabecular bone (shown in Fig. 3a), consistent with the idea that bone aging in this group was lowest. The changes in trabecular bone of the tibial epiphysis are visualized by 3D reconstructions in Fig. 4 (bottom panel).

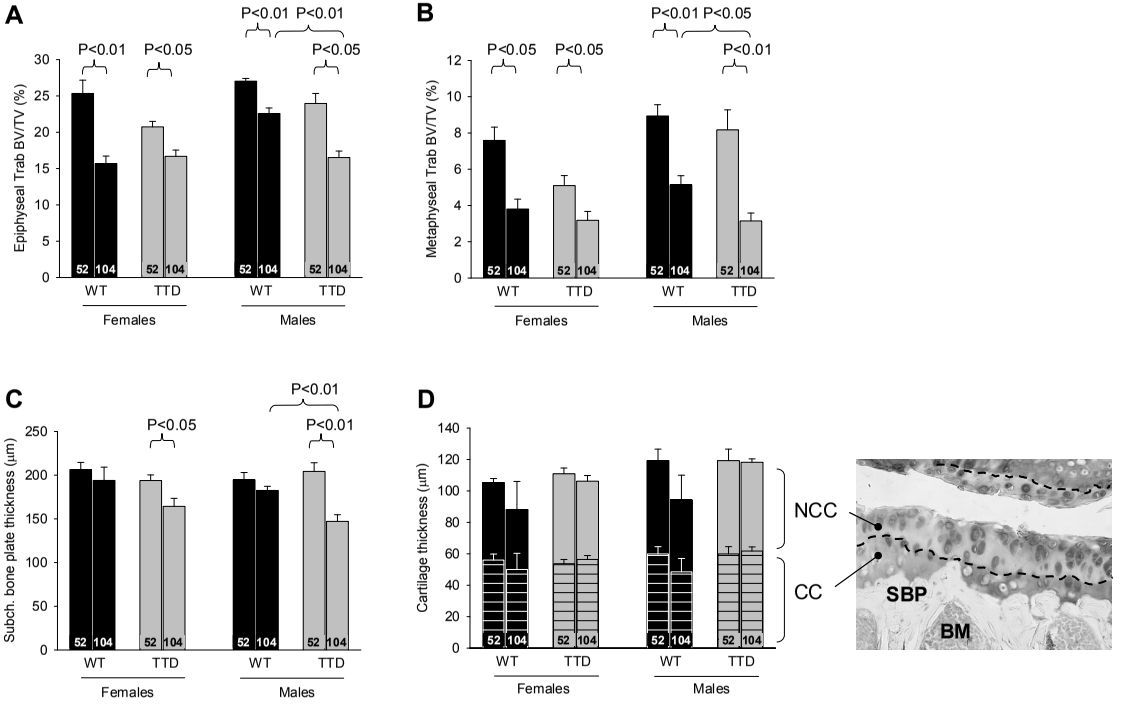

Figure 3. Bone changes in female and male WT and TTD mice, aged 52 and 104 weeks. A, trabecular bone volume fraction (Trab BV/TV) in tibial epiphysis. B, Trab BV/TV in tibial metaphysic. C, subchondral bone plate thickness in the tibial epiphysis. Please note that values refer to the average thickness of the medial and lateral subchondral bone plate. D, thickness of non-calcified (NCC) and calcified (CC) portion of the cartilage layer. Please note the decreased values and increased standard error in both sexes of the 104-week-old WT mice. This was caused due to the severe cartilage damage in two cases (one mouse in each group), for which it was not possible to obtain a thickness value. In these cases '0' was used as value. The histological section (magnification x200) is provided for anatomical context, the dashed line indicates the border between NCC and CC. Shown are averages ± SEM, significance was tested within genders, with $p<0.05$ considered significant. Ages are depicted inside the bars. NCC= non-calcified cartilage, CC= calcified cartilage, SBP= subchondral bone plate, BM= bone marrow.

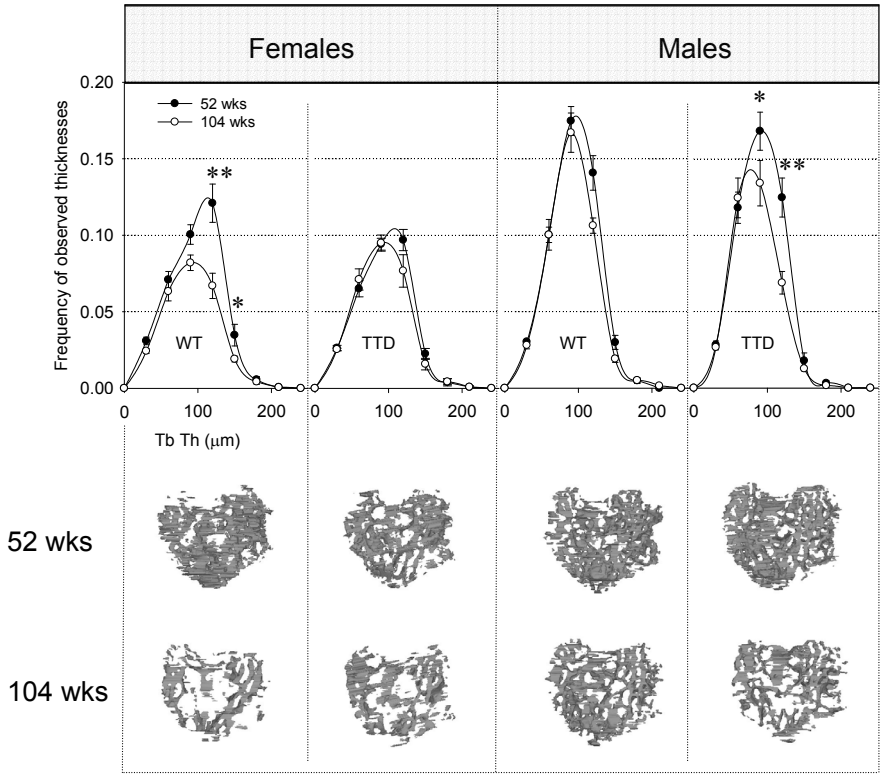

Figure 4. Top panel, thickness distributions of epiphyseal trabecular bone in female and male WT and TTD mice, aged 52 and 104 weeks. The number of observations of a measured thickness were counted and pooled in intervals of 30 μm of thickness. Please note that area under the curve depicts the total amount of trabecular bone (Trab BV). Trab BV in males is higher compared to females, since males are larger animals, but this is compensated by TV (not shown) and both sexes therefore have similar Trab BV/TV ratios as depicted in Fig. 2a, * $p<0.05$, ** $p<0.01$, 52 vs. 104 weeks. Bottom panel, 3D visualizations of the epiphyseal trabecular bone structure, as viewed from the top. The anatomical positioning is the same as shown in Fig. 1 (right).

Next to a decreased Trab BV (Fig. 4), the reduction in the amount of trabecular bone (i.e., Trab BV/TV, Fig. 3a) was also caused by an increase in the total amount of endocortical tissue volume (TV), thereby lowering the Trab BV/TV ratio (data not shown). The increased endocortical TV indicated that with aging, more space became present inside the epiphysis. Since the epiphysis itself was not significantly enlarged during aging in neither females nor males, we hypothesized that the endocortical thinning of the subchondral bone plate would explain the increased TV. We therefore studied the relation between the Sb.Pl.Th. and TV and found an inverse correlation in TTD, but not in WT mice (female TTD, 52 and 104 weeks, $r= -0.56$, $p=0.05$; male TTD, 52 and 104 weeks, $r= -0.72$, $p<0.01$). Thus, in 104-week-old TTD mice, which had the thinnest subchondral bone plate (Fig. 2a), TV was large, contributing to a decrease in Trab BV/TV.

Cartilage changes in knee joints of WT and TTD mice

The most commonly observed type of cartilage damage was superficial fibrillation, occasionally accompanied by small fissures down the non-calcified region, mainly at the lateral side of the tibial plateau (Fig. 5). This type of damage is similar what has been found by others in WT mice (195,200). Cartilage damage values ranged from ~10-30 points out of a maximum of 96 points in all groups of mice (Fig. 6a). In both sexes of WT mice, cartilage damage increased from mild at 52 weeks of age to moderate at 104 weeks of age, although this difference was only statistically significant in the female mice. In two cases clear disorganization throughout the joint was found: 1 out of n=7 in the group of 104-week-old WT males (summed cartilage damage score 61.3) and 1 out of n=6 in the group of 104-week-old WT females (summed cartilage damage score 70.8). Compared to WT females, the female TTD mice had significantly less cartilage damage both at 52 and 104 weeks of age. In males the amount of damage was more similar between genotypes, although the 52-week-old TTD mice had a trend towards more cartilage damage compared to age-matched WT mice (p=0.05).

To find out if a relation existed between the amount of cartilage damage and changes observed in the underlying subchondral bone plate, we plotted the average subchondral bone plate thickness against the amount of cartilage damage, but no relation was found between these parameters in any of the mouse groups. Because within every group of mice, the highest cartilage damage scores were consistently found at the lateral side, where the subchondral bone plate was thinner compared to the medial side (data not shown), we checked for a relation by plotting the separate medial and lateral subchondral bone plate and cartilage damage values for each anatomical site (i.e., medial and lateral tibial plateau), but no relation was found.

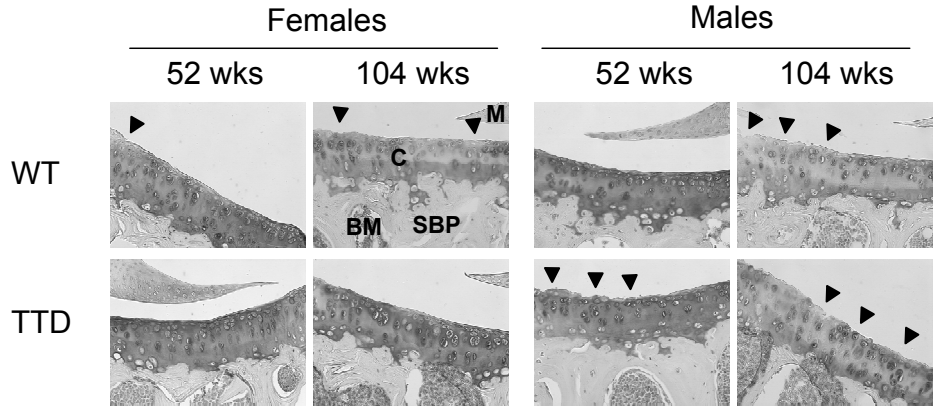

Figure 5. Representative examples of cartilage damage at the lateral tibial plateau in female and male WT and TTD mice, aged 52 and 104 weeks. Cartilage damage (arrowheads) in 104-week-old female TTD mice was only sporadically observed, contrary to the other groups of 104-week-old mice. In addition, Safranin O depletion indicating proteoglycan loss was observed in all 104-week-old mice, except for the TTD females. Magnification x200. C= cartilage, SBP= subchondral bone plate, M= meniscus, BM= bone marrow.

At 104 weeks of age, loss of proteoglycans as assessed by Safranin O depletion was observed in all but the female TTD mice, in which the cartilage phenotype remained relatively normal during aging (Figs. 5 and 6b). At 104 weeks of age, TTD females had significantly less proteoglycan depletion compared to age-matched female WT mice. In males a similar amount of proteoglycan depletion was found in both genotypes, which proved to be significantly different for TTD males and also had an upward trend for male WT animals (p=0.07; Fig. 6b).

Finally, osteophytes were observed in 52-week-old WT mice of both sexes (females, 4 out of n=6; males, 2 out of n=5), and prevalence rose to 100% in the 104-week-old animals (females, 6 out of n=6; males, 7 out of n=7). TTD mice had less osteophytosis at 52 weeks of age (females, 0 out of n=6; males, 1 out of n=6), and significantly less at 104-week-old of age (females, 1 out of n=7; males, 4 out of n=6) compared to age-matched WT animals (Fig. 6c).

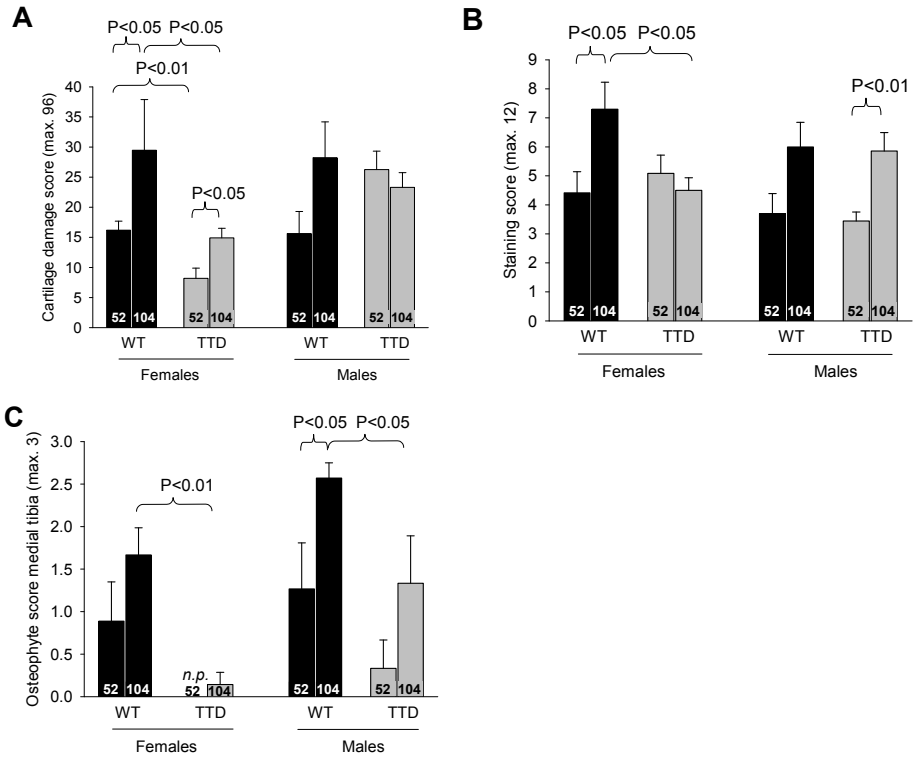

Figure 6. Quantification of histological OA characteristics in knee joints of female and male WT and TTD mice, aged 52 and 104 weeks. A, cartilage damage, scoring was performed according to the OARSI Working Group scoring system. B, proteoglycan loss. The staining score is inversely correlated with of the Safranin O staining intensity, a high score therefore indicates more proteoglycan loss. C, osteophyte presence at the medial tibia, a higher score meaning more mature (mineralized) osteophytes. Shown are averages ± SEM, significance was tested within genders, with p<0.05 considered significant. Ages are depicted inside the bars. n.p.= not present.

DISCUSSION

This is the first study that investigated the link between DNA repair deficiency as seen in a mouse model for the DNA repair compromised, premature aging disorder trichothiodystrophy, and OA-related changes in cartilage and subchondral bone with aging. Given the fact that both human TTD patients and TTD mice present a predominantly progeroid clinical picture, including prominent osteoporosis, it was expected that these mice would also display an increased cartilage damage, a hallmark characteristic of osteoarthritis (OA). Remarkably, however, not only did our findings indicate that this was not the case, we also found that female TTD mice were protected from cartilage damage. In sharp contrast, at the level of (subchondral) bone, we did confirm the accelerated bone aging phenotype, especially in TTD females.

The question then is, what explains this apparent tissue difference between bone and cartilage in aging TTD mice, and why are female mice affected more than males? Previous results already showed that other tissues in TTD mice also exhibit a paradoxically slower rate of aging-related pathology compared to WT mice. For instance, incidence of age-related cataract of the eye lens was decreased in TTD mice as compared to WT littermates (191). An interesting common denominator of both cartilage and lens tissue is the absence of any vascular, neuronal, or lymphatic tissue and the post-mitotic state of the cells, whereas bone (as most other tissues) is highly vascularized and has a higher turnover. Epithelial cells of the lens are nourished via the aqueous humor and anaerobic metabolism is the primary source of energy (201). Articular cartilage receives its nutrients via the surrounding synovial fluid which is encapsulated by the knee capsule, and via the underlying subchondral bone (74,202,203). Embedded inside their extracellular matrix, the chondrocytes survive under relative anoxic conditions, with oxygen tensions varying from around 6% at the joint surface to 1% in the deep layers of healthy articular cartilage (19). In contrast, blood vessels are commonly observed in subchondral bone (66), and oxygen is important for the survival of osteoblasts (204).

Vascularization of a tissue is important for nutrient and oxygen supply to tissues and cells and for determining the metabolic capacity of the cells. However, the downside of oxygen is the generation of DNA-damaging ROS, which are produced when oxygen is consumed in the aerobic respiratory chain of mitochondria. ROS are important for some cellular processes in both bone and cartilage (205-209), but high levels of ROS (i.e., oxidative stress) can lead to increased levels of oxidative DNA damage which may not be repaired sufficiently, thereby disturbing normal cellular metabolism and increasing the risk for pathology (183,184,210,211). The concept of ROS production in relation to age-related bone loss and development of osteoporosis has recently been carefully reviewed by Manolagas (212) and the significance of FoxO-mediated defense against oxidative stress for osteoblast function and skeletal homeostasis has recently been dem-

onstrated (206,207). A role for ROS in OA has also been discussed in the context of DNA damage, together with the effect of oxygen tension on *ex vivo* chondrocyte function and antioxidant intervention studies (213). However, it was concluded that the role of ROS in cartilage degradation and development of OA remained an open question.

The concept of ROS-induced oxidative stress leading to pathology is especially relevant for a situation in which the DNA repair system is compromised, as is the case in TTD. However, this concept also implies that less metabolic active and low oxygen consuming tissues (such as cartilage and the eye lens) have reduced sensitivity to age-related accumulation of DNA damage. Following this argument, oxidative stress in the nonvascularized cartilage and lens is expected to be limited compared to bone and other vascularized tissues, and the presence of only a partially functional DNA repair system would therefore suffice. Our current study therefore strongly indicates that oxidative damage does not play a major role in the age-related etiology of cartilage damage and OA. In this respect, the role of antioxidant treatment (either taken as supplements or via enriched dietary intake) may not be effective, and although in the last decades a number of randomized clinical trials have been performed which tested the use of supplements as treatment for OA, antioxidant supplementation so far has not shown clear efficacy (214-216). Subsequent direct proof that oxidative damage is not involved in OA should be provided by genetic studies and age-related cartilage-specific interference in metabolism, ROS production and cartilage degradation.

A second explanation for the observed age-related differences in cartilage and bone between WT and TTD mice has emerged from microarray expression profile analysis of other DNA repair-deficient progeroid mouse mutants, which revealed a 'survival response' involving suppression of the somatotrophic (IGF-1/growth hormone) axis (183,217-219). This survival response is a systemic adaptive response aimed at minimizing further damage to the DNA, by shifting the energy equilibrium of the organism from growth and proliferation to preservation of somatic maintenance. In addition to lowering IGF-1 production, the survival response stimulates cellular antioxidant systems and suppresses the production of certain hormones, such as estrogens, which may also explain why TTD mice have a lower bone mass compared to WT mice. This latter finding is of particularly interest, as the association of low amounts of cartilage damage associated with (subchondral) osteopenia point to the 'old' theory of an inverse relation between OA and osteoporosis (220). Here, IGF-1 may be a mechanistic link, since its levels were shown to be elevated in OA cartilage (221) but its production is generally found to decline with aging leading to osteoporosis (222). However, studies looking at the relation between IGF-1 levels and OA remain inconclusive (223). Interestingly, Biermasz and co-workers found that acromegaly patient having abnormally high circulating levels of IGF-1 showed an almost fourfold increased risk for radiological osteoarthritis of the hip (224). It would therefore be interesting to determine both circulating, but prob-

ably more important, local IGF-1 levels and IGF-I signaling inside the articular cartilage of old WT and TTD mice and assess a relation with cartilage damage.

Furthermore, it is possible that nonvascularized and non-proliferative tissues, such as the cells in the eye lens and cartilage, profit more from this systemic survival response, than they suffer from the consequences of the DNA repair defect in part derived from endogenous oxidative stress. As a net result these organs and tissues undergo less pathological changes with aging compared to vascularized tissues. However, it is currently unknown whether a (protective) survival response is also present in cartilage of (female) TTD mice, and cartilage-specific microarray studies will be instrumental to answer this question.

A final explanation for the observed differences in cartilage aging between WT and TTD mice, although speculative, is the absence of adipose tissue in the latter. In humans, obesity is one of the major risk factors for developing OA, and recent studies indicate that, next to increased body weight and thus increased mechanical joint load, the adipose tissue itself may also induce or exacerbate OA, by excreting pro-inflammatory cytokines such as leptin (225-228). However, if this will hold for TTD mice as well will necessitate extensive further analyses.

It is difficult to relate our results directly to observations in the human TTD patients since to our knowledge, no study has ever reported or looked at OA development in TTD patients, probably because of the extreme rarity of the disease and the fact that most patients die at an age too early for OA development. With regard to bone changes, some reports stated bone abnormalities including osteopenia in the long bones and osteosclerosis in the axial skeleton (190), but clear sex differences have not been described.

An intriguing and yet unexplained observation in our study was the difference between female and male TTD mice. Female TTD mice had less OA development than TTD males at both ages, whereas in WT mice the OA severity between both sexes was similar. Studies comparing spontaneous OA in both male and female WT mice are scarce but those that are published (usually serving as controls for genetically modified mice) do not report large differences between genders (229,230). However, in some OA susceptible mouse strains such as the STR/ORT mice, known to develop progressive cartilage damage at early age (10-20 weeks of age), males are affected more than females (231). This finding also holds for instability-induced OA (64,65). These studies indicate that male mice, when challenged (by joint instability or genetic modification) are more prone to develop OA than female mice. This difference between male and female mice might be further enhanced by changes in the levels of sex hormones (232-234).

To summarize, we found that TTD mice, despite their overall premature aging phenotype, did not have more, or even had less, OA characteristics compared to WT mice. This may be explained by a difference in response of a tissue to the 'survival response' triggered by the accumulation of DNA damage, or by a difference in sensitivity to the

DNA damage itself (or a combination). The outcome of this process is that some, preferentially nonvascularized, tissues will remain relatively unaffected, giving this disorder a segmental nature. This study therefore provides important clues as to why progeroid syndromes such as TTD show a segmental pattern of aging.

ACKNOWLEDGMENTS

We are grateful to Piet Kramer and Nicole Kops for their skilful technical assistance. This work was financially supported by National Institute of Health (NIH)/National Institute of Aging (NIA), grant number 1 PO1 AG-17242, NIEHS (1UO1 ES011044), Netherlands Organization for Scientific Research (NWO) through the foundation of the Research Institute Diseases of the Elderly, as well as grants from the Dutch Cancer Society (EUR 99-2004), and EC (QRTL-1999-02002).

OPEN ACCESS

Chapter 6

Osteoarthritis induction leads to early and temporal subchondral plate porosity in the tibial plateau of mice: an *in vivo* micro CT study.

S.M. Botter, G.J.V.M van Osch, S. Clockaerts, J.H. Waarsing, H. Weinans, J.P.T.M. van Leeuwen

Published in Arthritis & Rheumatism (2010)

ABSTRACT

In osteoarthritis (OA) changes occur both in cartilage and subchondral bone. The subchondral bone plate facilitates normal crosstalk between articular cartilage and trabecular subchondral bone, and adaptive changes in the plate due to OA may therefore disturb crosstalk homeostasis. To investigate these changes over time we examined the cartilage-subchondral bone interface using a combined approach of histology and *in vivo* micro CT. Male C57Bl/6 mice (*n*=8), aged 16 weeks, received intra-articular injections with collagenase in one joint to induce instability-related OA and saline into the contralateral knee joint (controls). At 2, 4, 6, 10 and 14 weeks post-injection, changes in the tibial subchondral bone plate and subchondral trabeculae were analyzed. At two weeks post-injection, collagenase injected joints had significantly more cartilage damage and osteophytosis than control joints. Osteoclast activity directly underneath the subchondral bone plate was significantly elevated (Oc.S./BS controls: 7.60± 0.81%; OA: 11.07± 0.79%), causing the plate to become thinner and creating a large increase in subchondral bone plate porosity (cumulative porosity volume controls: 0.05e-3 ± 0.04e-3 mm^3; OA: 2.52e-3 ± 0.69e-3 mm^3). At four weeks post-injection, the previously formed perforations disappeared, coinciding with a significant rise in osteoblast activity in the subchondral trabecular bone (bone formation rate controls: 0.30± 0.03, OA: 0.62± 0.13 $\mu m^3/\mu m^2$*day). The current study provides for the first time quantitative longitudinal data on the dynamic changes in the subchondral bone plate after OA induction. The development of plate perforations may enhance mutual interaction between subchondral trabeculae, bone marrow cells and the articular cartilage in OA.

INTRODUCTION

In osteoarthritis (OA) changes in bone are thought to accompany cartilage deterioration, although it remains unclear which process is responsible for the initial homeostatic disturbance. Because of its close proximity to the articular cartilage, the subchondral bone plate is responsible for structural support of the articular cartilage as well as providing a portal for biochemical interaction between cartilage and bone marrow and/or subchondral trabecular bone (24,66,129,235,236). Therefore, any changes in its structure may well have an effect on the overlying cartilage as well as the underlying subchondral bone. In OA, subchondral bone is hypomineralized and of inferior quality as a consequence of an abnormally high turnover rate (92,102,237-239). The exact cause of this increased bone turnover is as yet unknown, but the involvement of changes in the overlying articular cartilage as principal cause is proposed (69,133,134). In contrast, other studies state that the OA process starts with an increase in subchondral bone turnover, which in turn initiates cartilage damage (132-135). Whichever theory is true, mutual interactions between cartilage and subchondral bone are likely to occur. In 2003, Burr and co-workers proposed that microcracks in the subchondral bone plate or calcified cartilage may initiate targeted remodeling of the subchondral bone, accounting for the increased turnover and reduced material density of the subchondral plate (76). In addition, an increase in subchondral bone plate porosity has been described in human OA patients as well as in animal models of OA (103,182), but it is unclear if this increase in porosity also leads to increased interaction between cartilage and subchondral bone.

To study changes in the subchondral bone, the use of micro CT imaging has become an invaluable tool (87,154). Contrary to histology, micro CT enables 3D monitoring and -quantification of changes in dense tissues such as bone and in the last few years the use of *in vivo* micro CT has become the new standard (240). A major advantage of the use of *in vivo* micro CT is its ability to follow bone changes longitudinally within one animal, which makes it possible to better dissect cause and consequence. Nevertheless, relatively few studies have looked at *in vivo* changes in the subchondral bone plate, the structure that interfaces articular cartilage and trabecular subchondral bone (47,48). Therefore, in this study we examined the changes in subchondral bone plate with development of OA with a combined approach of histology and *in vivo* micro CT.

METHODS

OA induction

Thirty-two male C57Bl/6 mice (Harlan, Zeist, The Netherlands) aged 16 weeks were used. The animals were maintained on a 12:12 h light-dark cycle, housed in individually ven-

tilated cages with four littermates per cage and were fed *ad libitum*. Body weight of all animals was measured at weekly intervals throughout the experiment. For induction of osteoarthritis, we used the collagenase OA model as described previously (54,241,242). At day 0 of the experiment mice were anesthetized using a 5% isoflurane/N_2O/O_2 mixture and intra-articular injections of either six µl containing 1U of purified bacterial type VII collagenase (Sigma, St Louis, MO) dissolved in saline (right knee joints), or saline only (left knee joints, hereafter called control left knee joints), were given using a 33G syringe. The animal received pain medication subcutaneously while still under anesthesia (Temgesic, 0.01 mg/kg body weight). All injections were repeated on day 1.

Animals were randomly divided into four groups of eight mice. The first three groups were termed Cross/0-2, Cross/0-4, Cross/0-14 (Cross for cross sectional), with numbers referring to the time points at which scans were performed, in number of weeks. The fourth group of mice was named Lt/0-14 (Lt for longitudinal) in which scans took place at T=0, 2, 4, 6, 10 and 14 weeks post injection. Sixteen mice (Cross/0-2, *n*=4; Cross/0-4, *n*=4; Cross/0-14, *n*=8) received an intraperitoneal injection with calcein (0.01 mg/g body weight, Sigma, St Louis, MO) eight days and one day before sacrifice (i.e. after 2, 4, and 14 weeks, respectively). After sacrifice, performed by cervical dislocation, the hind legs of all animals were excised and fixed in 4% buffered formalin. All experiments were approved by the local animal ethics committee.

Micro CT

To monitor bone changes, we made use of the Skyscan 1076 *in vivo* X-ray microtomograph (Skyscan, Kontich, Belgium). Prior to scanning, each animal was anesthetized using a 5% isoflurane/N_2O/O_2 mixture for the duration of the procedure (~25 minutes) and a small synthetic foam block was mounted between its hind leg to clear the scan area of surrounding soft tissues (see figure 1A, left panel). The mouse was then placed supine inside the scanner in a polystyrene bed. The X-ray beam was directed at the proximal tibia so that only a scan area of 17 mm length was irradiated, leaving the rest of the animal shielded from radiation. The following settings were used: voxelsize 9 µm; voltage 40 keV; current 250 µA; exposure time 2356 ms; frame averaging 2; beam filtration filter 1 mm aluminum. Data were recorded every 1.5 degree rotation step through 180 degrees. Left and right legs were scanned in the same scan session. The total time per scan was 21 minutes, of which the hind legs were exposed to X-ray radiation for in total 11 minutes due to the use of a shutter that shielded the scan area in between recordings.

Mice in groups Cross/0-2, Cross/0-4 and Cross/0-14 were scanned prior to OA induction (performed directly after the T0 scan with the animal still anesthetized), and immediately after sacrifice at two (Cross/0-2), four (Cross/0-4) and fourteen weeks (Cross/0-14) post OA induction. Mice in group Lt/0-14 were scanned at zero (OA induction immediately after scan), two, four, six, ten and fourteen weeks post OA induction (see figure 1B). After

sacrifice all excised hind limbs were scanned again *ex vivo* using an extended scan protocol with improved signal/noise ratio: the rotation angle was lowered to 0.8 degrees, and frame averaging was increased to 3. All other settings remained unchanged.

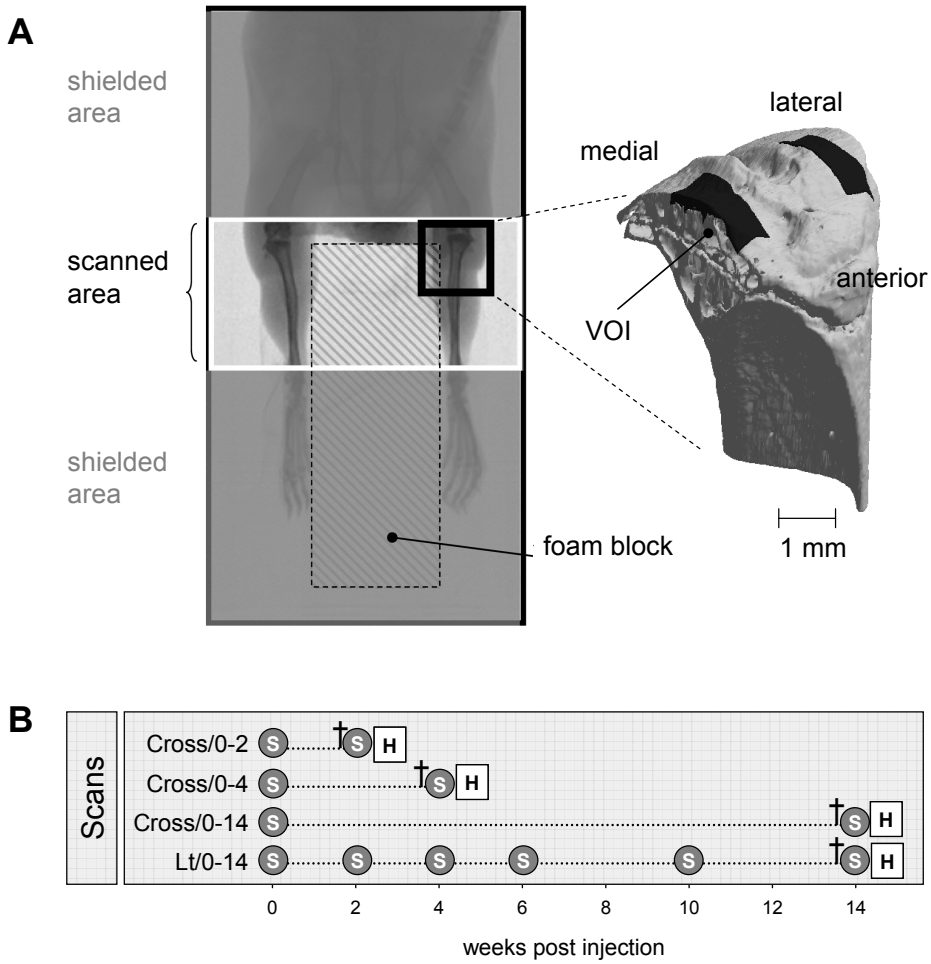

Figure 1. Schematic overview of the scanning procedure. A, After anesthetization, a foam block was placed between the animals' hind legs with soft adhesive tape, to prevent any soft tissue from entering the scanned area. The tail of the animal was bended out of view dorso-cranially. After a fast scout scan using low radiation dose for orientation, the X-ray beam was focused on the proximal tibia for the actual scan, leaving all areas outside shielded from radiation. On the right a 3D model of the proximal tibia is shown, with two volumes of interest (VOI) indicated in blue: one on the medial and one on the lateral side, which were chosen for analysis. These VOIs included the subchondral bone plate (dark blue) and subchondral trabeculae (light blue). B, time points at which animals of each group were scanned is indicated by 'S'. The first scan (at T=0 weeks) was performed just before the first of the two intra-articular injections, the last scan (at T=14 weeks) was performed immediately after sacrifice (indicated by †). After sacrifice, hind limbs of mice were processed for *ex vivo* scanning and histology ('H'). Cross= cross sectional group, Lt= longitudinal group.

Reconstruction was performed using Skyscan NRecon v1.4.3. Resulting grey-scale cross sections were composed of isotropic voxels measuring exactly 8.88 μm in all dimensions.

Radiation dose

Radiation dose per scan was measured with a Solidose 400 dosimeter equipped with a DCT16-77 ionisation chamber probe (RTI Electronics AB, Mölndal, Sweden). The received radiation dose was 0.08 Gray per minute using the *in vivo* scan settings. However, this dose rate needs to be corrected for tissue depth since part of the radiation dose will be absorbed by the skin and overlying tissues. Skyscan recommends a tissue correction factor of 0.656 for the mouse hind leg, which means that each animal received 11 minutes x 0.08 x 0.656 = 0.57 Gy on its hind legs per scan.

Quantification of bone morphometric parameters

Each knee joint scan, consisting of reconstructed cross sections that together formed a 3D dataset, was manually aligned to get the same spatial orientation for all knee joints. To distinguish calcified tissue from non-calcified tissue and noise, scans were segmented with a local threshold algorithm (88). Using 3D data analysis software (CTAnalyzer, Skyscan) the proximal tibia was selected for further analysis (figure 1A, right panel). The cortex, including the subchondral bone plate, and trabeculae of the proximal tibia were separated using in-house developed software (available upon request). By applying subsequent steps of image dilation and erosion on the binary datasets, the software returns the anatomical compartments of the proximal tibia: subchondral bone plate; subchondral trabeculae; bone marrow; perforations inside subchondral bone plate. Perforations were only identified as such when they tunneled the subchondral bone plate enabling contact between the articular cartilage and the subchondral bone marrow. The different compartments were analyzed separately with the freely available software package 3D-Calculator (*http://www.erasmusmc.nl/47460/386156/Downloads)* using a binary selection feature.

To measure subchondral bone plate thickness, medial and lateral subsections (0.50 mm medio-lateral width, 1.15 mm ventro-dorsal length; dark blue bands in figure 1A, right panel) of the weight-bearing region of the subchondral bone plate were selected and their thicknesses was measured. For reasons of clarity we present the thickness of the subchondral bone plate (Sb.Pl.Th., in μm) as the average of the medial and lateral side, since the direction and magnitude of change was similar for both sides.

When measuring the total volume of perforations inside the subchondral bone plate the medial and lateral subsections were expanded to 1.00 mm medio-lateral width. The total volume of subchondral plate perforations was then measured in each cross section and summed.

Below each subsection of subchondral bone plate, the subchondral trabeculae (light blue in figure 1A, right panel) were analyzed separately and the following 3D morphometric parameters were calculated: Trabecular bone volume fraction (Trab BV/TV), which is the ratio of trabecular bone volume (Trab BV, in mm^3) over endocortical tissue volume (TV, in mm^3), trabecular thickness (Tb.Th., in μm,), trabecular spacing (in μm) and connectivity density (mm^{-3}), indicating the number of trabecular connections per unit volume (90). Values were averaged for medial and lateral sides.

In order to evaluate if bone changes also occurred at distal sites in the mouse hind leg due to the collagenase injection, the ankle area of mice sacrificed 4 and 14 weeks post saline or collagenase injection was scanned using the *ex vivo* scan protocol and Trab BV/TV of the calcaneus was measured.

To visualize the subchondral bone changes that took place within one animal, scans derived from one animal at time points zero, four and fourteen weeks were spatially matched by rotation and translation using the registration software M.I.R.I.T. developed at the University of Leuven (243). This software uses an optimization criterion based on maximizing mutual information. The resulting rotated datasets were used to create overlaps between different time points post injection and differences were highlighted in colour-coding.

All 3D images were made using the software programme ANT (Skycan).

Histological analysis

Left and right hind limbs of sixteen animals (Cross/0-2, *n*=4; Cross/0-4, *n*=4; Lt/0-14, *n*=8) were decalcified in 10% EDTA/5% paraformaldehyde (PFA) for 14 days and embedded in paraffin. Hind limbs of the sixteen animals that received calcein injections remained undecalcified and were embedded in methyl metacrylate (MMA). Six μm thick coronal (frontal) histological sections were taken through the joint at 100 μm intervals.

Paraffin sections were stained with Safranin O and Fast green. Cartilage damage was scored at the medial and lateral tibial plateau using the semi-quantitative grading and staging system devised by the OARSI Working Group (18). In this system, a grade score (reflecting damage severity) and stage score (reflecting damage extent) is assigned to each analyzed location, and then multiplied. Three histological sections per joint were analyzed and the obtained medial and lateral damage values were first summed and then averaged for the three sections, yielding a maximum obtainable cartilage damage score of 48. Loss of proteoglycans (stained by Safranin O) was scored using a four-point scoring system from 0-3, where 0 represents no loss of proteoglycans and 3 indicates complete loss of staining for proteoglycans in more than half of the cartilage layer. Osteophyte presence was scored according to the 4-point scoring system from Kamekura *et al*. (52), with 0 - no osteophytes, 1 - formation of cartilage-like tissues, 2 - increase of cartilaginous matrix, 3 - endochondral ossification. Finally, osteoclasts were visualized

using histochemical staining for tartrate-resistant acid phosphatase (TRAP) activity as described previously (244), using Gill's haematoxylin as counter stain. Osteoclast quantification included osteoclast surface/bone surface (Oc.S./BS) and osteoclast number/bone surface (Oc.N./BS) using Bioquant Osteo v7.20 (Bioquant, Nashville, TN).

MMA sections were photographed in bright field and fluorescent light to visualize the outline of the bone and calcein labels, respectively. These photos were merged in Paint Shop Pro 7.02 (i.e. the bright field microphotograph was made 70% transparent and added as layer to the fluorescent microphotograph). The whole surface area of epiphyseal trabecular bone was analyzed and single and double labels were manually indicated using Bioquant Osteo v7.20. Mineralizing surface over bone surface (MS/BS, in %), mineral apposition rate (MAR, in μm/day) and bone formation rate (BFR/BS, in $\mu m^3/\mu m^2$*day) were then calculated.

Statistical analysis

Results were statistically analyzed with GraphPad Prism v5.02 (San Diego, CA). For the cartilage damage, osteophytosis, osteoblast and osteoclast data a repeated measures two-way ANOVA was applied with treatment (intra-articular injection with saline or collagenase) and time as factors and Bonferroni post tests. For the micro-CT derived morphometric data a two-way ANOVA was used with treatment (intra-articular injection with saline or collagenase) and time as factors and Bonferroni post tests. When studying effects in time within a single group or treatment a one-way ANOVA with Tukey's post test was chosen. In all cases $p<0.05$ was considered significantly different. In all graphs, data are presented as mean ± standard error of the mean (SEM).

RESULTS

Effect of the operation and scanning

All animals were closely monitored up to twelve hours after the operation, corresponding to the therapeutic effective time span of the applied analgesic, and since cage activity was normal no further analgesia was applied. Although some weight loss was measured in the first week after surgery (2-6% of the initial body weight at T=0), this change was not significant and all animals had normal weight gain thereafter. From ten weeks post injection onwards, average body weight of both the Cross/0-14 group (scanned two times of which once after sacrifice) and the Lt/0-14 group (scanned six times of which once after sacrifice) was significantly higher compared to the body weights measured at T=0 (data not shown). The bone volume fraction in the proximal tibia of control left knee joints was not statistically different between Cross/0-14 (12.6 ± 0.71%) and Lt/0-14 (10.17 ± 1.04%) at T=14 weeks, indicating that repeated scanning did not have

a measurable deleterious effect on normal bone metabolism. To assess if the animals would preferentially unload one of their hind legs due to the operation, we analyzed the amount of trabecular bone in the calcaneus of collagenase injected and contralateral control legs. Trabecular bone volume fraction (Trab BV/TV) was 104.9 ± 6.3 %, 98.6 ± 5.2 % and 96.0 ± 3.8 % and trabecular thickness was 95.7 ± 2.7%, 99.5 ± 1.9% and 96.9 ± 4.3% of contralateral controls at T=2, T=4 and T=14 weeks after collagenase injection, respectively. No significant differences were found between collagenase injected and contralateral control joints at any time point.

Osteoarthritis induction and subchondral bone changes

Two weeks after OA induction cartilage damage was significantly higher in collagenase injected knee joints compared to contralateral controls (figure 2A, left). Mineralized osteophytes were also observed after two weeks in collagenase injected joints (figure 2A, right). Reduction of Safranin O staining, indicative for proteoglycan loss was significant at 4 weeks after OA induction, but not at 2 or 14 weeks (data not shown).

In the subchondral volumes of interest (VOIs) of collagenase injected knee joints bone loss was observed. Compared to contralateral control knee joints, the thickness of the subchondral bone plate in the collagenase injected knee joints decreased from two weeks post injection onwards (figure 2B), indicating increased osteoclastic activity. This initial thickness decrease was temporary, since at 10 weeks post injection the bone plate returned to its initial thickness, although the average plate thickness as measured in the contralateral control joints (which also increased in time) could not be reached.

When we quantified the presence of osteoclasts located directly underneath the subchondral bone plate (figure 2C, top), we found similar time-dependent dynamics in osteoclast surface and osteoclast number in saline and collagenase injected knees. Only in the first period after injection (T=2) a significant increase in osteoclast surface (figure 2C, bottom left) was detected in collagenase injected knee joints. Osteoclast number (figure 2C, bottom right) was elevated as well although this difference did not reach significance (p=0.09). In the trabecular bone underlying the subchondral bone plate similar temporal bone loss patterns were found as assessed by bone volume fraction (Trab BV/TV: p-value between curves< 0.05, figure 3A, top) and trabecular thickness (Tb.Th.: p-value between curves <0.01, data not shown), whereas trabecular spacing was significantly elevated (Tb.Sp: p-value between curves=0.001, figure 3A, bottom) in collagenase injected knee joints versus contralateral controls. As previously found for the subchondral bone plate, the initial decrease in bone volume fraction was followed by an increase, indicating a rise in osteoblastic activity. This was confirmed by the calcein labeling, which showed increased osteoblast activity in the subchondral trabecular bone of collagenase injected knee joints at T=4 weeks (figure 3B). We observed significant increases in mineralized surface and bone formation rate (figure 3C) as well as mineral apposition rate (data not

shown) compared to contralateral control joints. At T=14 weeks, these parameters also increased significantly in control knee joint (figure 3C, compare grey bars), indicating normal growth and providing an explanation for the temporal increase in subchondral bone plate thickness in controls (see figure 2B).

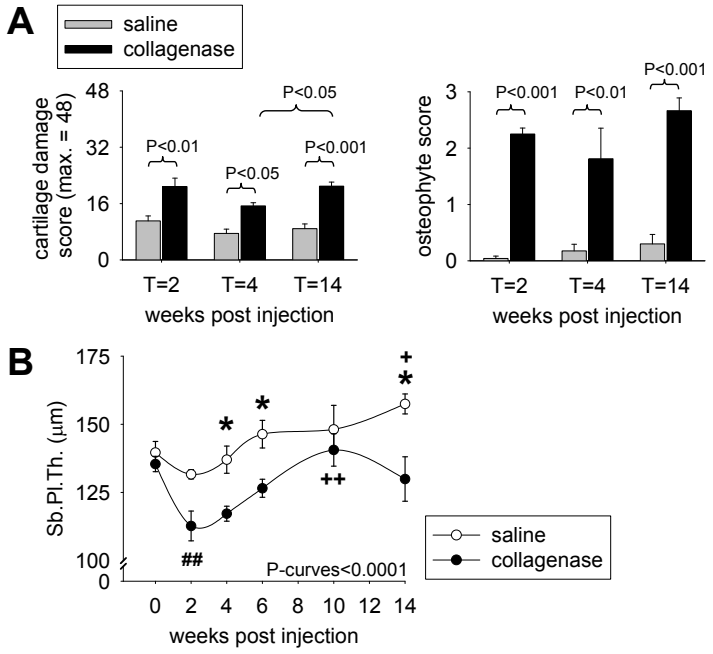

Figure 2. A, cartilage damage (left) and osteophyte presence (right) presence in collagenase injected knee joints and contralateral control knee joints. B, Temporal changes in subchondral bone plate thickness (Sb.Pl.Th.) over time. Shown are averages ± SEM, # $p<0.05$ vs. T=0 (within treatment); + $p<0.05$ vs. T=2 (within treatment); * $p<0.05$ between treatments. C, Microphotograph of tibial subchondral bone plate area (dotted area was examined). A TRAP positive osteoclast indicated by the arrow head is shown enlarged in the inset. M= meniscus, AC= articular cartilage, SBP= subchondral bone plate, BM= bone marrow, GP= growth plate (top), quantification of osteoclast activity in the dotted area after collagenase or saline injection (bottom). Osteoclast surface per bone surface (left) and number of osteoclasts per bone surface (right) were determined. For T=2 and T=4, $n=4$ for each bar, for T=14, $n=8$ (group Lt/0-14). All bar graphs show averages ± SEM, $p<0.05$ was considered significant.

The changes in subchondral bone (i.e. subchondral bone plate and subchondral trabeculae) within the same anatomical location in one animal are visualized in figure 4A. To further visualize the bone remodeling process, binarized grayscale images derived from T=0, T=2 and T=14 were overlapped and the differences in the amounts of bone between the time points was visualized (figure 4B). From these figures it becomes clear that at T=2, primarily bone loss (light blue) is observed at both the medial and lateral side of the tibial plateau, whereas at T=14 bone gain (dark blue) is more prominent.

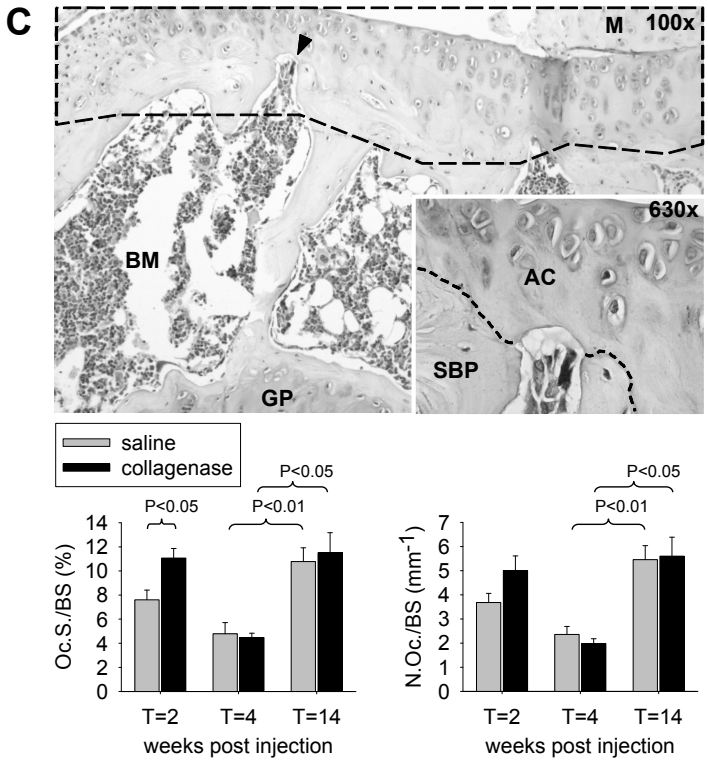

Figure 2. (continued)

Since we observed that subchondral bone plate thinning was one of the main outcomes of the experiment, we scrutinized the micro CT data of the subchondral bone plate. This analysis demonstrated that at multiple locations the subchondral bone plate had become so thin that perforations started to appear forming connecting tunnels between the subchondral trabecular bone/bone marrow and the articular cartilage (figure 5A, left, figure 5B). To exclude that the perforations were due to higher noise levels in the *in vivo* scans, we checked if the same perforations could also be found in scans made with the *ex vivo* scan protocol (which had a better signal-to-noise ratio) and this proved to be the case (figure 5A, right). In addition, we identified the perforations by histological analysis (figure 5C). Subchondral bone plate porosity was observed in both saline injected and collagenase injected knee joints, but the number and size of the perforations were larger in the collagenase injected knee joints (figure 6A). The perforation volume of the tibial plateau was significantly different between collagenase injected and contralateral control joints despite some temporal variation between the animals (figure 6B).

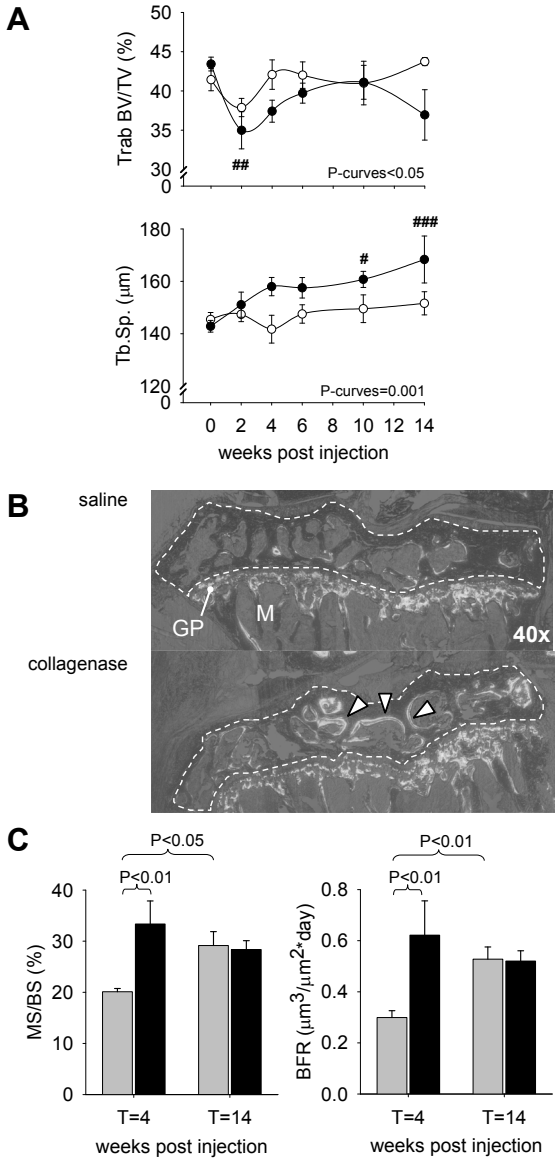

Figure 3. A, Temporal changes in the subchondral trabecular bone of collagenase injected knee joints and contralateral control knee joints. Bone volume fraction (top) and trabecular spacing (bottom). Shown are averages ± SEM, # $p<0.05$ vs. T=0 (within treatment). Although no differences were found at each individual time point, the ANOVA test ('P-curves') indicated that the curves are significantly different for both morphometric parameters. B, merged bright field and fluorescent microphotographs of the proximal tibia of a control knee joint and a collagenase injected knee joint at T=4 weeks post injection, with calcein labeling in green and the epiphysis delineated by the white dotted line. In the collagenase injected joint increased osteoblast activity is visible by the larger distance between the two labels (white arrowheads). GP= growth plate, M= metaphysis. C, quantification of osteoblast activity, in mineralizing surface (MS/BS, left) and bone formation rate (BFR, right). For T=4, n=4 for each bar, for T=14, n=8 (group Cross/0-14). Shown are averages ± SEM, $p<0.05$ was considered significant.

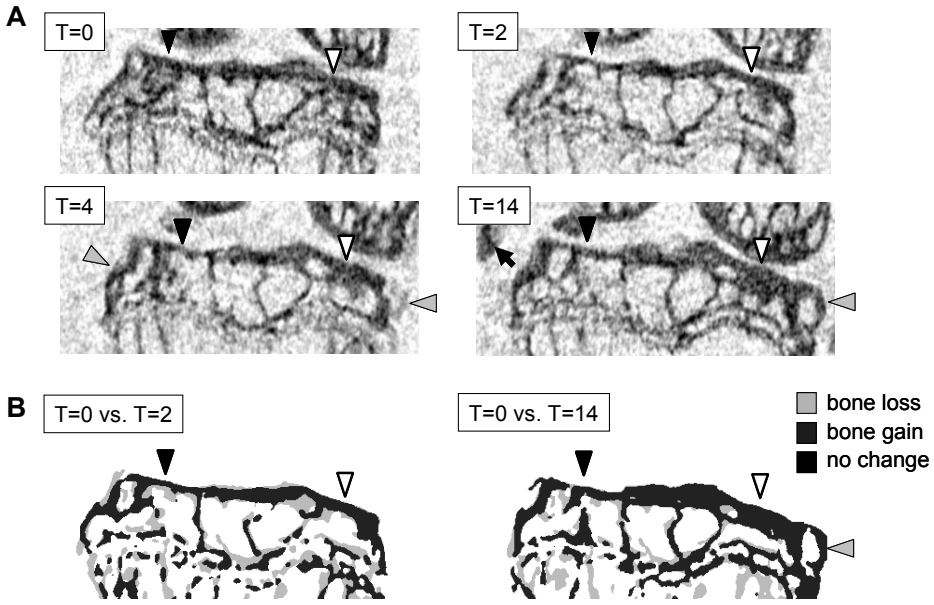

Figure 4. Visualization of subchondral bone changes within the proximal tibia of a single mouse (group Lt/0-14) at T=0, 2, 4 and 14 weeks post injection. A, At the beginning of follow-up (T=2), initial thinning of the subchondral bone plate was followed by thickening (T=4, T=14) at both the lateral (black arrowheads) and medial (white arrowheads) sides. Notice the development of mineralized osteophytes in this animal (grey arrowheads) at the medial and lateral sides of the tibial plateau from 4 weeks post injection onwards. In some cases ectopic calcifications were observed in the collateral ligaments, for example in week 14 post injection (black arrow). B, Segmented overlaps of the images shown in A, highlighting differences between T=0 vs. T=2 and T=0 vs. T=14. Changes in bone architecture are indicated by colour coding.

DISCUSSION

This study is the first to show quantitative longitudinal data on formation of perforations in the subchondral bone plate in an instability-induced model of osteoarthritis appearing within two weeks after induction. Increased osteoclast activity acting locally underneath the subchondral bone plate is the most likely cause of the formation of these perforations in the initial phase after inducing instability, followed by an increased osteoblast activity that repairs the perforations while cartilage damage progresses. These data show the high temporal dynamics in subchondral plate bone metabolism in OA. Finally, we demonstrated that *in vivo* micro CT is sensitive enough to quantify the anatomical changes following the altered osteoblast/osteoclast activities, without disturbing normal bone metabolism. Besides generating statistically powerful data, this technique also helps to reduce the amount of experimental animals needed.

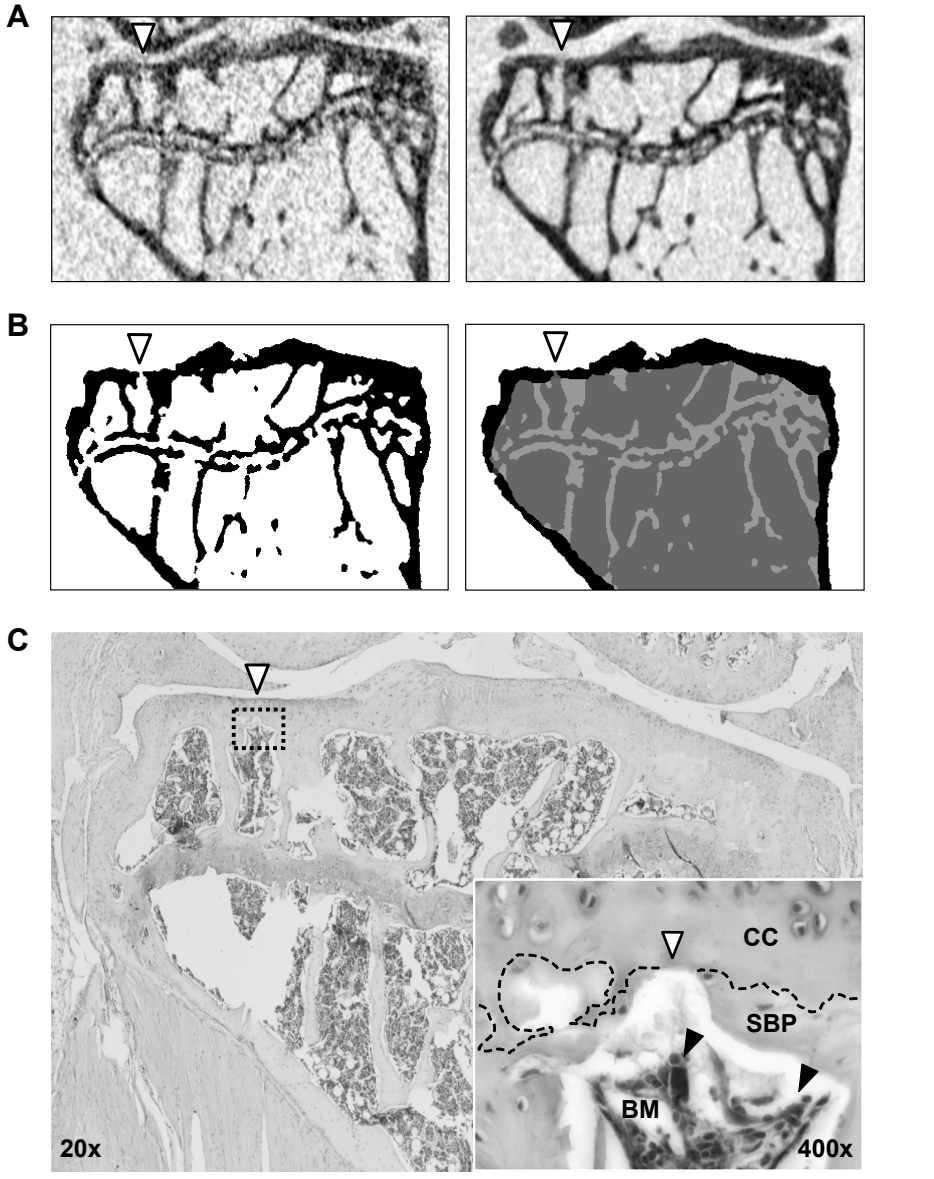

Figure 5. Example of a subchondral bone plate perforation that pierces the tibial plateau in a collagenase injected knee joint. All images were derived from the exact same anatomical location of the same animal, with the white arrowhead indicating the location of the subchondral bone plate perforation. A, Perforations are visible in *in vivo* obtained grey-scale images (left) as well in scans obtained with the *ex vivo* scan protocol which had a higher signal-to-noise ratio (right). B, In the segmented images (left) each anatomical component (cortex, trabeculae, plate perforation) was labeled with a different gray tone (right, plate perforation indicated in red). C, The accompanying histological section (dotted area enlarged as inset) confirmed the perforation to be present. TRAP stained osteoclasts (inset, black arrowheads) were observed in close vicinity of the perforation. CC= calcified cartilage, SBP= subchondral bone plate, BM= bone marrow.

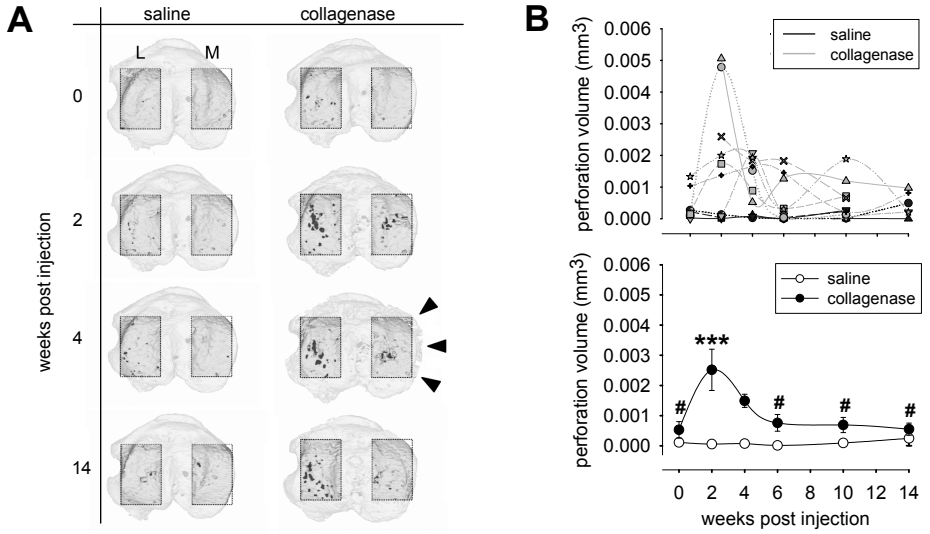

Figure 6. Formation of subchondral bone plate perforations in time. A, 3D top views of the tibial plateau at T=0, 2, 4 and 14 with subchondral bone perforations (purple) superimposed. Regions of interest (bright dotted areas) from which quantitative data was derived are indicated on the lateral (L) and medial (M) sides. Mineralization of an osteophyte at T=4 is indicated by arrowheads. B, Quantification of medial perforation volume in individual mice (top) belonging to group Lt/0-14. Some scans which had low quality due to movement artifacts were omitted, but it is clear that collagenase injected joints show larger and more dynamic temporal changes in subchondral plate porosity compared to contralateral control joints. At the bottom averages ± SEM are shown: $p<0.05$ was considered significant. # $p<0.05$ vs. T=2 (within treatment), * $p<0.05$ between treatments.

The dynamic changes in osteoarthritic subchondral bone that we found in the present study matches well with data published by others. For instance, Hayami *et al*. also found subchondral bone loss to occur in the rat knee within 2 weeks after surgical destabilization followed by significant increases in subchondral bone volume relative to sham up to 10 weeks post-surgery (30). Importantly, the authors observed increased vascular invasion into the calcified cartilage after one week, which coincided with the onset of cartilage surface fibrillation. In other studies with rats, McErlain *et al*., and Morenko *et al*., both using *in vivo* micro CT, also found early bone loss to occur in the rat knee after destabilization (47) or by using monosodium iodoacetate (48). Subchondral bone loss after knee joint destabilization was also found in dogs (182), guinea pigs (95), rabbits (94) and cats (85).

In human OA patients subchondral bone loss was also found to occur, especially in progressive OA. Bettica *et al.* found that urinary markers of collagen type I degradation were significantly higher in progressive knee OA patients, similar to patients having osteoporosis (239), and Buckland-Wright *et al.* concluded that risedronate was able to correct the subchondral trabecular bone loss found in progressive knee OA (245). Thus, although subchondral sclerosis is the final disease outcome, these data indicate that

bone loss generally occurs in OA, which may explain why net bone loss is observed at early stages of the disease process. To confirm this in human patients is difficult, since clinical data on changes in the subchondral bone plate is generally derived from patients with already established OA. This is a pity, since on the basis of our current data in depth analysis of the subchondral bone plate in case of (mild) joint complaints seems justified and may identify early stages of OA, which then may be modifiable or treatable.

Our finding that subchondral bone plate perforations are a) already present in normal tibial plateaus and b) are increased after inducing knee joint instability fit well with current literature finding. The first reports on holes penetrating the subchondral bone plate date from the 1980s, where Duncan et al.(27) described numerous perforations through the subchondral plate in non-arthritic tibial plateaus, some of which extending to the bone marrow (27). Similar findings were described by Lyons *et al*. (24) and Clark & Huber (246), and in the latter study the prevalence of these perforations in the human tibial plateau to estimated to be less than 10 /cm2. More recently, imaging studies have shown that small molecules such as gadolinium (129) or sodium fluorescein (247) are able to reach the articular cartilage from the bone marrow side, thereby passing through the subchondral bone plate. These studies showed that next to a mechanical interaction, biochemical interactions between bone and cartilage are very likely. Finally, Hwang *et al*., found a trend for increasing density of larger than normal canals penetrating the calcified cartilage in partially eroded samples, and were able to link this finding to increased hydraulic conductance of osteochondral tissue samples with progression of OA (26). These authors also postulated that the increase in hydraulic conductance of the subchondral bone plate may cause the articular cartilage to lose its high interstitial fluid pressurization (important to withstand joint loads) because of an abnormally high fluid exudation in the direction of the subchondral bone trabeculae and subchondral bone marrow.

From our current findings and data from literature discussed above, we would like to propose a concept of the consecutive events that take place in bone and cartilage in instability-induced OA in the murine knee joint. In this concept, we hypothesize that the increased perforation of the subchondral bone plate found in our current study leads to an increase in the mutual interaction between subchondral bone and cartilage: at T=0, directly after inducing instability, mechanical stress is induced on the articular cartilage and underlying subchondral bone, causing an increase in osteoclast activity just below the articular cartilage and decreasing subchondral bone plate thickness in the first two weeks. This gives rise to more and larger than normal perforations in the subchondral bone plate, increasing its permeability and causing a higher than normal fluid exudation towards the subchondral bone compartment, leading to a net loss of fluid from the cartilage which then becomes damaged. Meantime, in an attempt to repair, the damaged cartilage produces growth factors and/or cytokines which transfer the chondro-osseous

junction via the plate perforations. Other factors such as MMPs (248,249) may also end up in the subchondral trabecular bone and subchondral bone marrow via this route (as well as *vice versa*; factors derived from the subchondral bone going towards the articular cartilage: 133,135). This will start a cascade of events in which the fine balance of bone build up and break down becomes disturbed. In this process, osteocytes inside the subchondral bone plate, known to respond to fluid flow, may play a modulating role as well (250). Then, four weeks after inducing instability, the functional coupling that exist between osteoclasts and osteoblasts causes a rise in osteoblast activity in the subchondral trabecular bone, decreasing the amount of perforations back to control levels, and increasing the subchondral bone plate thickness. At this stage, osteoclast activity is suppressed. With more time progressing, osteoblast and osteoclast activity return to control levels, but the bone turnover is still in a disordered phase, and at the end of the follow up period (at T=14 weeks) the subchondral bone plate remains thinner compared to the contralateral controls. The fact that subchondral bone osteosclerosis was not observed might be explained by the still relative early phase of the osteoarthritis disease process in our experiment: despite the presence of fully mineralized osteophytes, the amount of cartilage damage after 14 weeks was mild, and full thickness erosion of the articular cartilage layer was only sporadically observed.

A limitation of the study is that a group of healthy animals was lacking from our study, therefore we cannot rule out that some of the parameters measured in the contralateral control joints may be different compared to intact (i.e., non-operated) joints, due to eg. altered cage activity. However, recurrent monitoring of the mice did not indicate any changes in daily cage activities until the end of the follow up (T=14 weeks), and we therefore have no reason to believe that this might be the case. Also, we did not notice progression of cartilage damage which is commonly observed in humans. The cause of this is yet unclear but may be a related to the OA model we used and/or be explained by the length of the follow up, which may still be too short.

In conclusion, we used a longitudinal approach in which subchondral bone changes in instability-induced OA were quantified using *in vivo* micro-CT combined with histological examination. We found that, as a result of increased osteoclast activity, subchondral bone loss occurred within two weeks after destabilization, resulting in increased subchondral bone plate perforation. These perforations directly connect two of the most affected tissues in OA, articular cartilage and subchondral bone, opening the possibility for increased crosstalk between cartilage and bone and contributing to disease progression. Finally, our findings may open up inspection of subchondral plate perforation as an early indicator of OA, and it will be a challenge to investigate this concept in a clinical study.

ACKNOWLEDGMENTS

We kindly acknowledge Yvonne Sniekers for help with operating the *in vivo* micro-CT scanner, Nicole Kops for assistance with histology and the personnel of the Experimental Animal Facility of the Erasmus MC for taking care of the animals during the experiment.

This research project was funded by the Erasmus Medical Centre, Rotterdam, The Netherlands.

Chapter 7

General discussion

Changes in bone form an inextricably part of the osteoarthritis (OA) disease process. These changes become apparent when an osteoarthritic joint is imaged, for instance by making a radiograph. Here, osteophytes can be visible at the margins of the joint. Also, the area of the subchondral bone is changed: the amount of subchondral trabecular bone is increased, and the subchondral bone plate is sclerotic.

Changes in subchondral bone have long been recognized as a hallmark of OA. Already in the 1970s, Radin and co-workers described these changes and recognized the potential impact of changes in the subchondral plate on the overlying articular cartilage (71,72). However, since an OA patient will only seek help once a joint becomes painful, often in late-stage OA, the early changes in subchondral bone remain elusive. Therefore, at the beginning of this thesis, we asked the question how skeletal alterations in the subchondral bone develop during the OA disease process. We have addressed this question by studying several mouse models of osteoarthritis, and made a division between primary or spontaneous OA, and secondary or instability-induced OA. In these models knee joints were digitized using micro-computed tomography (micro-CT). This technique allows non-invasive and three dimensional quantification of changes that occur in the subchondral bone, both at the level of the subchondral bone plate as well as in the subchondral trabeculae. In this chapter our most important findings on changes in subchondral bone are highlighted and a tantalizing perspective is given on how different subchondral bone phenotypes may influence the risk of developing OA.

KEY FINDINGS WITH RESPECT TO THE SUBCHONDRAL BONE PLATE AND SUBCHONDRAL TRABECULAE

Subchondral bone changes in instability-induced OA

With regard to changes in the subchondral bone plate we found, in almost all studies, an initial decrease in bone plate thickness following intra-articular collagenase injection to induce knee joint instability. This was shown for at least two strains of mice, C57Bl/6 and C3H/HeJ (Chapters 2, 4 and 6). The thickness decrease was found both at the medial and lateral sides of the tibial plateau. As shown in chapter 6, this initial thinning led to a striking increase in perforation of the subchondral bone plate, most likely caused by local osteoclastic recruitment, which enabled direct contact between articular cartilage and subchondral bone. In a later stage, this was followed by a recovery period in which increased osteoblast activity largely restored the bone plate thickness. Overall, these data demonstrate that in the early phases of OA subchondral bone becomes more dynamic as exemplified by increased bone resorption and formation.

Subchondral sclerosis, one of the OA hallmarks, was not always observed. It would therefore be interesting to see if with a longer follow-up period sclerosis will develop in

the collagenase model. This would be expected since the same order of events has been described in several other animal models as well (30,84,94,95). Subchondral sclerosis did occur in the study described in chapter 4, where ADAMTS5 knockout mice were compared to wild type (WT) animals. There are a number of possible explanations for this discrepancy. First of all, in this study knee joint instability was induced via a surgical procedure, destabilization of the medial meniscus (DMM), instead of an intra-articular collagenase injection. The arguments for this were mainly practical, since the procedure was carried out in the lab of one of the co-authors (Dr. S. Glasson, Wyeth Research, USA) who were familiar with the model and could relate the study outcomes to previous experiments. However, it would as well be interesting to see if a different method of inducing knee joint instability would lead to similar results as obtained by the collagenase model. Since this turned out not to be the case, the surgical procedure (in other words: the difference in mechanical redistribution of forces inside the joint following destabilization via collagenase or DMM) may form an explanatory factor.

Another explanation can be that the background of mice used in the study was different (129SvEv-Brd instead of C57Bl/6J in all other studies). We, as described in chapter 3 comparing C57Bl/6J to C3H/HeJ mice, and others (64,65) have shown that differences in mouse strain can lead to marked differences in study outcome. Differences in basal mechanical distribution in the joint and differences in bone turnover rate (see eg. Wise *et al*., reference 251) may therefore have caused the increased bone plate thickness in 129SvEv-Brd mice.

Lastly, it might still be possible that the observed bone plate sclerosis was preceded by initial thinning, since the time point at which sample assessment was performed was eight weeks instead of four (chapters 2, 3). Although still shorter than the 14-week follow-up period described in chapter 6, it may be that in this particular strain of mice subchondral changes occur faster compared to the early phase of bone loss. To answer this question, a longitudinal study using 129SvEv-Brd, and perhaps other inbred mouse strains, is warranted.

Besides changes in the subchondral bone plate, we also documented changes in the subchondral trabeculae. In the collagenase-induced models (chapters 2, 3, 6) trabecular bone loss was observed, although the magnitude depended on the strain that was used: in C3H/HeJ, the decrease was larger compared to C57Bl/6J. In the latter strain, the amount of trabecular bone returned to control levels due to increased osteoblast activity (chapter 6). In the DMM model however (chapter 5), no changes were observed in WT animals after DMM, whereas in ADAMTS5 knockout mice, a slight reduction in trabecular bone volume fraction (BV/TV) was observed at the medial side.

When the data discussed so far are compared to studies performed by others, we can observe some parallels. Subchondral bone loss including bone plate thinning has also been demonstrated in several other instability-related OA models using different animal

species (85,93,172,182,252-254), whereas later on in the disease process, bone gain occurred (30,94,95). It therefore appears that these subchondral bone adaptations, with initial bone loss followed by bone gain, are a general characteristic in instability-induced OA.

Subchondral bone changes in spontaneous OA

Thus far we can pose the provisional model that in instability-related OA, with progressively increasing cartilage damage, the bone changes develop in two phases, with initial subchondral bone loss, followed by bone gain later on. How does this model compare to spontaneous OA development? In chapter 5, this was studied in C57Bl/6J mice. Originally, this study was performed to find out if fast-aging trichothiodystrophy (TTD) mice, who have an accelerated bone aging phenotype (199), also had more OA compared to age-matched wild type (WT) animals. A second goal was to see if the subchondral bone plate changes (in both WT and TTD mice) would match those seen in the instability-induced mouse models. This turned out not to be the case, since the bone plate thickness in female WT C57Bl/6J mice did not change between 52 and 104 weeks of age, despite a significant increase in cartilage damage. Also in male WT mice the thickness of the plate remained intact. On the contrary, in TTD mice, the bone plate did become thinner, although the amount of cartilage damage was similar (TTD males) or even lower (TTD females) compared to WT mice. In all groups of mice, subchondral trabecular bone loss was observed.

Besides C57Bl/6J mice, only a few other spontaneous OA models are used. One of them is the Dunkin-Hartley strain of guinea pigs that develop cartilage damage from about 24 weeks of age. These animals are known to have a relatively thin subchondral bone plate and to develop sclerosis in the course of the disease (255-257). Importantly, prior to sclerosis a decrease in subchondral bone density was observed at 9 weeks of age (80), possibly indicating that in the Dunkin Hartley strain a similar mechanism of change occurs compared to instability-related OA as discussed above.

Another model organism which develops OA spontaneously, already used since the early 1970s, is the STR/ORT strain of mice. These mice start to develop OA around 26 weeks of age, eventually developing a sclerotic subchondral bone plate (258-260). However, initial thinning of the bone plate was not observed (261).

Two important problems arise when using spontaneous OA models. Firstly, the experimental variation between animals is generally larger compared to induced models, as not all OA-prone animals develop cartilage damage to the same extent (51). Secondly, no internal controls exist. Contrary to induced models, where contralateral limbs or a group of non-operated animals serve as controls, spontaneous models are compared to other strains that do not develop OA. For instance, nonarthritic CBA mice are generally used as controls for STR/ORT, and Weiser-Maple or Strain 13 guinea pigs for Dunkin Hart-

ley. These strains may differ considerably in (bio)mechanical properties compared to the spontaneous OA strain under study. When the study outcomes are compared to these controls, the relevance of the results may become questionable. For instance, when STR/ORT mice were compared with their non-OA counterparts instead of CBA mice as control, entirely different results were obtained (262). In this respect, the TTD mouse model, with its background equal to WT C57Bl/6J mice, holds a good internal control. Since female TTD mice are somehow protected from cartilage damage, further research on the exact cause of this protection is warranted. Although not extensively studied here, an interesting note in this respect is that TTD mice remain very lean throughout life, whereas an OA prone strain such as STR/ORT becomes obese (263). As stated in chapter 5, OA and obesity are linked. It is therefore tempting to speculate that adipose tissue, and in particular adipokines including, but not restricted to, leptin may form a mechanistic cause in the development of spontaneous OA (225-227,264). In this respect it is interesting to study OA development in TTD mice crossed with obese ob/ob mice. This substrain (TTD/ob) is already generated and available within the Erasmus MC for further studies.

Subchondral bone changes in clinical studies

How do the present results relate to findings in clinical studies, especially with respect to the proposed model of increased osteoclastic activation and initial subchondral bone loss? After all, subchondral sclerosis remains one of the OA hallmarks. To answer this question, our data must be compared to reports featuring mild OA patients, since in the animal models bone loss only occurred in early stages of OA. Karvonen *et al.* indeed showed that mild OA patients had lower subchondral bone mineral density (265). Another study by Bolbos *et al.* also demonstrated that patients with mild knee OA (K&L grades of 1 or 2) had subchondral trabecular bone loss prior to loss of cartilage, although morphological alterations in the latter were already present (266). Whether this early decrease in subchondral bone is (in part) due to subchondral bone marrow lesion (BML) formation (267) remains to be determined.

Also in more advanced stages of OA, subchondral bone loss could be demonstrated, albeit less generalized and most likely reflecting an increased bone turnover. Using peripheral quantitative computed tomography (pQCT), Bennell *et al.* found that some subchondral regions of the tibia of moderate OA patients (K&L score =3) had less trabecular bone compared to healthy controls, especially localized below less affected or unaffected cartilage compartments (268). Other regions however had more subchondral bone. Besides local changes, a generalized increase in bone resorption has also been described (110,239,269), although in the OA joint itself bone loss was limited (270). The increased bone loss was outcompeted by a parallel increase in bone formation (69), raising the net amount of bone in the OA joint (110).

Although the abovementioned data indicates parallels between our data and data from clinical studies, not all studies found a volumetric subchondral bone difference between mild OA patients and controls (102). To explain these differences, it may therefore also be important to look at the starting amount and architecture of subchondral bone. Recently, a prospective study by Doré *et al.* indicated that cartilage defects progressed in patients with high baseline subchondral bone BMD (271), indicating that high subchondral BMD in itself may be a risk factor for OA. In Chapter 3, we attempted to study this using mice with high and low bone mass phenotypes. Although we did not find a difference in overall cartilage damage, focal cartilage loss at the posterior side was significantly higher in high bone mass mice.

To conclude, there is certainly evidence from clinical studies to support the order of events we proposed, in which subchondral bone loss precedes subchondral sclerosis. However, more prospective patient data will be necessary to confirm this hypothesis.

MEANS OF CROSSTALK BETWEEN SUBCHONDRAL BONE AND CARTILAGE

A long-standing question regarding the osteochondral interface is whether articular cartilage and subchondral bone are able to influence each other's metabolism. This question becomes even more prominent since today OA is more widely regarded as a whole-organ disease, where interactions between different tissue types occur. Several *in vitro* studies already described effects of OA osteoblasts on articular cartilage and *vice versa* (130,133,134,272,273), but it is unclear if these influences also take place *in vivo*. As described in chapter 6, small molecules are able to reach the articular cartilage via the subchondral bone plate, probably via plate perforations connecting the subchondral bone marrow with the articular cartilage. The presence of these perforations (or subchondral bone resorption pits) is a normal property of the subchondral bone plate and is caused by osteoclastic invasion of the calcified cartilage. Importantly, their number correlates with the amount of cartilage damage in OA (120). We now demonstrated the dynamic appearance of these perforations, increasing in early stages of instability-induced OA, due to a localized osteoclastic invasion towards the subchondral bone plate, and decreasing thereafter. Since these perforations seem to form a common denominator of both clinical and pre-clinical OA, it would be interesting to know which process drives the osteoclastic induction that leads to the increase in bone plate perforations. To answer this question, it may be instructive to look at other processes where osteoclasts are active. For instance, in growth plate biology and endochondral bone formation, it is known that (chondro-)osteoclasts pave the way for vascular invasion that eventually leads to calcification of a cartilaginous matrix. In OA, a similar process takes place. In an extensive study on OA femoral heads already published in 1953, Harrison and co-workers noted

increased invasion of subchondral vasculature and noted that 'the stimulus to vessel growth and invasion is the same in all these cases- namely cartilage damage.' (274). Since then, preclinical as well as clinical data have confirmed this observation (30,275-277). In our studies we also found evidence in support of these findings (note the erythrocyte presence in figure 5C, Chapter 6). Thus, if osteoclasts also pave the way for blood vessel formation inside subchondral bone plate perforations, what would attract them? An obvious candidate for this task would be vascular endothelial growth factor (VEGF), a 46 to 48 kD glycoprotein involved both in *de novo* formation of blood vessels, a process called angiogenesis, and as chemoattractant for osteoclasts (278,279). VEGF also promotes survival of both osteoclasts (280,281) and osteoblasts (282). The source of VEGF may come from OA chondrocytes in reaction to mechanical stress (283,284) but also through stimulation by factors such as IL-1, IL-17, TNFα or TGFβ (285-287), or chemicals such as iodoacetate (288). Recently, Fransès *et al.* found that chondrocytic expression of VEGF was associated with greater chondropathy and with higher vascular density in non-calcified cartilage (289).

Blocking VEGF signaling leads to impaired angiogenesis and endochondral bone formation (290,291), and VEGF inhibitors may therefore qualify for a new class of disease modifying OA drugs. FDA-approved VEGF inhibitors are available and have the potential to repair osteochondral defects (292). An alternative strategy may come from inhibiting yet another growth factor, Nerve Growth Factor (NGF). Classically known to induce the growth of neuronal fibers, this neurotroph is also able to regulate VEGF expression in a variety of cell types (293-297). NGF is overexpressed in many inflammatory and degenerative rheumatic diseases among which osteoarthritis (298). Interestingly, NGF expression has also been demonstrated in subchondral bone plate perforations (276). Currently, phase II and III clinical trials using an anti-NGF antibody (Tanezumab, Pfizer) are ongoing (299). Since this compound is administered systemically, it is as yet unknown if local concentrations are high enough to exert an effect. In order to inhibit changes in the subchondral bone plate, a future challenge may be to locally deliver these inhibitors to the subchondral bone.

A WORKING HYPOTHESIS OF EARLY SUBCHONDRAL BONE CHANGES IN OA

Following the discussion above we would like to propose a hypothesis of one possible mechanism whereby subchondral bone changes may contribute to initiation and progression of osteoarthritis (figure 1).

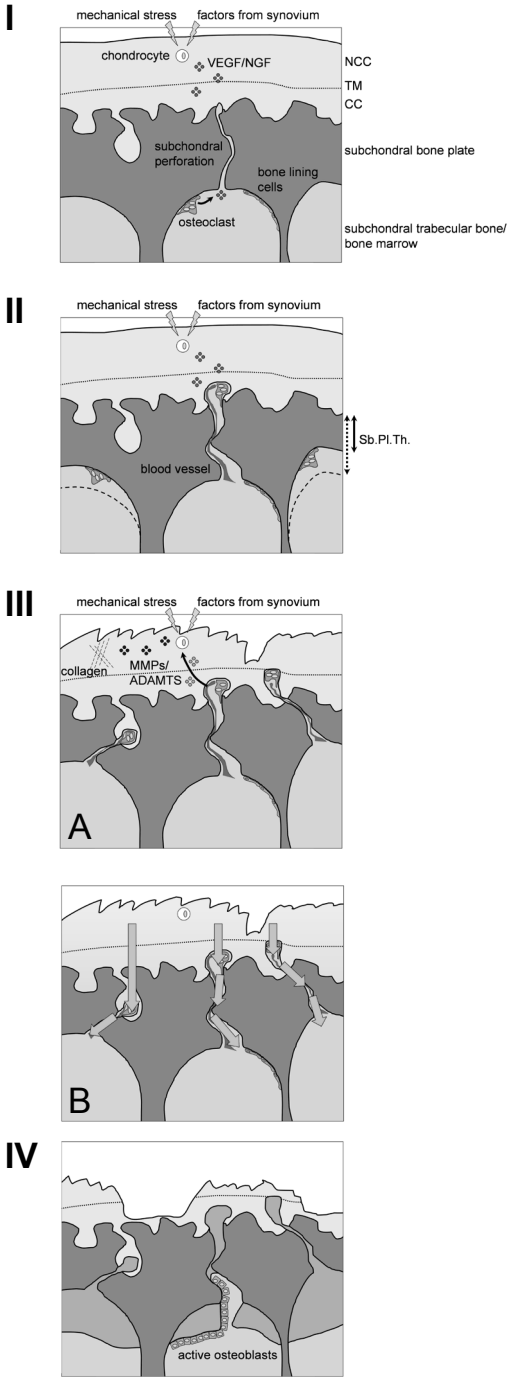

Phase I: occurence of the earliest changes, where an instability-inducing stimulus (in our case the chemical or surgical destabilization of the knee joint, or in aging-related osteoarthritis perhaps degeneration of the joint musculature) causes increased mechanical stress on the articular chondrocytes. These cells then start to produce angiogenic factors such as VEGF and/or NGF. Via normally present subchondral bone plate perforations, these growth factors reach osteoclasts residing in the subchondral bone.

Phase II: the osteoclasts follow the chemotactic gradient towards the chondrocytes, creating subchondral bone plate perforations in the process and decreasing subchondral bone plate thickness (Sb.Pl.Th.). In addition, newly formed blood vessels start to grow inside the plate perforations.

Phase III: with time progressing, more vessel-containing subchondral perforations are formed and enhanced crosstalk between subchondral bone and articular cartilage commences: bone-derived factors (depicted green) stimulate chondrocytes to produce matrix metalloproteinases and/or 'a disintegrin and metalloproteinase with a thrombospondin type 1 motif' (MMPs/ADAMTS, depicted blue) which destroy the collageneous structure of the cartilage extracellular matrix. Consequential, the first visual damage starts to appear (Phase IIIa). In addition, since the destruction of the cartilage matrix causes loss of the water-retaining GAGs, the articular cartilage loses fluid through the plate perforations with each mechanical compression (Phase IIIb, blue arrows). Without sufficient amounts of fluid the cartilage can no longer aptly withstand mechanical pressure, and is further degraded.

Phase IV: in the last phase, active osteoblasts, stimulated by the increased osteoclast activity and/or (growth) factors derived from the damaged cartilage, start to fill the bone plate perforations with newly formed, but poorly organized woven bone, and cause subchondral bone plate sclerosis in end-stage disease.

Figure 1. Hypothetical model of changes in cartilage and subchondral bone that may contribute to initiation and progression of osteoarthritis. VEGF= vascular endothelial growth factor, NGF= nerve growth factor, NCC= non-calcified cartilage, TM= tidemark, CC= calcified cartilage.

FUTURE PERSPECTIVES

In this thesis we have studied subchondral bone alterations in osteoarthritis. Using instability-induced models, we showed that the subchondral bone plate is subjected to considerable change during the course of this disease. However, these models may still not truly reflect the human situation, where in the majority of cases OA evolves more slowly and at later age. Our study in spontaneously aging C57Bl/6J mice unfortunately could not confirm the results found in the instability-induced models, however it should be kept in mind that only two time points were studied and that longitudinal follow-up over an extended time period may yield a different outcome.

We devised an order-of-events hypothesis in which osteoclasts plays a central role. Therefore, an alternative method of preventing these changes from happening is to inhibit osteoclast function. Several pre-clinical studies using bisphosphonates or calcitonin (167,169,170,172,300,301) have already indicated that this indeed reduces OA symptoms and clinical studies using these compounds are now in progress (299).

Micro-CT imaging is now a standard technique to assess the bone phenotype of human samples and the use of non-invasive imaging modalities such as pQCT (268) and MRI (37,266) is increasing. Recently, 3D bone density measurements of the subchondral bone plate in predominantly mild OA cases showed local increases in stiffness (302), which may finally confirm Radin's theory devised more than two decades ago (72). However, one major problem in clinical studies remains that the earliest changes are difficult to monitor, because of ethical boundaries with respect to the invasiveness of the monitoring technique, or simply because an OA patient may only seek help once complaints (usually pain) start to occur. It is then too late to trace back which changes preceded the deformation of the different tissues, which is important to identify which tissue type showed the earliest changes. Since prospective clinical studies are time-consuming and therefore expensive, it is here that animal models of OA are of great value. Whether OA is induced or develops spontaneously, the disease process can be precisely monitored, including its early stages. In addition, bodily fluids such as urine and blood are readily available, and can be collected longitudinally which is important to identify new early OA markers. We therefore expect that animal models of OA are still an essential tool to study the process of OA in the near future. Still, the number of longitudinal pre-clinical studies in the OA field is rather small. These studies are important for several reasons. Firstly, to better assess how changes in one tissue can exert changes elsewhere in the joint. Also, they may aid in answering the question whether subchondral bone changes precede cartilage changes or *vice versa*, and therefore, which tissue type should be targeted for intervention. Finally, but ethically important, the number of animals used in a longitudinal experiment can be reduced, while the statistical power of the study will increase since comparisons between time points are paired. Image registration

techniques make it able to detect small changes within the same animal which may not be as obvious when comparing different animals at consecutive time points.

A further recommendation may be to study a large variety of subchondral bone phenotypes. As we have shown in chapter 2, differences in the amount of subchondral bone and the thickness of the subchondral bone plate may yield considerably different results. Preferably, these studies should be conducted using a uniform strain background, using targeted, tissue-specific deletion of genes, causing for instance an increased bone phenotype. Likewise, different articular cartilage volume may be as important. These differences are set already early in life (303) and may also play a role in the ability of the tissue to withstand a changed mechanical and/or biochemical environment later on. Early monitoring of these models, preferably using a wide choice of imaging modalities (304) will have the highest potential to unravel the complex interactions that exist between subchondral bone and articular cartilage.

Summary

Osteoarthritis (OA), a disease in which normal functioning of a joint becomes impaired, forms the leading cause of chronic disability in the Western world. The term 'osteo' in OA points to the involvement of bone in the disease. During OA development, the subchondral bone that is located underneath the articular cartilage undergoes a pathological remodeling process leading to sclerosis. Specifically, the subchondral bone plate, bordering the calcified cartilage, becomes thicker. However, how the subchondral bone changes in the early stages of OA remains elusive. This process can be monitored in small laboratory animals such as mice, in both (controlled) induced as well as in spontaneously developed OA. Therefore, in this thesis we set out to answer the following question: *How do the skeletal alterations develop in the subchondral bone of the murine knee joint during the osteoarthritis disease process?*

Since the technique of choice to study these bone changes would be micro-computed tomography (micro-CT), our first task was to assess if micro-CT is indeed a suitable technique to detect early changes in the subchondral bone structure of murine joints. The findings in **Chapter 2** show that this is indeed the case. By injecting bacterial collagenase in the intra-articular space of murine knee joints, OA can be induced. Four weeks after this injection we found that the subchondral bone plate became thinner compared to contralateral control joints, and that the amount of subchondral trabecular bone was consistently reduced in all studied mice. These findings indicated that perhaps prior to sclerosis, a period of bone loss takes place first.

Next, we wanted to know if the same bone changes occur when either the initial subchondral bone phenotype or articular cartilage phenotype would differ. Therefore, in **Chapter 3**, we described which subchondral bone changes took place in two mouse strains, C57Bl/6J mice having a thin subchondral bone plate, and C3H/HeJ mice having a thick subchondral bone plate. Again using the collagenase model, we found that although both strains developed cartilage damage to a comparable extent, the location of damage on the tibial plateau differed significantly: C57Bl/6J mice had most damage at the lateral side, whereas in C3H/HeJ mice the medial side was more affected, with high focal damage. Nevertheless, overall thinning of the subchondral bone plate was found in both strains, as well as a reduction in subchondral trabecular bone volume, the latter more pronounced in C3H/HeJ mice. In addition, actively resorbing osteoclasts were found at to the bottom of the subchondral bone plate in both strains, creating perforations through the plate.

The effect of a modified articular cartilage phenotype on changes in the subchondral bone was studied in **Chapter 4**, where mice were examined that lack A Disintegrin And Metalloproteinase with ThromboSpondin-like motif type 5, or ADAMTS5 in short. Since ADAMTS5 is able to cleave aggrecan, absence of this protein significantly reduced the amount of cartilage damage after destabilization of the medial meniscus (DMM) compared to wild type (WT) knee joints. When we assessed the subchondral bone changes eight weeks after applying this surgical model, we found that in both genotypes the subchondral bone plate after DMM had become thicker compared to the contralateral control joints. In line with this, DMM joints of WT animals did not have more subchondral osteoclasts compared to the contralateral control joints, possibly reflecting that the osteoclast activation found in our previous studies had already ended. Importantly, the percentage increase in bone plate thickness in the DMM joints of ADAMTS5 knockout animals was significantly less compared to WT animals. Since ADAMTS5 knockout animals also developed less cartilage damage after DMM, this suggests that the amount of cartilage damage and the thickness of the subchondral bone plate may somehow be related.

So far we only focused on models in which OA was induced by creating joint instability. Since we wanted to know if the current results would also hold for spontaneous OA, **Chapter 5** describes a study in which cartilage damage and subchondral bone changes were examined in old-age mice. Besides WT C57Bl/6J mice, we also examined mice with an accelerated aging phenotype. These genetically modified mice contain a mutated form of the protein Xeroderma Pigmentosum group D (XPD), which serves a function both in the repair of daily sustained DNA damages as well as in basal cellular transcription. As result of this mutation, these mice suffer from the premature aging syndrome trichothiodystrophy (TTD). Not only do TTD mice die prematurely, during life they also develop a range of aging characteristics which are normally obtained much later. We measured the thickness of the subchondral bone plate at two time points in the lives of both genotypes, at 52 and 104 weeks of age. In WT mice we did not observe a thickness change despite significant increases in cartilage damage and osteophytosis. In TTD mice the subchondral bone plate did become thinner relative to WT mice, but unexpectedly OA development was generally reduced. This reduced pathology had previously been described for other tissues in TTD mice as well, which, like cartilage, lack blood vessel presence. We therefore theorized that our findings may be explained because of reduced levels of DNA damaging reactive oxygen species (ROS) in the the low-oxygen containing articular cartilage of both WT and TTD animals, whereas other, vascularized tissues produce higher levels of ROS that promote aging. Combined with an activated 'survival response', triggered by increased cellular stress in the rest of the body, cartilage damage may further be prevented.

These findings may reflect that spontaneous subchondral OA changes develop differently compared to induced changes. Because of the relative high ages studied, other bone remodeling events such as osteoporosis may also start to play a role. To unravel these processes, a longitudinal approach would be necessary, which is time consuming because of the extended time span of follow up. In **Chapter 6** we therefore returned to our induced collagenase model, and studied subchondral bone changes in WT mice over a 14-week period. Following joint destabilization, we again found that the subchondral bone plate became thinner due to increased local osteoclast presence. However, at four weeks this was followed by increased osteoblast activity, and at ten weeks the bone plate thickness returned to the level of the contralateral control joints. Furthermore, the initial phase of bone loss caused the subchondral bone plate to become so thin that increased numbers of perforations appeared which may form a direct route for (bidirectional) crosstalk between the articular cartilage and the subchondral bone.

Finally, in **Chapter 7**, we highlighted the most important finding with regard to subchondral bone changes in induced and spontaneous OA, and attempted to relate our findings to clinical studies. Contrary to the clinically observed subchondral sclerosis, considered as a typical OA characteristic, we found subchondral bone plate thinning as one of the main outcomes of our studies. However, subchondral bone plate thinning, as well as the formation of subchondral bone plate perforations, have also been found in a number of other (pre-)clinical studies as part of an early subchondral bone response. Importantly, some studies also found blood vessels to be present inside the plate perforations. We therefore hypothesize that (over)loading and/or cartilage damage leads to an increased expression of angiogenic factors such as VEGF in the deep cartilage layer, thereby triggering a dynamic subchondral remodeling process that involves osteoclast infiltration and neovascularization. This hypothesis has yet to be confirmed by future research.

Samenvatting

Artrose, een ziekte waarin het normaal functioneren van een gewricht sterk vermindert, is de hoofdoorzaak van blijvende invaliditeit in de Westerse maatschappij. In het Engels wordt artrose aangeduid als 'osteoarthritis'. De term 'osteo' hierin verwijst naar de betrokkenheid van bot in de ziekte. Het direct onder het kraakbeen gelegen subchondrale bot ondergaat gedurende het ziekteproces een pathologisch proces van remodellering, uiteindelijk leidend tot sclerose. Specifieker gezegd, de subchondrale botplaat, grenzend aan de gecalcificeerde kraakbeenlaag, wordt dikker. Hoe het subchondrale bot verandert in de vroege stadia van artrose is echter nog grotendeels onduidelijk. Dit proces kan bestudeerd worden in kleine proefdieren zoals de muis, waarin artrose kan worden geïnduceerd maar zich ook spontaan kan ontwikkelen. In dit proefschrift wilden we daarom de volgende vraag beantwoorden: *Hoe ontwikkelen skeletveranderingen zich in het subchondrale bot van het kniegewricht van de muis tijdens het ziekteverloop van artrose?*

Omdat we ervoor kozen om deze botveranderingen te bestuderen met micro-computer tomografie (micro-CT), was onze eerste taak om vast te stellen of de micro-CT techniek inderdaad geschikt is om vroege veranderingen te detecteren in de subchondrale botstructuur van muizengewrichten. De bevindingen in **Hoofdstuk 2** laten zien dat dit inderdaad het geval is. Door bacterieel collagenase te injecteren in de intra-articulaire knieholte van muizen kan artrose worden geïnduceerd. Vier weken na deze injectie vonden we dat de subchondrale botplaat dunner was geworden vergeleken met de contralaterale controlegewrichten, en dat tevens de hoeveelheid subchondraal trabeculair bot in alle bestudeerde dieren verlaagd was. Deze bevindingen geven aan dat voorafgaand aan de ontwikkeling van sclerose mogelijk eerst een periode van botverlies plaatsvindt.

Hierna wilden we weten of dezelfde botveranderingen zouden worden waargenomen als het initiële subchondrale botfenotype, of het kraakbeenfenotype, anders zou zijn. In **Hoofdstuk 3** hebben we daarom beschreven welke subchondrale botveranderingen zich voordeden in twee muizenlijnen, C57Bl/6J muizen met een dunne subchondrale botplaat, en C3H/HeJ muizen met een dikke subchondrale botplaat. Na wederom het collagenase model toegepast te hebben vonden we dat beide lijnen weliswaar een vergelijkbare hoeveelheid kraakbeenschade ontwikkelden, maar dat de locatie van deze schade op het gewrichtsoppervlak van de tibia sterk verschilde: C57Bl/6J muizen hadden de meeste schade aan de laterale zijde, terwijl bij C3H/HeJ muizen de mediale kant

meer was aangedaan, waarbij hoge focale schade werd waargenomen. Niettemin werd in beide lijnen een verdunning van de subchondrale botplaat waargenomen, naast een vermindering van de hoeveelheid subchondraal trabeculair bot, dit laatste met name in C3H/HeJ muizen. Tevens werden in beide lijnen actief resorberende osteoclasten waargenomen op de onderzijde van de subchondrale botplaat, die perforaties door de plaat veroorzaakten.

Het effect van een gemodificeerd kraakbeenfenotype op de veranderingen in het subchondrale bot werd onderzocht in **Hoofdstuk 4**, waar muizen werden bestudeerd die 'A Disintegrin And Metalloproteinase with ThromboSpondin-like motif type 5', afgekort tot ADAMTS5, misten. Omdat aggrecan door ADAMTS5 kan worden gekliefd, leidt het afwezig zijn van dit eiwit tot een significante vermindering van de hoeveelheid kraakbeenschade na destabilisatie van de mediale meniscus (DMM), vergeleken met kniegewrichten van wildtype (WT) dieren. Toen we acht weken na toepassing van dit chirurgische model vaststelden welke subchondrale botveranderingen hadden plaatsgevonden, vonden we dat in beide genotypen de subchondrale plaat na DMM dikker was geworden dan in de contralaterale controlegewrichten. Hierop aansluitend vonden we dat de hoeveelheid subchondrale osteoclasten in DMM gewrichten van WT dieren niet verhoogd was vergeleken met de contralaterale controlegewrichten, er mogelijk op duidend dat de osteoclast activatie gevonden in onze eerdere studies al had plaatsgevonden. Een belangrijk aspect was dat de procentuele toename in botplaatdikte in DMM gewrichten van ADAMTS5 knockout dieren significant minder was vergeleken met de WT dieren. Omdat ADAMTS5 knockout dieren ook minder kraakbeenschade ontwikkelden na DMM suggereert deze bevinding dat de hoeveelheid kraakbeenschade en de dikte van de subchondrale plaat op de een of andere manier aan elkaar gerelateerd zouden kunnen zijn.

Tot nu toe lag onze focus op modellen waarin artrose werd geïnduceerd door het veroorzaken van gewrichtsinstabiliteit. Omdat we wilden weten of de tot dan toe verkregen resultaten ook van toepassing zouden zijn in het geval van spontane artrose, beschrijven we in **Hoofdstuk 5** een studie waarin kraakbeenschade en subchondrale botveranderingen onderzocht werden in oude muizen. Naast WT C57Bl/6J muizen hebben we ook muizen onderzocht met een versneld verouderingsfenotype. Deze genetisch gemodificeerde muizen hebben een gemuteerde vorm van het eiwit Xeroderma Pigmentosum group D (XPD), dat zowel een functie vervult in het herstel van dagelijks opgelopen DNA schades alsook in basale cellulaire transcriptie. Als gevolg van deze mutatie lijden deze muizen aan het versneld verouderingssyndroom trichothiodystrofie (TTD). Niet alleen sterven TTD muizen voortijdig, ze ontwikkelen gedurende hun leven ook vele verouderingskenmerken die zich normaliter pas veel later openbaren. We maten de dikte van de subchondrale botplaat op twee tijdpunten in het leven van beide genotypen, op een leeftijd van 52 en 104 weken oud. In de WT muizen zagen we geen

dikteverandering, ondanks een significante toename in kraakbeenschade en osteofytvorming. In de TTD muizen werd de subchondrale botplaat wel dunner vergeleken met de WT muizen, maar onverwachts bleek de ontwikkeling van artrose over het algemeen verminderd te zijn. Deze vermindering in pathologie was eerder beschreven voor andere weefsels van TTD muizen, die net als kraakbeen geen bloedvaten bevatten. We theoriseerden daarom dat onze bevindingen verklaard zouden kunnen worden doordat het laag-zuurstof bevattende articulaire kraakbeen van zowel WT als TTD dieren een relatief lage hoeveelheid DNA-beschadigende reactieve zuurstof radicalen (eng.: *reactive oxygen species*, ROS) produceert, terwijl andere, gevascullariseerde weefsels grotere hoeveelheden ROS aanmaken die veroudering bevorderen. Gecombineerd met een geactiveerde 'overlevingsrespons', veroorzaakt door verhoogde cellulaire stress in de rest van het lichaam zou verdere kraakbeenschade voorkomen kunnen worden.

Deze bevindingen geven weer dat spontane subchondrale artrotische veranderingen wellicht anders verlopen dan geïnduceerde veranderingen. Daarnaast zouden gezien de relatief hoge leeftijd van de bestudeerde muizen andere botremodellerings-processen zoals osteoporose ook een rol kunnen beginnen te spelen. Om deze processen op te helderen is een longitudinale aanpak noodzakelijk, deze is echter tijdrovend gezien de zeer lange tijdsspanne van follow-up. Daarom keerden we in **Hoofdstuk 6** terug naar ons geïnduceerde collagenase model, en gedurende een periode van 14 weken onderzochten we subchondrale botveranderingen in WT muizen. Na gewrichtsdestabilisatie vonden we opnieuw dat de subchondrale plaat dunner werd door een lokale verhoging van de hoeveelheid aanwezige osteoclasten. Echter, na vier weken werd dit opgevolgd door een verhoogde osteoblast activiteit, en na tien weken keerde de botplaatdikte terug naar het niveau van de contralaterale controles. De initiële fase van botverlies zorgde er tevens voor dat de subchondrale botplaat zo dun werd dat verhoogde aantallen perforaties verschenen die wellicht een directe route zouden kunnen vormen voor (bidirectionele) *crosstalk* tussen het articulaire kraakbeen en het subchondrale bot.

Tot slot hebben we in **Hoofdstuk 7** de belangrijkste bevindingen uitgelicht met betrekking tot subchondrale botveranderingen in geïnduceerde en spontane artrose, en geprobeerd om onze bevindingen te relateren aan klinische studies. In tegenstelling tot de klinisch waargenomen subchondrale sclerose, welke beschouwd wordt als typisch artrose kenmerk, vonden we subchondrale botplaat verdunning als een van de belangrijkste uitkomsten uit onze studies. Echter, subchondrale botplaat verdunning alsmede de vorming van subchondrale botplaat perforaties werd ook gevonden in een aantal andere (pre-)klinische studies als onderdeel van een vroege subchondrale botrespons. Daarnaast toonden sommige studies ook aan dat zich in de plaatperforaties bloedvaten bevonden. We hypothetiseren daarom dat (over)belasting en/of kraakbeenschade leidt tot een verhoogde expressie van angiogene factoren zoals VEGF in de diepe kraakbeenlaag, welke een dynamisch subchondraal remodelleringsproces veroorzaakt

gepaard gaand met osteoclast infiltratie en neovascularisatie. Deze hypothese zal door toekomstig onderzoek nog moeten worden bevestigd.

References

1. Bondeson J, Blom AB, Wainwright S, Hughes C, Caterson B, Van den Berg WB. The role of synovial macrophages and macrophage-produced mediators in driving inflammatory and destructive responses in osteoarthritis. Arthritis Rheum 2010;62:647-57.
2. Clockaerts S, Bastiaansen-Jenniskens YM, Runhaar J, Van Osch GJ, Van Offel JF, Verhaar JA et al. The infrapatellar fat pad should be considered as an active osteoarthritic joint tissue: a narrative review. Osteoarthritis Cartilage 2010;18:876-82.
3. Tan AL, Grainger AJ, Tanner SF, Shelley DM, Pease C, Emery P et al. High-resolution magnetic resonance imaging for the assessment of hand osteoarthritis. Arthritis Rheum 2005;52:2355-65.
4. Hurley MV. The role of muscle weakness in the pathogenesis of osteoarthritis. Rheum Dis Clin North Am 1999;25:283-98, vi.
5. Brandt KD, Radin EL, Dieppe PA, Van de Putte L. Yet more evidence that osteoarthritis is not a cartilage disease. Ann Rheum Dis 2006;65:1261-4.
6. Peterfy CG, Guermazi A, Zaim S, Tirman PF, Miaux Y, White D et al. Whole-Organ Magnetic Resonance Imaging Score (WORMS) of the knee in osteoarthritis. Osteoarthritis Cartilage 2004;12:177-90.
7. McGonagle D, Tan AL, Carey J, Benjamin M. The anatomical basis for a novel classification of osteoarthritis and allied disorders. J Anat 2010;216:279-91.
8. Day JS, Van der Linden JC, Bank RA, Ding M, Hvid I, Sumner DR et al. Adaptation of subchondral bone in osteoarthritis. Biorheology 2004;41:359-68.
9. Karsdal MA, Leeming DJ, Dam EB, Henriksen K, Alexandersen P, Pastoureau P et al. Should subchondral bone turnover be targeted when treating osteoarthritis? Osteoarthritis Cartilage 2008;16:638-46.
10. Alcaraz MJ, Megias J, Garcia-Arnandis I, Clerigues V, Guillen MI. New molecular targets for the treatment of osteoarthritis. Biochem Pharmacol 2010;80:13-21.
11. Zhang Y, Jordan JM. Epidemiology of osteoarthritis. Rheum Dis Clin North Am 2008;34:515-29.
12. Cheung PP, Gossec L, Dougados M. What are the best markers for disease progression in osteoarthritis (OA)? Best Pract Res Clin Rheumatol 2010;24:81-92.
13. Van Meurs JB, Bierma-Zeinstra SM, and Uitterlinden AG. RIVM: Nationaal Kompas Volksgezondheid, www.nationaalkompas.nl/gezondheid-en-ziekte/ziekten-en-aandoeningen/bewegingsstelsel-en-bindweefsel/artrose/artrose-samengevat/. 2010
14. Shane AA, Loeser RF. Why is osteoarthritis an age-related disease? Best Pract Res Clin Rheumatol 2010;24:15-26.
15. Kellgren JH, LAWRENCE JS. Radiological assessment of osteo-arthrosis. Ann Rheum Dis 1957;16:494-502.
16. Wenham CY, Conaghan PG. Imaging the painful osteoarthritic knee joint: what have we learned? Nat Clin Pract Rheumatol 2009;5:149-58.

17. Mankin HJ, Dorfman H, Lippiello L, Zarins A. Biochemical and metabolic abnormalities in articular cartilage from osteo-arthritic human hips. II. Correlation of morphology with biochemical and metabolic data. J Bone Joint Surg Am 1971;53:523-37.
18. Pritzker KP, Gay S, Jimenez SA, Ostergaard K, Pelletier JP, Revell PA et al. Osteoarthritis cartilage histopathology: grading and staging. Osteoarthritis Cartilage 2006;14:13-29.
19. Pfander D, Gelse K. Hypoxia and osteoarthritis: how chondrocytes survive hypoxic environments. Curr Opin Rheumatol 2007;19:457-62.
20. Ferguson VL, Bushby AJ, Boyde A. Nanomechanical properties and mineral concentration in articular calcified cartilage and subchondral bone. J Anat 2003;203:191-202.
21. Burr DB. Anatomy and physiology of the mineralized tissues: role in the pathogenesis of osteoarthrosis. Osteoarthritis Cartilage 2004;12 Suppl A:S20-S30.
22. Wang F, Ying Z, Duan X, Tan H, Yang B, Guo L et al. Histomorphometric analysis of adult articular calcified cartilage zone. J Struct Biol 2009;168:359-65.
23. Henrotin Y, Pesesse L, Sanchez C. Subchondral bone in osteoarthritis physiopathology: state-of-the art and perspectives. Biomed Mater Eng 2009;19:311-6.
24. Lyons TJ, McClure SF, Stoddart RW, McClure J. The normal human chondro-osseous junctional region: evidence for contact of uncalcified cartilage with subchondral bone and marrow spaces. BMC Musculoskelet Disord 2006;7:52.
25. Madry H, Van Dijk CN, Mueller-Gerbl M. The basic science of the subchondral bone. Knee Surg Sports Traumatol Arthrosc 2010;18:419-33.
26. Hwang J, Bae WC, Shieu W, Lewis CW, Bugbee WD, Sah RL. Increased hydraulic conductance of human articular cartilage and subchondral bone plate with progression of osteoarthritis. Arthritis Rheum 2008;58:3831-42.
27. Duncan H, Jundt J, Riddle JM, Pitchford W, Christopherson T. The tibial subchondral plate. A scanning electron microscopic study. J Bone Joint Surg Am 1987;69:1212-20.
28. Bailey AJ, Mansell JP. Do subchondral bone changes exacerbate or precede articular cartilage destruction in osteoarthritis of the elderly? Gerontology 1997;43:296-304.
29. Burr DB. The importance of subchondral bone in osteoarthrosis. Curr Opin Rheumatol 1998;10:256-62.
30. Hayami T, Pickarski M, Zhuo Y, Wesolowski GA, Rodan GA, Duong lT. Characterization of articular cartilage and subchondral bone changes in the rat anterior cruciate ligament transection and meniscectomized models of osteoarthritis. Bone 2006;38:234-43.
31. Lajeunesse D. The role of bone in the treatment of osteoarthritis. Osteoarthritis Cartilage 2004;12 Suppl A:S34-S38.
32. Quasnichka HL, Anderson-Mackenzie JM, Bailey AJ. Subchondral bone and ligament changes precede cartilage degradation in guinea pig osteoarthritis. Biorheology 2006;43:389-97.
33. Pottenger LA, Phillips FM, Draganich LF. The effect of marginal osteophytes on reduction of varus-valgus instability in osteoarthritic knees. Arthritis Rheum 1990;33:853-8.
34. Van der Kraan PM, Van den Berg WB. Osteophytes: relevance and biology. Osteoarthritis Cartilage 2007;15:237-44.
35. Taljanovic MS, Graham AR, Benjamin JB, Gmitro AF, Krupinski EA, Schwartz SA et al. Bone marrow edema pattern in advanced hip osteoarthritis: quantitative assessment with magnetic resonance imaging and correlation with clinical examination, radiographic findings, and histopathology. Skeletal Radiol 2008;37:423-31.
36. Link TM, Steinbach LS, Ghosh S, Ries M, Lu Y, Lane N et al. Osteoarthritis: MR imaging findings in different stages of disease and correlation with clinical findings. Radiology 2003;226:373-81.

37. Crema MD, Roemer FW, Marra MD, Guermazi A. Magnetic resonance imaging assessment of subchondral bone and soft tissues in knee osteoarthritis. Rheum Dis Clin North Am 2009;35:557-77.
38. Hunter DJ, Gerstenfeld L, Bishop G, Davis AD, Mason ZD, Einhorn TA et al. Bone marrow lesions from osteoarthritis knees are characterized by sclerotic bone that is less well mineralized. Arthritis Res Ther 2009;11:R11.
39. Felson DT, Niu J, Guermazi A, Roemer F, Aliabadi P, Clancy M et al. Correlation of the development of knee pain with enlarging bone marrow lesions on magnetic resonance imaging. Arthritis Rheum 2007;56:2986-92.
40. Daheshia M, Yao JQ. The bone marrow lesion in osteoarthritis. Rheumatol Int 2010;Epub ahead of print:DOI: 10.1007/s00296-010-1454-x.
41. Lo GH, McAlindon TE, Niu J, Zhang Y, Beals C, Dabrowski C et al. Bone marrow lesions and joint effusion are strongly and independently associated with weight-bearing pain in knee osteoarthritis: data from the osteoarthritis initiative. Osteoarthritis Cartilage 2009;17:1562-9.
42. Roemer FW, Neogi T, Nevitt MC, Felson DT, Zhu Y, Zhang Y et al. Subchondral bone marrow lesions are highly associated with, and predict subchondral bone attrition longitudinally: the MOST study. Osteoarthritis Cartilage 2010;18:47-53.
43. Dieppe PA, Reichenbach S, Williams S, Gregg P, Watt I, Juni P. Assessing bone loss on radiographs of the knee in osteoarthritis: a cross-sectional study. Arthritis Rheum 2005;52:3536-41.
44. Reichenbach S, Guermazi A, Niu J, Neogi T, Hunter DJ, Roemer FW et al. Prevalence of bone attrition on knee radiographs and MRI in a community-based cohort. Osteoarthritis Cartilage 2008;16:1005-10.
45. Neogi T, Nevitt M, Niu J, Sharma L, Roemer F, Guermazi A et al. Subchondral bone attrition may be a reflection of compartment-specific mechanical load: the MOST Study. Ann Rheum Dis 2010;69:841-4.
46. Piscaer TM, Waarsing JH, Kops N, Pavljasevic P, Verhaar JA, Van Osch GJ et al. In vivo imaging of cartilage degeneration using microCT-arthrography. Osteoarthritis Cartilage 2008;16:1011-7.
47. McErlain DD, Appleton CT, Litchfield RB, Pitelka V, Henry JL, Bernier SM et al. Study of subchondral bone adaptations in a rodent surgical model of OA using in vivo micro-computed tomography. Osteoarthritis Cartilage 2008;16:458-69.
48. Morenko BJ, Bove SE, Chen L, Guzman RE, Juneau P, Bocan TM et al. In vivo micro computed tomography of subchondral bone in the rat after intra-articular administration of monosodium iodoacetate. Contemp Top Lab Anim Sci 2004;43:39-43.
49. Waarsing JH, Day JS, Van der Linden JC, Ederveen AG, Spanjers C, De Clerck N et al. Detecting and tracking local changes in the tibiae of individual rats: a novel method to analyse longitudinal in vivo micro-CT data. Bone 2004;34:163-9.
50. Yamamoto K, Shishido T, Masaoka T, Imakiire A. Morphological studies on the ageing and osteoarthritis of the articular cartilage in C57 black mice. J Orthop Surg (Hong Kong) 2005;13:8-18.
51. Ameye LG, Young MF. Animal models of osteoarthritis: lessons learned while seeking the "Holy Grail". Curr Opin Rheumatol 2006;18:537-47.
52. Kamekura S, Hoshi K, Shimoaka T, Chung U, Chikuda H, Yamada T et al. Osteoarthritis development in novel experimental mouse models induced by knee joint instability. Osteoarthritis Cartilage 2005;13:632-41.
53. Glasson SS, Blanchet TJ, Morris EA. The surgical destabilization of the medial meniscus (DMM) model of osteoarthritis in the 129/SvEv mouse. Osteoarthritis Cartilage 2007;15:1061-9.

54. Van der Kraan PM, Vitters EL, Van Beuningen HM, Van de Putte LBA, Van den Berg WB. Degenerative Knee-Joint Lesions in Mice After A Single Intraarticular Collagenase Injection - A New Model of Osteoarthritis. Journal of Experimental Pathology 1990;71:19-31.
55. Van Osch GJ, Van der Kraan PM, Van den Berg WB. Site-specific cartilage changes in murine degenerative knee joint disease induced by iodoacetate and collagenase. J Orthop Res 1994;12:168-75.
56. Guzman RE, Evans MG, Bove S, Morenko B, Kilgore K. Mono-iodoacetate-induced histologic changes in subchondral bone and articular cartilage of rat femorotibial joints: an animal model of osteoarthritis. Toxicol Pathol 2003;31:619-24.
57. Marijnissen AC, Van Roermund PM, TeKoppele JM, Bijlsma JW, Lafeber FP. The canine 'groove' model, compared with the ACLT model of osteoarthritis. Osteoarthritis Cartilage 2002;10:145-55.
58. Pfeiffer M, Pfeiffer D. Important macroscopic and microscopic differences in the bony and cartilaginous regions adjacent to the lumbar intervertebral disc between animal and man: a caveat to overinterpretation of animal experiments: comment to the article: Primary stability of anterior lumbar stabilization: interdependence of implant type and endplate retention or removal (C.H. Flamme et al.). Eur Spine J 2006;15:819-20.
59. Alini M, Eisenstein SM, Ito K, Little C, Kettler AA, Masuda K et al. Are animal models useful for studying human disc disorders/degeneration? Eur Spine J 2008;17:2-19.
60. Miyazaki T, Kobayashi S, Takeno K, Meir A, Urban J, Baba H. A phenotypic comparison of proteoglycan production of intervertebral disc cells isolated from rats, rabbits, and bovine tails; which animal model is most suitable to study tissue engineering and biological repair of human disc disorders? Tissue Eng Part A 2009;15:3835-46.
61. Joshi MD, Suh JK, Marui T, Woo SL. Interspecies variation of compressive biomechanical properties of the meniscus. J Biomed Mater Res 1995;29:823-8.
62. Kaab MJ, Gwynn IA, Notzli HP. Collagen fibre arrangement in the tibial plateau articular cartilage of man and other mammalian species. J Anat 1998;193 (Pt 1):23-34.
63. Glasson SS, Askew R, Sheppard B, Carito B, Blanchet T, Ma HL et al. Deletion of active ADAMTS5 prevents cartilage degradation in a murine model of osteoarthritis. Nature 2005;434:644-8.
64. Van Osch GJ, Van der Kraan PM, Vitters EL, Blankevoort L, Van den Berg WB. Induction of osteoarthritis by intra-articular injection of collagenase in mice. Strain and sex related differences. Osteoarthritis Cartilage 1993;1:171-7.
65. Ma HL, Blanchet TJ, Peluso D, Hopkins B, Morris EA, Glasson SS. Osteoarthritis severity is sex dependent in a surgical mouse model. Osteoarthritis Cartilage 2007;15:695-700.
66. Imhof H, Sulzbacher I, Grampp S, Czerny C, Youssefzadeh S, Kainberger F. Subchondral bone and cartilage disease: a rediscovered functional unit. Invest Radiol 2000;35:581-8.
67. Kawcak CE, McIlwraith CW, Norrdin RW, Park RD, James SP. The role of subchondral bone in joint disease: a review. Equine Vet J 2001;33:120-6.
68. Bobinac D, Spanjol J, Zoricic S, Maric I. Changes in articular cartilage and subchondral bone histomorphometry in osteoarthritic knee joints in humans. Bone 2003;32:284-90.
69. Matsui H, Shimizu M, Tsuji H. Cartilage and subchondral bone interaction in osteoarthrosis of human knee joint: a histological and histomorphometric study. Microsc Res Tech 1997;37:333-42.
70. Bruyere O, Dardenne C, Lejeune E, Zegels B, Pahaut A, Richy F et al. Subchondral tibial bone mineral density predicts future joint space narrowing at the medial femoro-tibial compartment in patients with knee osteoarthritis. Bone 2003;32:541-5.
71. Radin EL, Paul IL, Tolkoff MJ. Subchondral bone changes in patients with early degenerative joint disease. Arthritis Rheum 1970;13:400-5.

72. Radin EL, Rose RM. Role of subchondral bone in the initiation and progression of cartilage damage. Clin Orthop 1986;34-40.
73. Burr DB, Schaffler MB. The involvement of subchondral mineralized tissues in osteoarthrosis: quantitative microscopic evidence. Microsc Res Tech 1997;37:343-57.
74. Imhof H, Breitenseher M, Kainberger F, Rand T, Trattnig S. Importance of subchondral bone to articular cartilage in health and disease. Top Magn Reson Imaging 1999;10:180-92.
75. Lajeunesse D, Reboul P. Subchondral bone in osteoarthritis: a biologic link with articular cartilage leading to abnormal remodeling. Curr Opin Rheumatol 2003;15:628-33.
76. Burr DB, Radin EL. Microfractures and microcracks in subchondral bone: are they relevant to osteoarthrosis? Rheum Dis Clin North Am 2003;29:675-85.
77. Bonnet CS, Walsh DA. Osteoarthritis, angiogenesis and inflammation. Rheumatology (Oxford) 2005;44:7-16.
78. Ding M, Odgaard A, Hvid I. Changes in the three-dimensional microstructure of human tibial cancellous bone in early osteoarthritis. J Bone Joint Surg Br 2003;85:906-12.
79. Mason RM, Chambers MG, Flannelly J, Gaffen JD, Dudhia J, Bayliss MT. The STR/ort mouse and its use as a model of osteoarthritis. Osteoarthritis Cartilage 2001;9:85-91.
80. Anderson-Mackenzie JM, Quasnichka HL, Starr RL, Lewis EJ, Billingham ME, Bailey AJ. Fundamental subchondral bone changes in spontaneous knee osteoarthritis. Int J Biochem Cell Biol 2005;37:224-36.
81. Hayami T, Pickarski M, Wesolowski GA, McLane J, Bone A, Destefano J et al. The role of subchondral bone remodeling in osteoarthritis: reduction of cartilage degeneration and prevention of osteophyte formation by alendronate in the rat anterior cruciate ligament transection model. Arthritis Rheum 2004;50:1193-206.
82. Van Beuningen HM, Glansbeek HL, Van der Kraan PM, Van den Berg WB. Osteoarthritis-like changes in the murine knee joint resulting from intra-articular transforming growth factor-beta injections. Osteoarthritis Cartilage 2000;8:25-33.
83. Van Osch GJ, Blankevoort L, Van der Kraan PM, Janssen B, Hekman E, Huiskes R et al. Laxity characteristics of normal and pathological murine knee joints in vitro. J Orthop Res 1995;13:783-91.
84. Dedrick DK, Goldstein SA, Brandt KD, O'Connor BL, Goulet RW, Albrecht M. A longitudinal study of subchondral plate and trabecular bone in cruciate-deficient dogs with osteoarthritis followed up for 54 months. Arthritis Rheum 1993;36:1460-7.
85. Boyd SK, Muller R, Leonard T, Herzog W. Long-term periarticular bone adaptation in a feline knee injury model for post-traumatic experimental osteoarthritis. Osteoarthritis Cartilage 2005;13:235-42.
86. Dedrick DK, Goulet R, Huston L, Goldstein SA, Bole GG. Early bone changes in experimental osteoarthritis using microscopic computed tomography. J Rheumatol Suppl 1991;27:44-5.
87. Wachsmuth L, Engelke K. High-resolution imaging of osteoarthritis using microcomputed tomography. Methods Mol Med 2004;101:231-48.
88. Waarsing JH, Day JS, Weinans H. An improved segmentation method for in vivo microCT imaging. J Bone Miner Res 2004;19:1640-50.
89. Hildebrand T, Ruegsegger P. Quantification of Bone Microarchitecture with the Structure Model Index. Comput Methods Biomech Biomed Engin 1997;1:15-23.
90. Odgaard A, Gundersen HJ. Quantification of connectivity in cancellous bone, with special emphasis on 3-D reconstructions. Bone 1993;14:173-82.
91. Hildebrand T, Ruegsegger P. A new method for the model-independent assessment of thickness in three-dimensional images. J Microscopy 1997;185:67-75.

92. Grynpas MD, Alpert B, Katz I, Lieberman I, Pritzker KPH. Subchondral Bone in Osteoarthritis. Calcified Tissue International 1991;49:20-6.
93. Boyd SK, Matyas JR, Wohl GR, Kantzas A, Zernicke RF. Early regional adaptation of periarticular bone mineral density after anterior cruciate ligament injury. J Appl Physiol 2000;89:2359-64.
94. Batiste DL, Kirkley A, Laverty S, Thain LM, Spouge AR, Holdsworth DW. Ex vivo characterization of articular cartilage and bone lesions in a rabbit ACL transection model of osteoarthritis using MRI and micro-CT. Osteoarthritis Cartilage 2004;12:986-96.
95. Pastoureau PC, Chomel AC, Bonnet J. Evidence of early subchondral bone changes in the meniscectomized guinea pig. A densitometric study using dual-energy X-ray absorptiometry subregional analysis. Osteoarthritis Cartilage 1999;7:466-73.
96. Bailey AJ, Mansell JP, Sims TJ, Banse X. Biochemical and mechanical properties of subchondral bone in osteoarthritis. Biorheology 2004;41:349-58.
97. Lavigne P, Benderdour M, Lajeunesse D, Reboul P, Shi Q, Pelletier JP et al. Subchondral and trabecular bone metabolism regulation in canine experimental knee osteoarthritis. Osteoarthritis Cartilage 2005;13:310-7.
98. Mansell JP, Bailey AJ. Abnormal cancellous bone collagen metabolism in osteoarthritis. J Clin Invest 1998;101:1596-603.
99. O'Connor BL, Visco DM, Heck DA, Myers SL, Brandt KD. Gait alterations in dogs after transection of the anterior cruciate ligament. Arthritis Rheum 1989;32:1142-7.
100. Clarke KA, Heitmeyer SA, Smith AG, Taiwo YO. Gait analysis in a rat model of osteoarthrosis. Physiol Behav 1997;62:951-4.
101. Odding E, Valkenburg HA, Stam HJ, Hofman A. Determinants of locomotor disability in people aged 55 years and over: the Rotterdam Study. Eur J Epidemiol 2001;17:1033-41.
102. Day JS, Ding M, Van der Linden JC, Hvid I, Sumner DR, Weinans H. A decreased subchondral trabecular bone tissue elastic modulus is associated with pre-arthritic cartilage damage. J Orthop Res 2001;19:914-8.
103. Li B, Marshall D, Roe M, Aspden RM. The electron microscope appearance of the subchondral bone plate in the human femoral head in osteoarthritis and osteoporosis. J Anat 1999;195 (Pt 1):101-10.
104. Carlson CS, Loeser RF, Purser CB, Gardin JF, Jerome CP. Osteoarthritis in cynomolgus macaques. III: Effects of age, gender, and subchondral bone thickness on the severity of disease. J Bone Miner Res 1996;11:1209-17.
105. Layton MW, Goldstein SA, Goulet RW, Feldkamp LA, Kubinski DJ, Bole GG. Examination of subchondral bone architecture in experimental osteoarthritis by microscopic computed axial tomography. Arthritis Rheum 1988;31:1400-5.
106. Fahlgren A, Messner K, Aspenberg P. Meniscectomy leads to an early increase in subchondral bone plate thickness in the rabbit knee. Acta Orthop Scand 2003;74:437-41.
107. Naitou K, Kushida K, Takahashi M, Ohishi T, Inoue T. Bone mineral density and bone turnover in patients with knee osteoarthritis compared with generalized osteoarthritis. Calcif Tissue Int 2000;66:325-9.
108. Hochberg MC, Lethbridge-Cejku M, Tobin JD. Bone mineral density and osteoarthritis: data from the Baltimore Longitudinal Study of Aging. Osteoarthritis Cartilage 2004;12 Suppl A:S45-S48.
109. Hart DJ, Cronin C, Daniels M, Worthy T, Doyle DV, Spector TD. The relationship of bone density and fracture to incident and progressive radiographic osteoarthritis of the knee: the Chingford Study. Arthritis Rheum 2002;46:92-9.

110. Burger H, Van Daele PL, Odding E, Valkenburg HA, Hofman A, Grobbee DE et al. Association of radiographically evident osteoarthritis with higher bone mineral density and increased bone loss with age. The Rotterdam Study. Arthritis Rheum 1996;39:81-6.
111. Bergink AP, Uitterlinden AG, Van Leeuwen JP, Hofman A, Verhaar JA, Pols HA. Bone mineral density and vertebral fracture history are associated with incident and progressive radiographic knee osteoarthritis in elderly men and women: the Rotterdam Study. Bone 2005;37:446-56.
112. Van Osch GJ, Van der Kraan PM, Blankevoort L, Huiskes R, Van den Berg WB. Relation of ligament damage with site specific cartilage loss and osteophyte formation in collagenase induced osteoarthritis in mice. J Rheumatol 1996;23:1227-32.
113. Scheven BA, Kawilarang-De Haas EW, Wassenaar AM, Nijweide PJ. Differentiation kinetics of osteoclasts in the periosteum of embryonic bones in vivo and in vitro. Anat Rec 1986;214:418-23.
114. Chen C, Kalu DN. Strain differences in bone density and calcium metabolism between C3H/HeJ and C57BL/6J mice. Bone 1999;25:413-20.
115. Richman C, Kutilek S, Miyakoshi N, Srivastava AK, Beamer WG, Donahue LR et al. Postnatal and pubertal skeletal changes contribute predominantly to the differences in peak bone density between C3H/HeJ and C57BL/6J mice. J Bone Miner Res 2001;16:386-97.
116. Sheng MH, Lau KH, Beamer WG, Baylink DJ, Wergedal JE. In vivo and in vitro evidence that the high osteoblastic activity in C3H/HeJ mice compared to C57BL/6J mice is intrinsic to bone cells. Bone 2004;35:711-9.
117. Koller DL, Schriefer J, Sun Q, Shultz KL, Donahue LR, Rosen CJ et al. Genetic effects for femoral biomechanics, structure, and density in C57BL/6J and C3H/HeJ inbred mouse strains. J Bone Miner Res 2003;18:1758-65.
118. Akhter MP, Iwaniec UT, Covey MA, Cullen DM, Kimmel DB, Recker RR. Genetic variations in bone density, histomorphometry, and strength in mice. Calcif Tissue Int 2000;67:337-44.
119. Wang VM, Banack TM, Tsai CW, Flatow EL, Jepsen KJ. Variability in tendon and knee joint biomechanics among inbred mouse strains. J Orthop Res 2006;24:1200-7.
120. Shibakawa A, Yudoh K, Masuko-Hongo K, Kato T, Nishioka K, Nakamura H. The role of subchondral bone resorption pits in osteoarthritis: MMP production by cells derived from bone marrow. Osteoarthritis Cartilage 2005;13:679-87.
121. Frost HM. The regional acceleratory phenomenon: a review. Henry Ford Hosp Med J 1983;31:3-9.
122. Bikle DD, Halloran BP. The response of bone to unloading. J Bone Miner Metab 1999;17:233-44.
123. Squire M, Donahue LR, Rubin C, Judex S. Genetic variations that regulate bone morphology in the male mouse skeleton do not define its susceptibility to mechanical unloading. Bone 2004;35:1353-60.
124. Judex S, Garman R, Squire M, Busa B, Donahue LR, Rubin C. Genetically linked site-specificity of disuse osteoporosis. J Bone Miner Res 2004;19:607-13.
125. Amblard D, Lafage-Proust MH, Laib A, Thomas T, Ruegsegger P, Alexandre C et al. Tail suspension induces bone loss in skeletally mature mice in the C57BL/6J strain but not in the C3H/HeJ strain. J Bone Miner Res 2003;18:561-9.
126. Dedrick DK, Goulet RW, O'Connor BL, Brandt KD. Preliminary report: increased porosity of the subchondral plate in an accelerated canine model of osteoarthritis. Osteoarthritis Cartilage 1997;5:71-4.
127. Calvo E, Palacios I, Delgado E, Ruiz-Cabello J, Hernandez P, Sanchez-Pernaute O et al. High-resolution MRI detects cartilage swelling at the early stages of experimental osteoarthritis. Osteoarthritis Cartilage 2001;9:463-72.

128. Bush PG, Hall AC. The volume and morphology of chondrocytes within non-degenerate and degenerate human articular cartilage. Osteoarthritis Cartilage 2003;11:242-51.
129. Burstein D, Velyvis J, Scott KT, Stock KW, Kim YJ, Jaramillo D et al. Protocol issues for delayed Gd(DTPA)(2-)-enhanced MRI (dGEMRIC) for clinical evaluation of articular cartilage. Magn Reson Med 2001;45:36-41.
130. Nakaoka R, Hsiong SX, Mooney DJ. Regulation of chondrocyte differentiation level via co-culture with osteoblasts. Tissue Eng 2006;12:2425-33.
131. Jiang J, Nicoll SB, Lu HH. Co-culture of osteoblasts and chondrocytes modulates cellular differentiation in vitro. Biochem Biophys Res Commun 2005;338:762-70.
132. Westacott CI, Webb GR, Warnock MG, Sims JV, Elson CJ. Alteration of cartilage metabolism by cells from osteoarthritic bone. Arthritis Rheum 1997;40:1282-91.
133. Westacott C. Interactions between subchondral bone and cartilage in OA. Cells from osteoarthritic bone can alter cartilage metabolism. J Musculoskelet Neuronal Interact 2002;2:507-9.
134. Sanchez C, Deberg MA, Piccardi N, Msika P, Reginster JY, Henrotin YE. Subchondral bone osteoblasts induce phenotypic changes in human osteoarthritic chondrocytes. Osteoarthritis Cartilage 2005;13:988-97.
135. Sanchez C, Deberg MA, Piccardi N, Msika P, Reginster JY, Henrotin YE. Osteoblasts from the sclerotic subchondral bone downregulate aggrecan but upregulate metalloproteinases expression by chondrocytes. This effect is mimicked by interleukin-6, -1beta and oncostatin M pre-treated non-sclerotic osteoblasts. Osteoarthritis Cartilage 2005;13:979-87.
136. Burr DB. Increased biological activity of subchondral mineralized tissues underlies the progressive deterioration of articular cartilage in osteoarthritis. J Rheumatol 2005;32:1156-8.
137. Sandy JD, Neame PJ, Boynton RE, Flannery CR. Catabolism of aggrecan in cartilage explants. Identification of a major cleavage site within the interglobular domain. J Biol Chem 1991;266:8683-5.
138. Plaas A, Osborn B, Yoshihara Y, Bai Y, Bloom T, Nelson F et al. Aggrecanolysis in human osteoarthritis: confocal localization and biochemical characterization of ADAMTS5-hyaluronan complexes in articular cartilages. Osteoarthritis Cartilage 2007;15:719-34.
139. Sandy JD, Verscharen C. Analysis of aggrecan in human knee cartilage and synovial fluid indicates that aggrecanase (ADAMTS) activity is responsible for the catabolic turnover and loss of whole aggrecan whereas other protease activity is required for C-terminal processing in vivo. Biochem J 2001;358:615-26.
140. Lark MW, Bayne EK, Flanagan J, Harper CF, Hoerrner LA, Hutchinson NI et al. Aggrecan degradation in human cartilage. Evidence for both matrix metalloproteinase and aggrecanase activity in normal, osteoarthritic, and rheumatoid joints. J Clin Invest 1997;100:93-106.
141. Sandy JD, Flannery CR, Neame PJ, Lohmander LS. The structure of aggrecan fragments in human synovial fluid. Evidence for the involvement in osteoarthritis of a novel proteinase which cleaves the Glu 373-Ala 374 bond of the interglobular domain. J Clin Invest 1992;89:1512-6.
142. Lohmander LS, Neame PJ, Sandy JD. The structure of aggrecan fragments in human synovial fluid. Evidence that aggrecanase mediates cartilage degradation in inflammatory joint disease, joint injury, and osteoarthritis. Arthritis Rheum 1993;36:1214-22.
143. Chockalingam PS, Zeng W, Morris EA, Flannery CR. Release of hyaluronan and hyaladherins (aggrecan G1 domain and link proteins) from articular cartilage exposed to ADAMTS-4 (aggrecanase 1) or ADAMTS-5 (aggrecanase 2). Arthritis Rheum 2004;50:2839-48.
144. Kuno K, Kanada N, Nakashima E, Fujiki F, Ichimura F, Matsushima K. Molecular cloning of a gene encoding a new type of metalloproteinase-disintegrin family protein with thrombospondin motifs as an inflammation associated gene. J Biol Chem 1997;272:556-62.

145. Kuno K, Okada Y, Kawashima H, Nakamura H, Miyasaka M, Ohno H et al. ADAMTS-1 cleaves a cartilage proteoglycan, aggrecan. FEBS Lett 2000;478:241-5.
146. Tortorella MD, Burn TC, Pratta MA, Abbaszade I, Hollis JM, Liu R et al. Purification and cloning of aggrecanase-1: a member of the ADAMTS family of proteins. Science 1999;284:1664-6.
147. Abbaszade I, Liu RQ, Yang F, Rosenfeld SA, Ross OH, Link JR et al. Cloning and characterization of ADAMTS11, an aggrecanase from the ADAMTS family. J Biol Chem 1999;274:23443-50.
148. Fosang AJ, Rogerson FM, East CJ, Stanton H. ADAMTS-5: the story so far. Eur Cell Mater 2008;15:11-26.
149. Malfait AM, Liu RQ, Ijiri K, Komiya S, Tortorella MD. Inhibition of ADAM-TS4 and ADAM-TS5 prevents aggrecan degradation in osteoarthritic cartilage. J Biol Chem 2002;277:22201-8.
150. Tortorella MD, Malfait AM, Deccico C, Arner E. The role of ADAM-TS4 (aggrecanase-1) and ADAM-TS5 (aggrecanase-2) in a model of cartilage degradation. Osteoarthritis Cartilage 2001;9:539-52.
151. Tortorella MD, Liu RQ, Burn T, Newton RC, Arner E. Characterization of human aggrecanase 2 (ADAM-TS5): substrate specificity studies and comparison with aggrecanase 1 (ADAM-TS4). Matrix Biol 2002;21:499-511.
152. Stanton H, Rogerson FM, East CJ, Golub SB, Lawlor KE, Meeker CT et al. ADAMTS5 is the major aggrecanase in mouse cartilage in vivo and in vitro. Nature 2005;434:648-52.
153. Glasson SS, Askew R, Sheppard B, Carito BA, Blanchet T, Ma HL et al. Characterization of and osteoarthritis susceptibility in ADAMTS-4-knockout mice. Arthritis Rheum 2004;50:2547-58.
154. Botter SM, Van Osch GJ, Waarsing JH, Day JS, Verhaar JA, Pols HA et al. Quantification of subchondral bone changes in a murine osteoarthritis model using micro-CT. Biorheology 2006;43:379-88.
155. Chambers MG, Cox L, Chong L, Suri N, Cover P, Bayliss MT et al. Matrix metalloproteinases and aggrecanases cleave aggrecan in different zones of normal cartilage but colocalize in the development of osteoarthritic lesions in STR/ort mice. Arthritis Rheum 2001;44:1455-65.
156. Van Meurs JB, Van Lent PL, Joosten LA, Van der Kraan PM, Van den Berg WB. Quantification of mRNA levels in joint capsule and articular cartilage of the murine knee joint by RT-PCR: kinetics of stromelysin and IL-1 mRNA levels during arthritis. Rheumatol Int 1997;16:197-205.
157. Malinin T, Ouellette EA. Articular cartilage nutrition is mediated by subchondral bone: a long-term autograft study in baboons. Osteoarthritis Cartilage 2000;8:483-91.
158. Raisz LG. Prostaglandins and bone: physiology and pathophysiology. Osteoarthritis Cartilage 1999;7:419-21.
159. Masuko-Hongo K, Berenbaum F, Humbert L, Salvat C, Goldring MB, Thirion S. Up-regulation of microsomal prostaglandin E synthase 1 in osteoarthritic human cartilage: critical roles of the ERK-1/2 and p38 signaling pathways. Arthritis Rheum 2004;50:2829-38.
160. Amin AR, Attur M, Patel RN, Thakker GD, Marshall PJ, Rediske J et al. Superinduction of cyclooxygenase-2 activity in human osteoarthritis-affected cartilage. Influence of nitric oxide. J Clin Invest 1997;99:1231-7.
161. Sanchez C, Deberg MA, Bellahcene A, Castronovo V, Msika P, Delcour JP et al. Phenotypic characterization of osteoblasts from the sclerotic zones of osteoarthritic subchondral bone. Arthritis Rheum 2008;58:442-55.
162. de Hooge AS, Van de Loo FA, Bennink MB, Arntz OJ, de Hooge P, Van den Berg WB. Male IL-6 gene knock out mice developed more advanced osteoarthritis upon aging. Osteoarthritis Cartilage 2005;13:66-73.
163. Massicotte F, Lajeunesse D, Benderdour M, Pelletier JP, Hilal G, Duval N et al. Can altered production of interleukin-1beta, interleukin-6, transforming growth factor-beta and prostaglandin E(2)

by isolated human subchondral osteoblasts identify two subgroups of osteoarthritic patients. Osteoarthritis Cartilage 2002;10:491-500.

164. Sanchez C, Deberg MA, Burton S, Devel P, Reginster JY, Henrotin YE. Differential regulation of chondrocyte metabolism by oncostatin M and interleukin-6. Osteoarthritis Cartilage 2004;12:801-10.
165. Lisignoli G, Piacentini A, Toneguzzi S, Grassi F, Cocchini B, Ferruzzi A et al. Osteoblasts and stromal cells isolated from femora in rheumatoid arthritis (RA) and osteoarthritis (OA) patients express IL-11, leukaemia inhibitory factor and oncostatin M. Clin Exp Immunol 2000;119:346-53.
166. Huebner AK, Schinke T, Priemel M, Schilling S, Schilling AF, Emeson RB et al. Calcitonin deficiency in mice progressively results in high bone turnover. J Bone Miner Res 2006;21:1924-34.
167. Papaioannou NA, Triantafillopoulos IK, Khaldi L, Krallis N, Galanos A, Lyritis GP. Effect of calcitonin in early and late stages of experimentally induced osteoarthritis. A histomorphometric study. Osteoarthritis Cartilage 2007;15:386-95.
168. El Hajjaji H, Williams JM, Devogelaer JP, Lenz ME, Thonar EJ, Manicourt DH. Treatment with calcitonin prevents the net loss of collagen, hyaluronan and proteoglycan aggregates from cartilage in the early stages of canine experimental osteoarthritis. Osteoarthritis Cartilage 2004;12:904-11.
169. Sondergaard BC, Wulf H, Henriksen K, Schaller S, Oestergaard S, Qvist P et al. Calcitonin directly attenuates collagen type II degradation by inhibition of matrix metalloproteinase expression and activity in articular chondrocytes. Osteoarthritis Cartilage 2006;14:759-68.
170. Karsdal MA, Tanko LB, Riis BJ, Sondergard BC, Henriksen K, Altman RD et al. Calcitonin is involved in cartilage homeostasis: is calcitonin a treatment for OA? Osteoarthritis Cartilage 2006;14:617-24.
171. Lin Z, Pavlos NJ, Cake MA, Wood DJ, Xu J, Zheng MH. Evidence that human cartilage and chondrocytes do not express calcitonin receptor. Osteoarthritis Cartilage 2008;16:450-7.
172. Behets C, Williams JM, Chappard D, Devogelaer JP, Manicourt DH. Effects of calcitonin on subchondral trabecular bone changes and on osteoarthritic cartilage lesions after acute anterior cruciate ligament deficiency. J Bone Miner Res 2004;19:1821-6.
173. Adamopoulos IE, Danks L, Itonaga I, Locklin RM, Sabokbar A, Ferguson DJ et al. Stimulation of osteoclast formation by inflammatory synovial fluid. Virchows Arch 2006;449:69-77.
174. Danks L, Sabokbar A, Gundle R, Athanasou NA. Synovial macrophage-osteoclast differentiation in inflammatory arthritis. Ann Rheum Dis 2002;61:916-21.
175. Adamopoulos IE, Sabokbar A, Wordsworth BP, Carr A, Ferguson DJ, Athanasou NA. Synovial fluid macrophages are capable of osteoclast formation and resorption. J Pathol 2006;208:35-43.
176. Mackie EJ, Ahmed YA, Tatarczuch L, Chen KS, Mirams M. Endochondral ossification: how cartilage is converted into bone in the developing skeleton. Int J Biochem Cell Biol 2008;40:46-62.
177. East CJ, Stanton H, Golub SB, Rogerson FM, Fosang AJ. ADAMTS-5 deficiency does not block aggrecanolysis at preferred cleavage sites in the chondroitin sulfate-rich region of aggrecan. J Biol Chem 2007;282:8632-40.
178. Nakamura M, Sone S, Takahashi I, Mizoguchi I, Echigo S, Sasano Y. Expression of versican and ADAMTS1, 4, and 5 during bone development in the rat mandible and hind limb. J Histochem Cytochem 2005;53:1553-62.
179. Lind T, McKie N, Wendel M, Racey SN, Birch MA. The hyalectan degrading ADAMTS-1 enzyme is expressed by osteoblasts and up-regulated at regions of new bone formation. Bone 2005;36:408-17.
180. Walton M, Elves MW. Bone thickening in osteoarthrosis. Observations of an osteoarthrosis-prone strain of mouse. Acta Orthop Scand 1979;50:501-6.

181. Botter SM, Van Osch GJ, Waarsing JH, Van der Linden JC, Verhaar JA, Pols HA et al. Cartilage damage pattern in relation to subchondral plate thickness in a collagenase-induced model of osteoarthritis. Osteoarthritis Cartilage 2008;16:506-14.
182. Sniekers YH, Intema F, Lafeber FP, Van Osch GJ, Van Leeuwen JP, Weinans H et al. A role for subchondral bone changes in the process of osteoarthritis; a micro-CT study of two canine models. BMC Musculoskelet Disord 2008;9:20.
183. Garinis GA, Uittenboogaard LM, Stachelscheid H, Fousteri M, Van Ijcken W, Breit TM et al. Persistent transcription-blocking DNA lesions trigger somatic growth attenuation associated with longevity. Nat Cell Biol 2009;11:604-15.
184. Hoeijmakers JH. Genome maintenance mechanisms for preventing cancer. Nature 2001;411:366-74.
185. Hanawalt PC, Spivak G. Transcription-coupled DNA repair: two decades of progress and surprises. Nat Rev Mol Cell Biol 2008;9:958-70.
186. Schumacher B, Garinis GA, Hoeijmakers JH. Age to survive: DNA damage and aging. Trends Genet 2008;24:77-85.
187. Hoeijmakers JH. DNA damage, aging, and cancer. N Engl J Med 2009;361:1475-85.
188. de Boer J, de Wit J, Van Steeg H, Berg RJ, Morreau H, Visser P et al. A mouse model for the basal transcription/DNA repair syndrome trichothiodystrophy. Mol Cell 1998;1:981-90.
189. de Boer J, Andressoo JO, de Wit J, Huijmans J, Beems RB, Van Steeg H et al. Premature aging in mice deficient in DNA repair and transcription. Science 2002;296:1276-9.
190. Faghri S, Tamura D, Kraemer KH, Digiovanna JJ. Trichothiodystrophy: a systematic review of 112 published cases characterises a wide spectrum of clinical manifestations. J Med Genet 2008;45:609-21.
191. Wijnhoven SW, Beems RB, Roodbergen M, Van den Berg J, Lohman PH, Diderich K et al. Accelerated aging pathology in ad libitum fed Xpd(TTD) mice is accompanied by features suggestive of caloric restriction. DNA Repair (Amst) 2005;4:1314-24.
192. Dillon CF, Rasch EK, Gu Q, Hirsch R. Prevalence of knee osteoarthritis in the United States: arthritis data from the Third National Health and Nutrition Examination Survey 1991-94. J Rheumatol 2006;33:2271-9.
193. de Boer J, de Wit J, Van Steeg H, Berg RJ, Morreau H, Visser P et al. A mouse model for the basal transcription/DNA repair syndrome trichothiodystrophy. Mol Cell 1998;1:981-90.
194. Dollé ME, Busuttil RA, Garcia AM, Wijnhoven S, Van Drunen E, Niedernhofer LJ et al. Increased genomic instability is not a prerequisite for shortened lifespan in DNA repair deficient mice. Mutat Res 2006;596:22-35.
195. Stoop R, Van der Kraan PM, Buma P, Hollander AP, Billinghurst RC, Poole AR et al. Type II collagen degradation in spontaneous osteoarthritis in C57Bl/6 and BALB/c mice. Arthritis Rheum 1999;42:2381-9.
196. Blaney Davidson EN, Vitters EL, Van Beuningen HM, Van de Loo FA, Van den Berg WB, Van der Kraan PM. Resemblance of osteophytes in experimental osteoarthritis to transforming growth factor beta-induced osteophytes: limited role of bone morphogenetic protein in early osteoarthritic osteophyte formation. Arthritis Rheum 2007;56:4065-73.
197. Halloran BP, Ferguson VL, Simske SJ, Burghardt A, Venton LL, Majumdar S. Changes in bone structure and mass with advancing age in the male C57BL/6J mouse. J Bone Miner Res 2002;17:1044-50.
198. Ferguson VL, Ayers RA, Bateman TA, Simske SJ. Bone development and age-related bone loss in male C57BL/6J mice. Bone 2003;33:387-98.

199. Diderich KE (2010). Bone aging in DNA repair deficient trichothiodystrophy mice. Dissertation, Erasmus University Rotterdam, The Netherlands
200. Lapvetelainen T, Nevalainen T, Parkkinen JJ, Arokoski J, Kiraly K, Hyttinen M et al. Lifelong moderate running training increases the incidence and severity of osteoarthritis in the knee joint of C57BL mice. Anat Rec 1995;242:159-65.
201. Harding JJ (1997). Biochemistry of the Eye. Chapman & Hall Medical, London
202. Benedek TG. A history of the understanding of cartilage. Osteoarthritis Cartilage 2006;14:203-9.
203. Huber M, Trattnig S, Lintner F. Anatomy, biochemistry, and physiology of articular cartilage. Invest Radiol 2000;35:573-80.
204. Sun X, Wei Y. The role of hypoxia-inducible factor in osteogenesis and chondrogenesis. Cytotherapy 2009;11:261-7.
205. Kim MS, Yang YM, Son A, Tian YS, Lee SI, Kang SW et al. RANKL-mediated ROS pathway that induces long-lasting Ca2+ oscillations essential for osteoclastogenesis. J Biol Chem 2010;285:6913-21.
206. Rached MT, Kode A, Xu L, Yoshikawa Y, Paik JH, Depinho RA et al. FoxO1 is a positive regulator of bone formation by favoring protein synthesis and resistance to oxidative stress in osteoblasts. Cell Metab 2010;11:147-60.
207. Ambrogini E, Almeida M, Martin-Millan M, Paik JH, Depinho RA, Han L et al. FoxO-mediated defense against oxidative stress in osteoblasts is indispensable for skeletal homeostasis in mice. Cell Metab 2010;11:136-46.
208. Morita K, Miyamoto T, Fujita N, Kubota Y, Ito K, Takubo K et al. Reactive oxygen species induce chondrocyte hypertrophy in endochondral ossification. J Exp Med 2007;204:1613-23.
209. Gibson JS, Milner PI, White R, Fairfax TP, Wilkins RJ. Oxygen and reactive oxygen species in articular cartilage: modulators of ionic homeostasis. Pflugers Arch 2008;455:563-73.
210. Wauquier F, Leotoing L, Coxam V, Guicheux J, Wittrant Y. Oxidative stress in bone remodelling and disease. Trends Mol Med 2009;15:468-77.
211. Giorgio M, Trinei M, Migliaccio E, Pelicci PG. Hydrogen peroxide: a metabolic by-product or a common mediator of ageing signals? Nat Rev Mol Cell Biol 2007;8:722-8.
212. Manolagas SC. From Estrogen-Centric to Aging and Oxidative Stress: A Revised Perspective of the Pathogenesis of Osteoporosis. Endocr Rev 2010;31:266-300.
213. Henrotin Y, Kurz B, Aigner T. Oxygen and reactive oxygen species in cartilage degradation: friends or foes? Osteoarthritis Cartilage 2005;13:643-54.
214. Wluka AE, Stuckey S, Brand C, Cicuttini FM. Supplementary vitamin E does not affect the loss of cartilage volume in knee osteoarthritis: a 2 year double blind randomized placebo controlled study. J Rheumatol 2002;29:2585-91.
215. Canter PH, Wider B, Ernst E. The antioxidant vitamins A, C, E and selenium in the treatment of arthritis: a systematic review of randomized clinical trials. Rheumatology (Oxford) 2007;46:1223-33.
216. Brien S, Prescott P, Bashir N, Lewith H, Lewith G. Systematic review of the nutritional supplements dimethyl sulfoxide (DMSO) and methylsulfonylmethane (MSM) in the treatment of osteoarthritis. Osteoarthritis Cartilage 2008;16:1277-88.
217. Niedernhofer LJ, Garinis GA, Raams A, Lalai AS, Robinson AR, Appeldoorn E et al. A new progeroid syndrome reveals that genotoxic stress suppresses the somatotroph axis. Nature 2006;444:1038-43.
218. Schumacher B, Van der Pluijm I, Moorhouse MJ, Kosteas T, Robinson AR, Suh Y et al. Delayed and accelerated aging share common longevity assurance mechanisms. PLoS Genet 2008;4:e1000161.

219. Van de Ven M, Andressoo JO, Holcomb VB, Hasty P, Suh Y, Van Steeg H et al. Extended longevity mechanisms in short-lived progeroid mice: identification of a preservative stress response associated with successful aging. Mech Ageing Dev 2007;128:58-63.
220. Dequeker J, Aerssens J, Luyten FP. Osteoarthritis and osteoporosis: clinical and research evidence of inverse relationship. Aging Clin Exp Res 2003;15:426-39.
221. Schneiderman R, Rosenberg N, Hiss J, Lee P, Liu F, Hintz RL et al. Concentration and size distribution of insulin-like growth factor-I in human normal and osteoarthritic synovial fluid and cartilage. Arch Biochem Biophys 1995;324:173-88.
222. Perrini S, Laviola L, Carreira MC, Cignarelli A, Natalicchio A, Giorgino F. The GH/IGF1 axis and signaling pathways in the muscle and bone: mechanisms underlying age-related skeletal muscle wasting and osteoporosis. J Endocrinol 2010;205:201-10.
223. Denko CW, Malemud CJ. Role of the growth hormone/insulin-like growth factor-1 paracrine axis in rheumatic diseases. Semin Arthritis Rheum 2005;35:24-34.
224. Biermasz NR, Wassenaar MJ, Van der Klaauw AA, Pereira AM, Smit JW, Roelfsema F et al. Pretreatment insulin-like growth factor-I concentrations predict radiographic osteoarthritis in acromegalic patients with long-term cured disease. J Clin Endocrinol Metab 2009;94:2374-9.
225. Otero M, Lago R, Lago F, Casanueva FF, Dieguez C, Gomez-Reino JJ et al. Leptin, from fat to inflammation: old questions and new insights. FEBS Lett 2005;579:295-301.
226. Gabay O, Hall DJ, Berenbaum F, Henrotin Y, Sanchez C. Osteoarthritis and obesity: experimental models. Joint Bone Spine 2008;75:675-9.
227. Sandell LJ. Obesity and osteoarthritis: is leptin the link? Arthritis Rheum 2009;60:2858-60.
228. Yusuf E, Nelissen RG, Ioan-Facsinay A, Stojanovic-Susulic V, De Groot J, Van Osch G et al. Association between weight or body mass index and hand osteoarthritis: a systematic review. Ann Rheum Dis 2010;69:761-5.
229. Bohm BB, Aigner T, Roy B, Brodie TA, Blobel CP, Burkhardt H. Homeostatic effects of the metalloproteinase disintegrin ADAM15 in degenerative cartilage remodeling. Arthritis Rheum 2005;52:1100-9.
230. Lories RJ, Peeters J, Szlufcik K, Hespel P, Luyten FP. Deletion of frizzled-related protein reduces voluntary running exercise performance in mice. Osteoarthritis Cartilage 2008;17:390-6.
231. Munasinghe JP, Tyler JA, Hodgson RJ, Barry MA, Gresham GA, Evans R et al. Magnetic resonance imaging, histology, and x-ray of three stages of damage to the knees of STR/ORT mice. Invest Radiol 1996;31:630-8.
232. Schwartz Z, Nasatzky E, Ornoy A, Brooks BP, Soskolne WA, Boyan BD. Gender-specific, maturation-dependent effects of testosterone on chondrocytes in culture. Endocrinology 1994;134:1640-7.
233. Sowers MF, Hochberg M, Crabbe JP, Muhich A, Crutchfield M, Updike S. Association of bone mineral density and sex hormone levels with osteoarthritis of the hand and knee in premenopausal women. Am J Epidemiol 1996;143:38-47.
234. Sniekers YH, Weinans H, Bierma-Zeinstra SM, Van Leeuwen JP, Van Osch GJ. Animal models for osteoarthritis: the effect of ovariectomy and estrogen treatment - a systematic approach. Osteoarthritis Cartilage 2008;16:533-41.
235. Ogata K, Whiteside LA, Lesker PA. Subchondral route for nutrition to articular cartilage in the rabbit. Measurement of diffusion with hydrogen gas in vivo. J Bone Joint Surg Am 1978;60:905-10.
236. Arkill KP, Winlove CP. Solute transport in the deep and calcified zones of articular cartilage. Osteoarthritis Cartilage 2008;16:708-14.
237. Li B, Aspden RM. Mechanical and material properties of the subchondral bone plate from the femoral head of patients with osteoarthritis or osteoporosis. Ann Rheum Dis 1997;56:247-54.

238. Stewart A, Black A, Robins SP, Reid DM. Bone density and bone turnover in patients with osteoarthritis and osteoporosis. J Rheumatol 1999;26:622-6.
239. Bettica P, Cline G, Hart DJ, Meyer J, Spector TD. Evidence for increased bone resorption in patients with progressive knee osteoarthritis: longitudinal results from the Chingford study. Arthritis Rheum 2002;46:3178-84.
240. Waarsing JH, Day JS, Weinans H. Longitudinal micro-CT scans to evaluate bone architecture. J Musculoskelet Neuronal Interact 2005;5:310-2.
241. Blom AB, Van Lent PL, Holthuysen AE, Van der Kraan PM, Roth J, Van Rooijen N et al. Synovial lining macrophages mediate osteophyte formation during experimental osteoarthritis. Osteoarthritis Cartilage 2004;12:627-35.
242. van Osch GJ, Van der Kraan PM, Vitters EL, Blankevoort L, Van den Berg WB. Induction of osteoarthritis by intra-articular injection of collagenase in mice. Strain and sex related differences. Osteoarthritis Cartilage 1993;1:171-7.
243. Maes F, Collignon A, Van der Meulen D, Marchal G, Suetens P. Multimodality image registration by maximization of mutual information. IEEE Trans Med Imaging 1997;16:187-98.
244. Erlebacher A, Derynck R. Increased expression of TGF-beta 2 in osteoblasts results in an osteoporosis-like phenotype. J Cell Biol 1996;132:195-210.
245. Buckland-Wright JC, Messent EA, Bingham CO, III, Ward RJ, Tonkin C. A 2 yr longitudinal radiographic study examining the effect of a bisphosphonate (risedronate) upon subchondral bone loss in osteoarthritic knee patients. Rheumatology (Oxford) 2007;46:257-64.
246. Clark JM, Huber JD. The structure of the human subchondral plate. J Bone Joint Surg Br 1990;72:866-73.
247. Pan J, Zhou X, Li W, Novotny JE, Doty SB, Wang L. In situ measurement of transport between subchondral bone and articular cartilage. J Orthop Res 2009;27:1347-52.
248. De Croos JN, Dhaliwal SS, Grynpas MD, Pilliar RM, Kandel RA. Cyclic compressive mechanical stimulation induces sequential catabolic and anabolic gene changes in chondrocytes resulting in increased extracellular matrix accumulation. Matrix Biol 2006;25:323-31.
249. Huang J, Ballou LR, Hasty KA. Cyclic equibiaxial tensile strain induces both anabolic and catabolic responses in articular chondrocytes. Gene 2007;404:101-9.
250. Klein-Nulend J, Nijweide PJ, Burger EH. Osteocyte and bone structure. Curr Osteoporos Rep 2003;1:5-10.
251. Wise LM, Wang Z, Grynpas MD. The use of fractography to supplement analysis of bone mechanical properties in different strains of mice. Bone 2007;41:620-30.
252. Yu LP, Jr., Burr DB, Brandt KD, O'Connor BL, Rubinow A, Albrecht M. Effects of oral doxycycline administration on histomorphometry and dynamics of subchondral bone in a canine model of osteoarthritis. J Rheumatol 1996;23:137-42.
253. Doschak MR, Wohl GR, Hanley DA, Bray RC, Zernicke RF. Antiresorptive therapy conserves some periarticular bone and ligament mechanical properties after anterior cruciate ligament disruption in the rabbit knee. J Orthop Res 2004;22:942-8.
254. Intema F, Hazewinkel HA, Gouwens D, Bijlsma JW, Weinans H, Lafeber FP et al. In early OA, thinning of the subchondral plate is directly related to cartilage damage: results from a canine ACLT-meniscectomy model. Osteoarthritis Cartilage 2010;18:691-8.
255. Jimenez PA, Glasson SS, Trubetskoy OV, Haimes HB. Spontaneous osteoarthritis in Dunkin Hartley guinea pigs: histologic, radiologic, and biochemical changes. Lab Anim Sci 1997;47:598-601.

256. Huebner JL, Hanes MA, Beekman B, TeKoppele JM, Kraus VB. A comparative analysis of bone and cartilage metabolism in two strains of guinea-pig with varying degrees of naturally occurring osteoarthritis. Osteoarthritis Cartilage 2002;10:758-67.
257. Muraoka T, Hagino H, Okano T, Enokida M, Teshima R. Role of subchondral bone in osteoarthritis development: a comparative study of two strains of guinea pigs with and without spontaneously occurring osteoarthritis. Arthritis Rheum 2007;56:3366-74.
258. Walton M. Degenerative joint disease in the mouse knee; radiological and morphological observations. J Pathol 1977;123:97-107.
259. Evans RG, Collins C, Miller P, Ponsford FM, Elson CJ. Radiological scoring of osteoarthritis progression in STR/ORT mice. Osteoarthritis Cartilage 1994;2:103-9.
260. Naruse K, Urabe K, Jiang SX, Uchida K, Kozai Y, Minehara H et al. Osteoarthritic changes of the patellofemoral joint in STR/OrtCrlj mice are the earliest detectable changes and may be caused by internal tibial torsion. Connect Tissue Res 2009;50:243-55.
261. Stok KS, Pelled G, Zilberman Y, Kallai I, Goldhahn J, Gazit D et al. Revealing the interplay of bone and cartilage in osteoarthritis through multimodal imaging of murine joints. Bone 2009;45:414-22.
262. Sarukawa J, Takahashi M, Doi M, Suzuki D, Nagano A. A longitudinal analysis of urinary biochemical markers and bone mineral density in STR/Ort mice as a model of spontaneous osteoarthritis. Arthritis Rheum 2010;62:463-71.
263. Uchida K, Urabe K, Naruse K, Ogawa Z, Mabuchi K, Itoman M. Hyperlipidemia and hyperinsulinemia in the spontaneous osteoarthritis mouse model, STR/Ort. Exp Anim 2009;58:181-7.
264. Griffin TM, Fermor B, Huebner JL, Kraus VB, Rodriguiz RM, Wetsel WC et al. Diet-induced obesity differentially regulates behavioral, biomechanical, and molecular risk factors for osteoarthritis in mice. Arthritis Res Ther 2010;12:R130.
265. Karvonen RL, Miller PR, Nelson DA, Granda JL, Fernandez-Madrid F. Periarticular osteoporosis in osteoarthritis of the knee. J Rheumatol 1998;25:2187-94.
266. Bolbos RI, Zuo J, Banerjee S, Link TM, Ma CB, Li X et al. Relationship between trabecular bone structure and articular cartilage morphology and relaxation times in early OA of the knee joint using parallel MRI at 3 T. Osteoarthritis Cartilage 2008;16:1150-9.
267. Javaid MK, Lynch JA, Tolstykh I, Guermazi A, Roemer F, Aliabadi P et al. Pre-radiographic MRI findings are associated with onset of knee symptoms: the most study. Osteoarthritis Cartilage 2010;18:323-8.
268. Bennell KL, Creaby MW, Wrigley TV, Hunter DJ. Tibial subchondral trabecular volumetric bone density in medial knee joint osteoarthritis using peripheral quantitative computed tomography technology. Arthritis Rheum 2008;58:2776-85.
269. Hunter DJ, Hart D, Snieder H, Bettica P, Swaminathan R, Spector TD. Evidence of altered bone turnover, vitamin D and calcium regulation with knee osteoarthritis in female twins. Rheumatology (Oxford) 2003;42:1311-6.
270. Arden NK, Nevitt MC, Lane NE, Gore LR, Hochberg MC, Scott JC et al. Osteoarthritis and risk of falls, rates of bone loss, and osteoporotic fractures. Study of Osteoporotic Fractures Research Group. Arthritis Rheum 1999;42:1378-85.
271. Doré D, Quinn S, Ding C, Winzenberg T, Cicuttini F, Jones G. Subchondral bone and cartilage damage: a prospective study in older adults. Arthritis Rheum 2010;62:1967-73.
272. Prasadam I, Van Gennip S, Friis T, Shi W, Crawford R, Xiao Y. ERK-1/2 and p38 in the regulation of hypertrophic changes of normal articular cartilage chondrocytes induced by osteoarthritic subchondral osteoblasts. Arthritis Rheum 2010;62:1349-60.

273. Prasadam I, Friis T, Shi W, Van Gennip S, Crawford R, Xiao Y. Osteoarthritic cartilage chondrocytes alter subchondral bone osteoblast differentiation via MAPK signalling pathway involving ERK1/2. Bone 2010;46:226-35.
274. Harrison MH, Schajowicz F, Trueta J. Osteoarthritis of the hip: a study of the nature and evolution of the disease. J Bone Joint Surg Br 1953;35-B:598-626.
275. Suri S, Gill SE, Massena dC, Wilson D, McWilliams DF, Walsh DA. Neurovascular invasion at the osteochondral junction and in osteophytes in osteoarthritis. Ann Rheum Dis 2007;66:1423-8.
276. Walsh DA, McWilliams DF, Turley MJ, Dixon MR, Franses RE, Mapp PI et al. Angiogenesis and nerve growth factor at the osteochondral junction in rheumatoid arthritis and osteoarthritis. Rheumatology (Oxford) 2010;Epub ahead of print:doi:10.1093/rheumatology/keq188.
277. Mapp PI, Avery PS, McWilliams DF, Bowyer J, Day C, Moores S et al. Angiogenesis in two animal models of osteoarthritis. Osteoarthritis Cartilage 2008;16:61-9.
278. Engsig MT, Chen QJ, Vu TH, Pedersen AC, Therkidsen B, Lund LR et al. Matrix metalloproteinase 9 and vascular endothelial growth factor are essential for osteoclast recruitment into developing long bones. J Cell Biol 2000;151:879-89.
279. Henriksen K, Karsdal M, Delaisse JM, Engsig MT. RANKL and vascular endothelial growth factor (VEGF) induce osteoclast chemotaxis through an ERK1/2-dependent mechanism. J Biol Chem 2003;278:48745-53.
280. Nakagawa M, Kaneda T, Arakawa T, Morita S, Sato T, Yomada T et al. Vascular endothelial growth factor (VEGF) directly enhances osteoclastic bone resorption and survival of mature osteoclasts. FEBS Lett 2000;473:161-4.
281. Yang Q, McHugh KP, Patntirapong S, Gu X, Wunderlich L, Hauschka PV. VEGF enhancement of osteoclast survival and bone resorption involves VEGF receptor-2 signaling and beta3-integrin. Matrix Biol 2008;27:589-99.
282. Street J, Lenehan B. Vascular endothelial growth factor regulates osteoblast survival - evidence for an autocrine feedback mechanism. J Orthop Surg Res 2009;4:19.
283. Tanaka E, Aoyama J, Miyauchi M, Takata T, Hanaoka K, Iwabe T et al. Vascular endothelial growth factor plays an important autocrine/paracrine role in the progression of osteoarthritis. Histochem Cell Biol 2005;123:275-81.
284. Pufe T, Lemke A, Kurz B, Petersen W, Tillmann B, Grodzinsky AJ et al. Mechanical overload induces VEGF in cartilage discs via hypoxia-inducible factor. Am J Pathol 2004;164:185-92.
285. Murata M, Yudoh K, Masuko K. The potential role of vascular endothelial growth factor (VEGF) in cartilage: how the angiogenic factor could be involved in the pathogenesis of osteoarthritis? Osteoarthritis Cartilage 2008;16:279-86.
286. Honorati MC, Cattini L, Facchini A. IL-17, IL-1beta and TNF-alpha stimulate VEGF production by dedifferentiated chondrocytes. Osteoarthritis Cartilage 2004;12:683-91.
287. Pulsatelli L, Dolzani P, Silvestri T, Frizziero L, Facchini A, Meliconi R. Vascular endothelial growth factor activities on osteoarthritic chondrocytes. Clin Exp Rheumatol 2005;23:487-93.
288. Sniekers YH, Van Osch GJ, Jahr H, Weinans H, Van Leeuwen JP. Estrogen modulates iodoacetate-induced gene expression in bovine cartilage explants. J Orthop Res 2010;28:607-15.
289. Fransès RE, McWilliams DF, Mapp PI, Walsh DA. Osteochondral angiogenesis and increased protease inhibitor expression in OA. Osteoarthritis Cartilage 2010;18:563-71.
290. Gerber HP, Vu TH, Ryan AM, Kowalski J, Werb Z, Ferrara N. VEGF couples hypertrophic cartilage remodeling, ossification and angiogenesis during endochondral bone formation. Nat Med 1999;5:623-8.

291. Maes C, Carmeliet P, Moermans K, Stockmans I, Smets N, Collen D et al. Impaired angiogenesis and endochondral bone formation in mice lacking the vascular endothelial growth factor isoforms VEGF164 and VEGF188. Mech Dev 2002;111:61-73.
292. Nagai T, Sato M, Kutsuna T, Kokubo M, Ebihara G, Ohta N et al. Intravenous administration of anti-vascular endothelial growth factor humanized monoclonal antibody bevacizumab improves articular cartilage repair. Arthritis Res Ther 2010;12:R178.
293. Campos X, Munoz Y, Selman A, Yazigi R, Moyano L, Weinstein-Oppenheimer C et al. Nerve growth factor and its high-affinity receptor trkA participate in the control of vascular endothelial growth factor expression in epithelial ovarian cancer. Gynecol Oncol 2007;104:168-75.
294. Julio-Pieper M, Lozada P, Tapia V, Vega M, Miranda C, Vantman D et al. Nerve growth factor induces vascular endothelial growth factor expression in granulosa cells via a trkA receptor/mitogen-activated protein kinase-extracellularly regulated kinase 2-dependent pathway. J Clin Endocrinol Metab 2009;94:3065-71.
295. Park HJ, Kim MN, Kim JG, Bae YH, Bae MK, Wee HJ et al. Up-regulation of VEGF expression by NGF that enhances reparative angiogenesis during thymic regeneration in adult rat. Biochim Biophys Acta 2007;1773:1462-72.
296. Romon R, Adriaenssens E, Lagadec C, Germain E, Hondermarck H, Le B, X. Nerve growth factor promotes breast cancer angiogenesis by activating multiple pathways. Mol Cancer 2010;9:157.
297. Sakata N, Chan NK, Chrisler J, Obenaus A, Hathout E. Bone marrow cells produce nerve growth factor and promote angiogenesis around transplanted islets. World J Gastroenterol 2010;16:1215-20.
298. Seidel MF, Herguijuela M, Forkert R, Otten U. Nerve Growth Factor in Rheumatic Diseases. Semin Arthritis Rheum 2009;doi:10.1016/j.semarthrit.2009.03.002:
299. Berenbaum F. Targeted therapies in osteoarthritis: a systematic review of the trials on www.clinicaltrials.gov. Best Pract Res Clin Rheumatol 2010;24:107-19.
300. Bagger YZ, Tanko LB, Alexandersen P, Karsdal MA, Olson M, Mindeholm L et al. Oral salmon calcitonin induced suppression of urinary collagen type II degradation in postmenopausal women: a new potential treatment of osteoarthritis. Bone 2005;37:425-30.
301. Sniekers YH (2009). Estrogen effects on cartilage and bone changes in models for osteoarthritis. Dissertation, Erasmus University Rotterdam, The Netherlands
302. Johnston JD, Kontulainen SA, Masri BA, Wilson DR. A comparison of conventional maximum intensity projection with a new depth-specific topographic mapping technique in the CT analysis of proximal tibial subchondral bone density. Skeletal Radiol 2010;39:867-76.
303. Jones G, Ding C, Glisson M, Hynes K, Ma D, Cicuttini F. Knee articular cartilage development in children: a longitudinal study of the effect of sex, growth, body composition, and physical activity. Pediatr Res 2003;54:230-6.
304. Piscaer TM, Van Osch GJ, Verhaar JA, Weinans H. Imaging of experimental osteoarthritis in small animal models. Biorheology 2008;45:355-64.

Appendices

Dankwoord

Curriculum Vitae

PhD portfolio

List of publications

Colour figures

Dankwoord

De meest gevreesde gedachte bij het schrijven van een dankwoord is waarschijnlijk toch wel '…heb ik iemand vergeten?!' Toch zal dat onherroepelijk gebeuren, gezien de grote hoeveelheid mensen die, direct of indirect, aan dit boekje hebben bijgedragen. Enfin, ik zal toch een poging wagen…

Allereerst mijn beide promotoren, Hans van Leeuwen en Harrie Weinans. Beste Hans, gedurende vier jaar heb ik bij jou op het lab gezeten, en heb samen met jou meegemaakt hoe de aanvankelijk compacte onderzoeksgroep groter en meer divers werd. Deze periode is voor mij erg vormend geweest, als wetenschapper maar ook als mens! Je hebt me geleerd een manuscript of experiment kritisch te beoordelen en een wetenschappelijke boodschap efficiënt over te brengen. Ik hoop dat we onze samenwerking in de toekomst kunnen voortzetten.

Beste Harrie, via jou ben ik uiteindelijk aan deze promotie begonnen. Ik herinner mij nog mijn sollicitatiegesprek, in de zomer van 2003. Ook al wist ik vrijwel niets van bot, je gaf me een kans en liet me vrij om mijn eigen weg te zoeken binnen het project, bedankt daarvoor. Ook je (Noordelijke?) nuchtere houding heb ik altijd erg kunnen waarderen.

Dan mijn copromotor, Gerjo van Osch. Beste Gerjo, je nooit aflatende enthousiasme is mij zeker tot steun geweest de afgelopen jaren. Steeds als ik dacht dat het werk echt nooit af zou geraken, wist jij me weer moed in te spreken, zodat ik weer met een opgewekt gemoed je kamer verliet. Je bent de perfecte 'mental coach'!

Graag wil ik ook alle (overige) leden van de promotiecommissie hartelijk bedanken voor hun deelname als opponent tijdens de verdediging van mijn proefschrift.

Next, I would like to thank all my co-authors for their critical view and their help with carrying out the experiments: Stefan Clockaerts, Judd Day, Martijn Dollé, Sonya Glasson, Jan Hoeijmakers, Bei Hopkins, Jacqueline van der Linden, Huib Pols, Harry van Steeg, Erwin Waarsing, Jan Verhaar, Michel Zar. Ook ben ik dank verschuldigd aan Ton de Jong, Piet Kramer, Bas Karels, Nicole Kops en alle medewerkers van het Erasmus Dierexperimenteel Centrum voor hun technische ondersteuning en goede zorg.

Mijn paranimfen, Marco en Marieke. Marieke, op het Nassau college merkte ik je aanvankelijk niet op ☺ maar gelukkig heb je me dat vergeven en zijn we goede vrienden geworden. Hopelijk blijven we dat nog lange tijd! Ik wens je alle succes in je werk en bovenal alle geluk in je leven samen met Mehdi.

Marco, met jou heb ik vele sport- en Paddy-sessies doorstaan, waar ik zeer goede herinneringen aan heb. Toen ik hier begon te werken kende ik bijna niemand, maar al snel nodigde je me uit om samen Rotterdam te ontdekken. Ik waardeer je vriendschap en collegialiteit zeer en wens je alle succes in je 'corporate' carrière.

Alle collega's en oud-collega's van het 'bottenlab' van de afdeling inwendige geneeskunde en de orthopedie/KNO. Ook al was ik een beetje uit beeld sinds mijn overstap naar Genetica, ik voelde me altijd erg welkom als ik weer eens langskwam. Aan alle 'buitenschoolse' activiteiten de afgelopen jaren houd ik leuke herinneringen. Specifiek wil ik graag bedanken Yvonne BJ en Marieke (a.k.a. Waaibiedzjeej & Mik) voor de Chez Orthopédique dinertjes; Ruud & Eric, thanks guys for putting up with me in your appartment and for letting me crawl through your furniture every now and then, and of course for all the quiet beers; Yvonne S voor de filmavondjes en de hulp met het in elkaar zetten van Henk (R.I.P.); Nicole & Wendy voor hun altijd zonnige humeur; de 'loopclub' van de 5e: Bram, Martijn, Rodrigo en Marco, die gezamenlijke sportieve prestaties tot ongekende hoogtes brachten (en voor het vieren van deze sportieve prestaties in de Mac na afloop); de studenten die ik heb begeleid: Jan-Floris, Michel, Stefan: ook jullie hebben meegeholpen aan het tot stand komen van dit boekje. En 'last but not least' bedank ik ook de collega's van Ee730, ook jullie hebben het een en ander meegekregen van mijn proefschrift. Dank voor jullie belangstelling en tips!

De afdeling Genetica (Prof.dr. Jan Hoeijmakers) en DNage B.V. (Dr. Gerben Zondag, Dr. Ingrid van der Pluijm). Beste Jan, Gerben, ook al was mijn proefschrift nog niet geheel af, jullie gaven alvast het groene licht voor mijn vervolgaanstelling. Het heeft allemaal wat langer geduurd dan aanvankelijk de bedoeling was, maar jullie bleven vertrouwen houden. Bedankt hiervoor.

Mijn vrienden; Bas, Lisette, Maarten, Jessica, Ilja. Ondanks alle veranderingen zijn we door de jaren heen contact blijven houden, en ook al zien we elkaar soms lange tijd niet, het voelt altijd weer vertrouwd als we elkaar weer ontmoeten. Ik hoop dat we dat nog lang blijven doen!

Mijn ouders en zus. André en Aline, jullie hebben wellicht het langst uitgezien naar het voltooien van dit boekje. Ook al hebben jullie inhoudelijk niet echt kunnen bijdragen, jullie hebben me altijd met raad en daad bijgestaan en op deze manier waren jullie echt onmisbaar! Dank voor alle belangstelling (én geduld!), dit was voor mij een belangrijke ondersteuning.

En dan ben ik toch nog iemand vergeten. Lieve Marie! Tja, was ik 's avonds niet op de 16e bezig geweest met 'PS-en' dan was het tussen ons wellicht nooit wat geworden ☺ Gelukkig is het nu dan af. Dank voor al je liefde en gezelligheid, ik hou van jou!

Curriculum Vitae

Sander Martijn Botter was born on the 31st of May, 1979 in Driebergen-Rijsenburg. From 1996-1998, he attended the Dr Nassau College (Atheneum) in Assen. After graduating he went on to study medical biology at the State university in Groningen. In 2002 and 2003, he completed two internships. The first one involved structurally modified antibodies to target tumor endothelium, under the supervision of Dr. Astrid Schraa and Prof.dr. Ingrid Molema at the University Medical Center Groningen (UMCG). In 2002, he participated in setting up a co-operation between the UMCG and the University of Heidelberg, Germany. As part of this conjunction, he joined the Gastroenterology laboratory of the University clinic in Mannheim for a period of six months. Supervised by Prof.dr. Matthias Löhr and dr. Ralf Jesnowski he studied signal transduction in several pancreatic tumor cell lines. After completing this second internship he returned to The Netherlands in 2003, and received his degree *cum laude*. He then applied for a position as PhD student at the Erasmus University in Rotterdam and until 2007 he worked on the project: 'Osteoarthritis: skeletal alterations' under the supervison of Prof.dr.ir. Harrie Weinans (Department of Orthopaedics) and Prof.dr. Hans van Leeuwen (Department of Internal Medicine). Since 2007 he is employed as a post-doctoral researcher at the department of Genetics (lead by Prof.dr. Jan Hoeijmakers) at the Erasmus Medical Center in Rotterdam where he is studying the bone phenotype and gene expressional behavior of premature aging mice.

Sander Martijn Botter werd geboren op 31 mei 1979 te Driebergen-Rijsenburg. Van 1996-1998 doorliep hij het Atheneum aan het Dr. Nassau College in Assen. Na het behalen van zijn VWO diploma ging hij medische biologie studeren aan de Rijksuniversiteit Groningen. In 2002 en 2003 voltooide hij twee stages. Tijdens de eerste stage werkte hij met structureel gemodificeerde antilichamen gericht tegen tumorendotheel, onder de supervisie van Dr. Astrid Schraa en Prof.dr. Ingrid Molema in het Universitair Medisch Centrum Groningen (UMCG). In 2002 participeerde hij in het opzetten van een samenwerkingsverband tussen het UMCG en de Universiteit van Heidelberg (Duitsland). Als onderdeel van deze samenwerking werkte hij gedurende zes maanden in het laboratorium Gastroenterologie van de Universiteitskliniek Mannheim. Begeleid door Prof.dr. Matthias Löhr en dr. Ralf Jesnowski onderzocht hij signaaltransductie processen in verschillende alvleesklier-tumorcellijnen. Na het afronden van deze tweede stage keerde hij terug naar Nederland in 2003 en ontving hij zijn bul *cum laude*. Vervolgens solliciteerde hij naar een positie als promovendus bij de Erasmus Universiteit in Rotterdam en werkte tot 2007 aan het project: `Artrose: skeletveranderingen' onder supervisie van Prof.dr.ir.

Harrie Weinans (afdeling Orthopedie) en Prof.dr. Hans van Leeuwen (afdeling Inwendige geneeskunde). Sinds 2007 werkt is hij verbonden als post-doctoraal onderzoeker aan de afdeling Genetica (geleid door Prof.dr. Jan Hoeijmakers) van het Erasmus Medisch Centrum te Rotterdam waar hij het botfenotype en de genexpressie van voortijdig verouderende muizen bestudeert.

PhD Portfolio

SUMMARY OF PHD TRAINING AND TEACHING ACTIVITIES

Name PhD student:	Sander Martijn Botter
Erasmus MC Departments:	Orthopaedics
	Internal Medicine
Research School:	MUSC (Musculoskeletal Science Center)
	MolMed
PhD period:	September 2003 – September 2007
Promotors:	Prof.dr. J.P.T.M. van Leeuwen
	Prof.dr.ir. H. Weinans
Co-promotor:	Dr. G.J.V.M. van Osch

PhD training activities

General courses	
Biomedical English Writing and Communication	2004
Classical methods for data-analysis (NIHES)	2005
Basic didactics (Risbo, previously OECR)	2005
Specific courses	
Biomedical research techniques (MolMed)	2003
Research methods for the movement apparatus (MUSC)	2004
Presentations at (inter)national conferences	
Podium:	
14th Annual Meeting of the Dutch Society for Calcium and Bone Metabolism (NVCB), Zeist, The Netherlands	2004
Annual meeting of the Dutch Society for Matrix Biology (NVMB), Lunteren, The Netherlands	2005
16th Annual Meeting of the Dutch Society for Calcium and Bone Metabolism (NVCB), Zeist, The Netherlands	2006
Annual meeting of the Dutch Orthopaedic Association (NOV), Amsterdam, The Netherlands	2006

Osteoarthritis Research Society International (OARSI) World Congress on Osteoarthritis, Fort Lauderdale, USA (including Young Investigator Award)	2007

Poster:

51st Annual meeting of the Orthopaedic Research Society (ORS), Washington DC, USA	2005
2nd Joint meeting of the European Calcified Tissue Society (ECTS) and International Bone and Mineral Society (IBMS), Geneva, Switzerland	2005
9th Annual Molecular Medicine Day, Rotterdam, The Netherlands	2005
Osteoarthritis Research Society International (OARSI) World Congress on Osteoarthritis, Prague, Czech Republic	2006
34th European Symposium on Calcified Tissues (ECTS), Copenhagen, Denmark	2007
53rd Annual meeting of the Orthopaedic Research Society (ORS), San Diego, USA	2007

Attended in addition:

Annual Meeting of the Dutch Society for Calcium and Bone Metabolism (NVCB)	2003-2007
Annual meeting of the Dutch Society for Matrix Biology (NVMB), Lunteren, The Netherlands	2004, 2005
4th International Symposium on Mechanobiology of Cartilage and Chondrocyte, Budapest, Hungary	2005
Annual meeting of the Tissue Engineering & Regenerative Medicine International Society (TERMIS), Rotterdam, The Netherlands	2006
Symposium 'Artrose, the state of the art 2006', Rotterdam, The Netherlands	2006
Science day Orthopaedics	2004-2007
Science day Internal Medicine	2003-2007
MUSC retreat	2004, 2006
Osteoarthritis research discussion of the Departments of General Practice, Rheumatology, Orthopaedics, and Internal Medicine (every two months)	2005-2007
Rotterdam – Leiden meeting (every two months)	2003-2007
Research and literature discussions at the Department of Orthopaedics (weekly)	2003-2007
Research and literature discussions of the 'Bone group' at Department of Internal Medicine (weekly)	2003-2007
Research and literature discussions of the Endocrinology group at Department of Internal Medicine (every two months)	2003-2007

Teaching activities

Supervising practicals and excursions	
Histological practical 'Bone pathology', 2nd year medical students	2005, 2006
High school students (one week)	2006
Supervising student internships	
Internship MSc. student Biomedical Engineering, TU/e (three months)	2005
Internship MSc. student Medicine, Erasmus University Rotterdam (ten months)	2005, 2006
Internship MSc. student Medicine, Antwerp University, Antwerp, Belgium (two months)	2006
Lecturing	
'Vaardigheidsonderwijs' hypothalamus-hypophysis-thyroid axis, 2nd year medical students	2005-2007

List of publications

Botter SM, van Osch GJ, Clockaerts S, Waarsing JH, Weinans H, van Leeuwen JP. Osteoarthritis induction leads to early and temporal subchondral plate porosity in the tibial plateau of mice: an *in vivo* micro CT study. *Published in Arthritis & Rheumatism (2010).*

Botter SM, Zar M, van Osch GJ, van Steeg H, Dollé ME, Hoeijmakers JH, Weinans H, van Leeuwen JP. Analysis of osteoarthritis in a mouse model of the progeroid human DNA repair syndrome trichothiodystrophy. *Age (Dordr). 2010 Sep 7. [Epub ahead of print]*

Botter SM, Glasson SS, Hopkins B, Clockaerts S, Weinans H, van Leeuwen JP, van Osch GJ. ADAMTS5-/- mice have less subchondral bone changes after induction of osteoarthritis through surgical instability: implications for a link between cartilage and subchondral bone changes. *Osteoarthritis Cartilage. 2009 May;17(5):636-45.*

Botter SM, van Osch GJ, Waarsing JH, van der Linden JC, Verhaar JA, Pols HA, van Leeuwen JP, Weinans H. Cartilage damage pattern in relation to subchondral plate thickness in a collagenase-induced model of osteoarthritis. *Osteoarthritis Cartilage. 2008 Apr;16(4):506-14.*

Botter SM, van Osch GJ, Waarsing JH, Day JS, Verhaar JA, Pols HA, van Leeuwen JP, Weinans H. Quantification of subchondral bone changes in a murine osteoarthritis model using micro-CT. Biorheology. *2006;43(3-4):379-88.*

Schraa AJ, Kok RJ, Botter SM, Withoff S, Meijer DK, de Leij LF, Molema G. RGD-modified anti-CD3 antibodies redirect cytolytic capacity of cytotoxic T lymphocytes toward alphavbeta3-expressing endothelial cells. *Int J Cancer. 2004 Nov 1;112(2):279-85.*

Colour figures

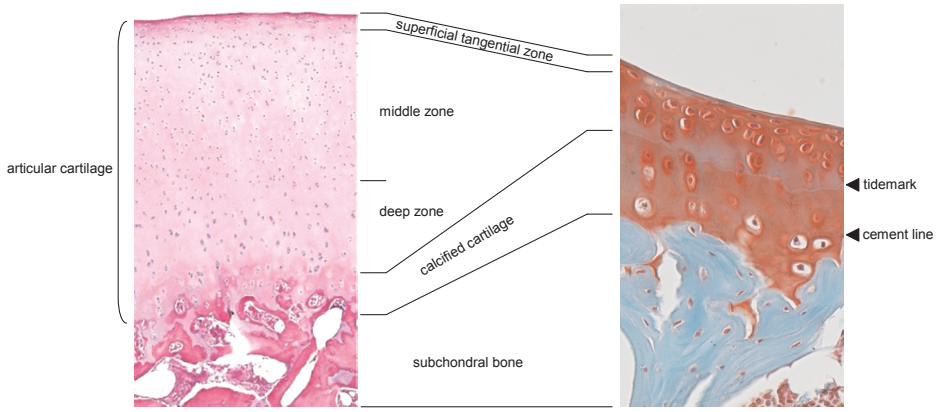

Chapter 1, Figure 1. The osteochondral interface in humans (left) and mice (right). In mice, the middle and deep zones of the articular cartilage are more difficult to discern. The tidemark delineates the boundary between the non-calcified (superficial, middle and deep zones) and the calcified cartilage. The cement line demarcates the boundary between calcified cartilage and the subchondral bone plate.

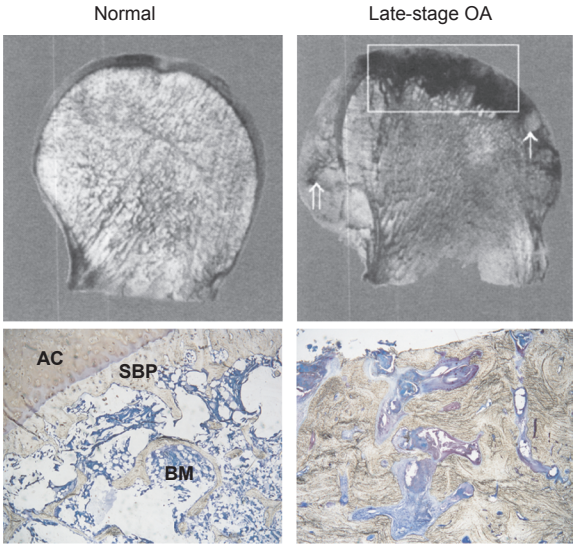

Chapter 1, Figure 2. A normal healthy (left) and advanced osteoarthritic femoral head (right). Macroscopically, osteophyte formation (top right, left arrow), subchondral edema (right arrow) and subchondral sclerosis (rectangle) can be readily identified. Below, histological images of the subchondral bone plate (SBP) area show changes at the microscopic level. Note the increase in subchondral bone, resulting in smaller bone marrow (BM) cavities, and the absence of articular cartilage (AC). Modified from Day *et al*. (8).

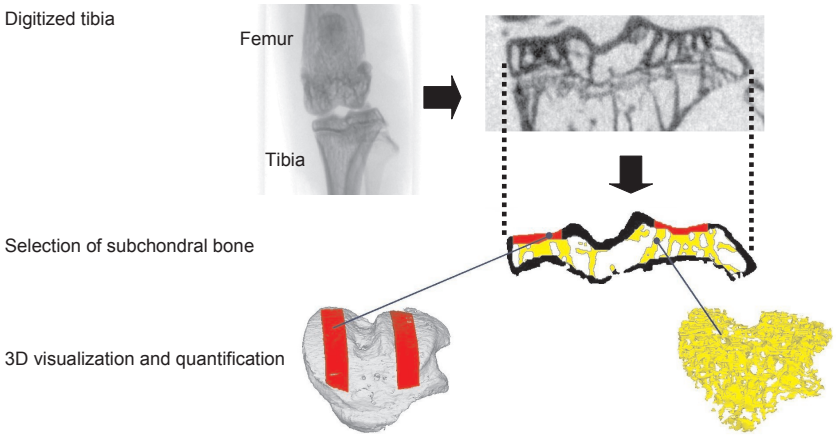

Chapter 1, Figure 3. A technique that was used in every study in this thesis was micro computed tomography (micro-CT). Here, a bone specimen (a murine knee joint is shown here) is digitized, the raw grey-scale images are binarized and separated into several anatomical components (red: subchondral bone plate, yellow: subchondral trabeculae) that can be analyzed separately.

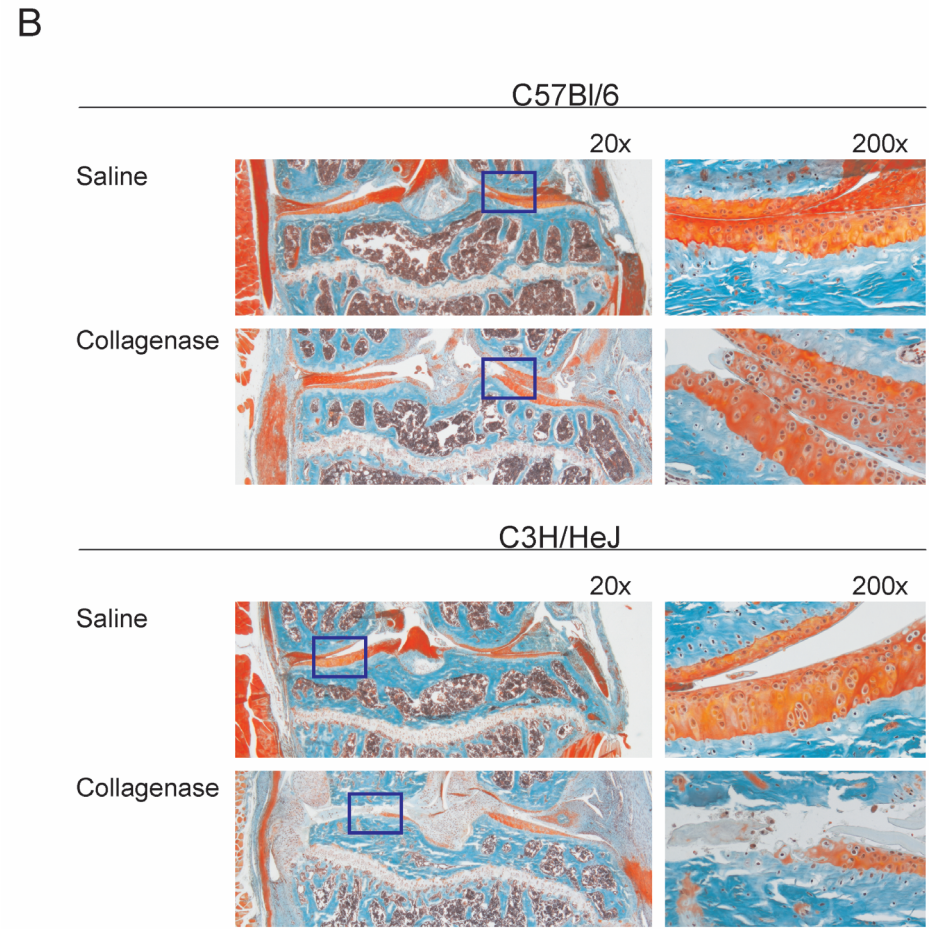

Chapter 3, Figure 3. B, histology of the posterior region in knee joints of control and osteoarthritic knee joints. Note the exposure of the subchondral bone at the medial side in collagenase-injected joints of C3H/HeJ mice. The blue boxes indicate a magnification of the lateral (C57Bl/6) and medial (C3H/HeJ) sides, shown on the right.

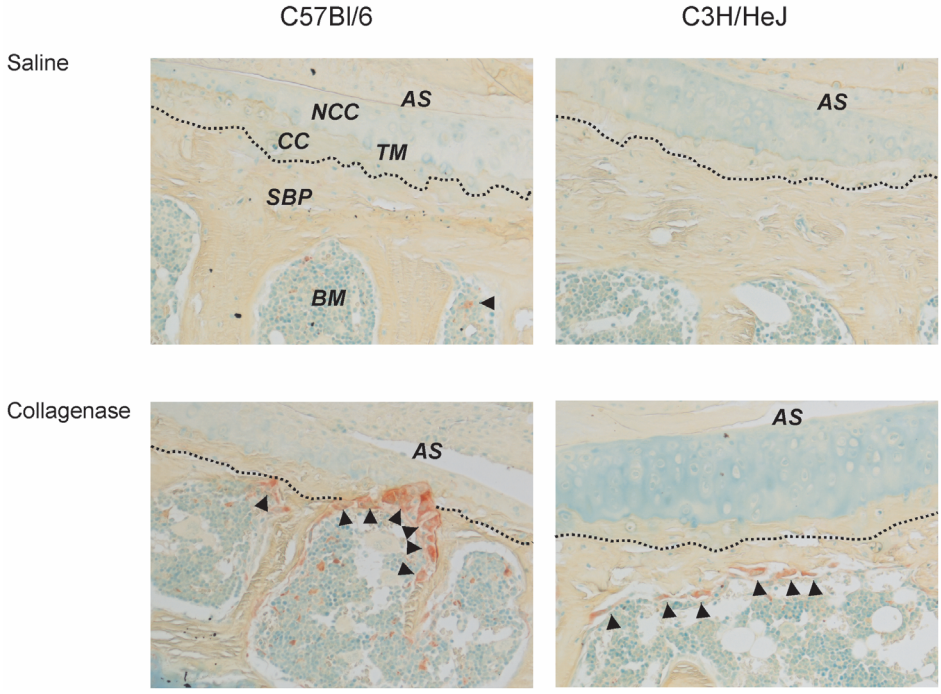

Chapter 3, Figure 5. TRAP staining in histological sections of saline-injected and collagenase-injected knee joints. In saline-injected joints, osteoclasts (arrowheads) were observed occasionally. At some locations in collagenase-injected joints osteoclasts resorbed the subchondral bone plate up to the noncalcified cartilage. The division between the calcified cartilage and the subchondral bone plate is indicated by a dotted line. AS= articular surface, NCC= noncalcified cartilage, CC= calcified cartilage, SBP= subchondral bone plate, TM= tidemark. Original magnification 200x.

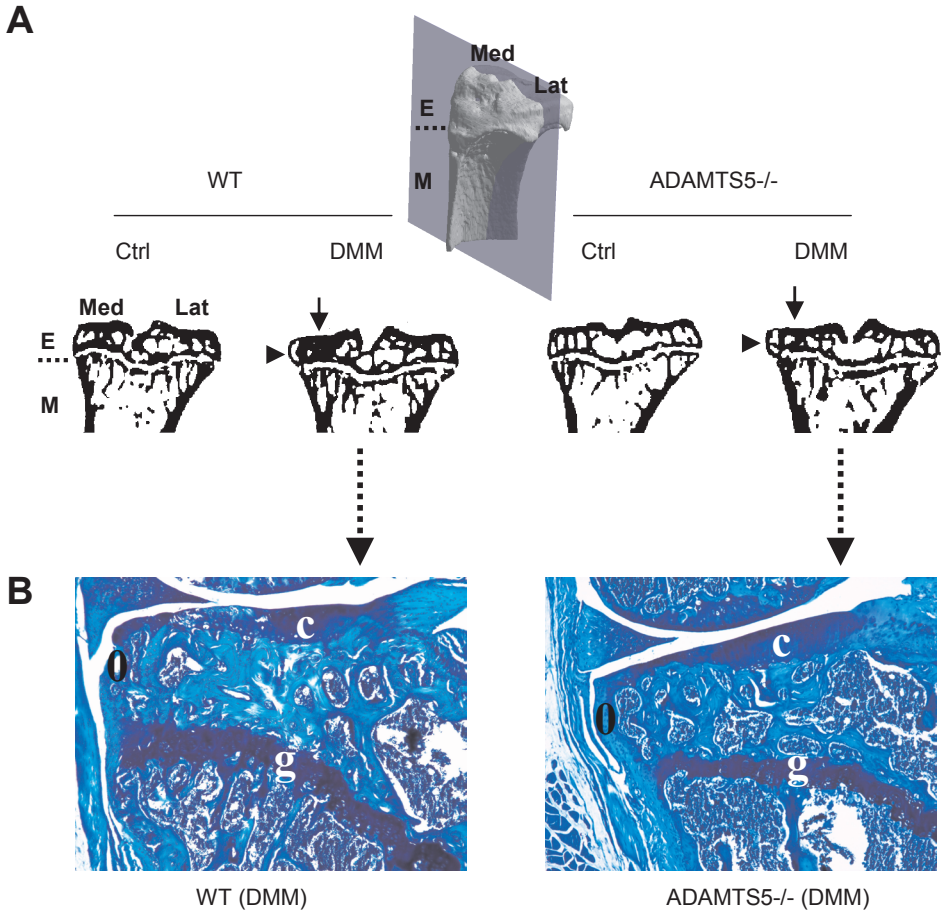

Chapter 4, Figure 3. A, representative cross-sections of tibiae from WT and ADAMTS5-/- mice, both left unoperated control (Ctrl) and right DMM. The inset shows a 3D reconstruction of a proximal tibia with a plane indicating the location from which the cross-sections were taken. Epiphysis (E), metaphysis (M) and growth plate (dotted line) are indicated, as well as the medial (Med) and lateral (Lat) tibial plateau. Subchondral sclerosis was found in the medial region of the epiphysis (arrows), and medial osteophytes were observed as well (arrowheads). B, histological images of the medial tibia from DMM WT and ADAMTS5-/- mice, stained with toluidine-blue. Please note the pronounced sclerosis of the subchondral bone plate in the WT mice, whereas ADAMTS5-/- mice only showed mild sclerosis. Magnification 100x. C= cartilage, O= osteophyte, G= growth plate.

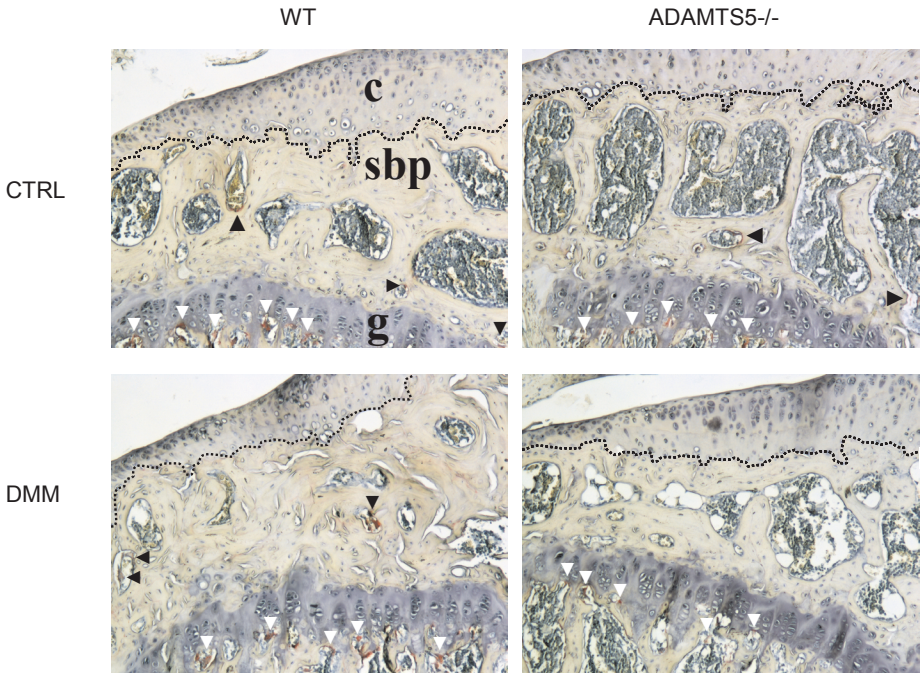

Chapter 4, Figure 5. Examples of TRAP-stained osteoclasts in the medial tibia of WT and ADAMTS5-/- mice, both left unoperated control (Ctrl) and right DMM. Osteoclasts in the subchondral bone (black arrowheads) were observed in Ctrl and DMM joints of both genotypes, in addition to osteoclasts beneath the growth plate (white arrowheads). Please note that in DMM joints of ADAMTS5-/- mice, very few if any osteoclasts were observed despite the presence of osteoclasts beneath the growth plate. Also note the thinner subchondral bone plate in the ADAMTS5-/- joints and the subchondral sclerosis after DMM in the WT joint. Magnification 100x. C= cartilage, SBP= subchondral bone plate, G= growth plate.

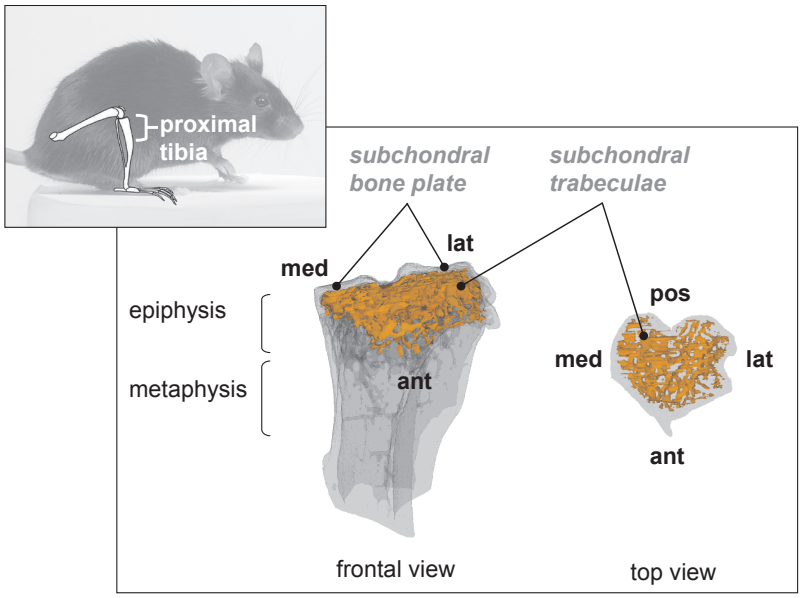

Chapter 5, Figure 1. Analysis of bone phenotype of WT and TTD mice. Anatomical context with the analyzed region (proximal tibia) is indicated in the smaller panel. The larger panel shows a transparent 3D model of the proximal tibia. The subchondral (epiphyseal) trabecular bone structure is indicated in orange (left: frontal view, right: top view). The model was build from a transaxial stack of cross-sections of 10 μm thickness. Med= medial, lat= lateral, pos= posterior, ant= anterior.

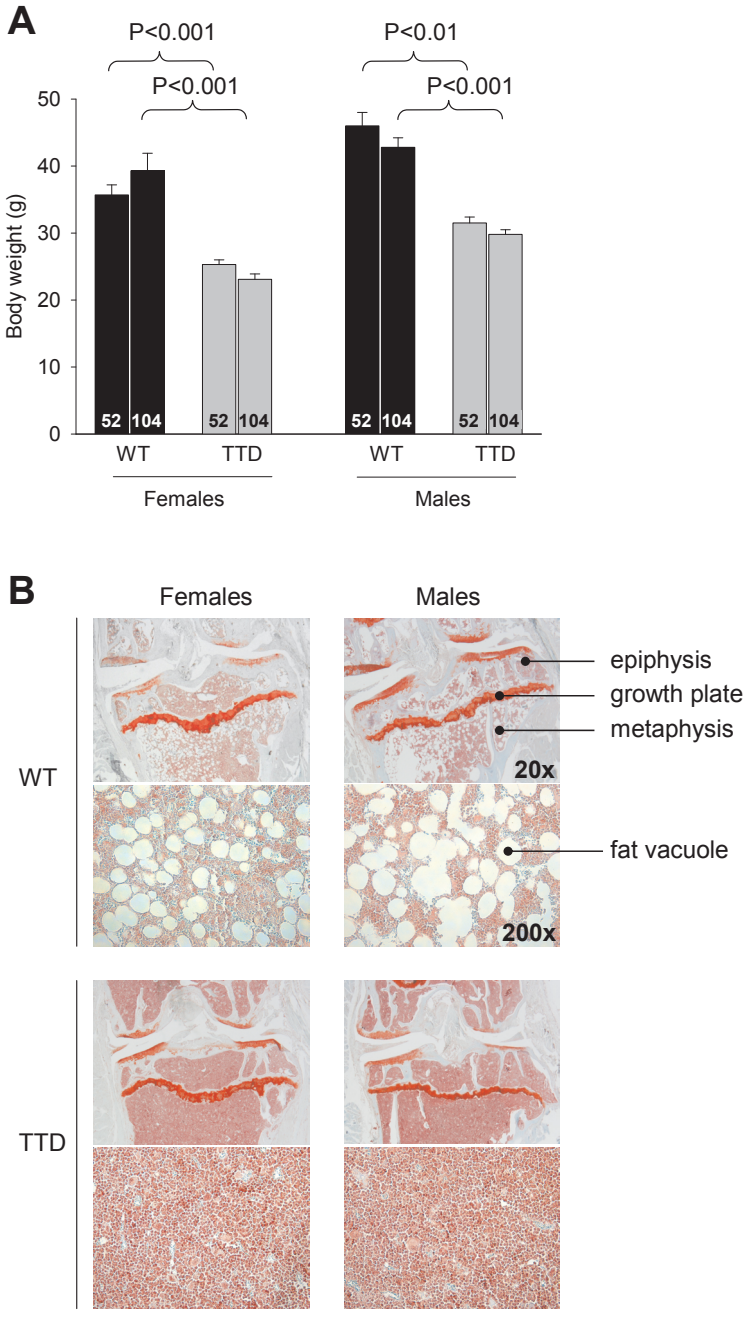

Chapter 5, Figure 2. A, body weights of female and male WT and TTD, aged 52 and 104 weeks. B, gross histological overview of the proximal tibia of WT and TTD mice, aged 104 weeks. An enlargement (magnification x200) of the metaphyseal bone marrow is shown below each of the overview pictures (magnification x20). Please note the absence of fat vacuoles in the bone marrow of TTD mice. This difference was already visible at 52 weeks, albeit less clearly (images not shown).

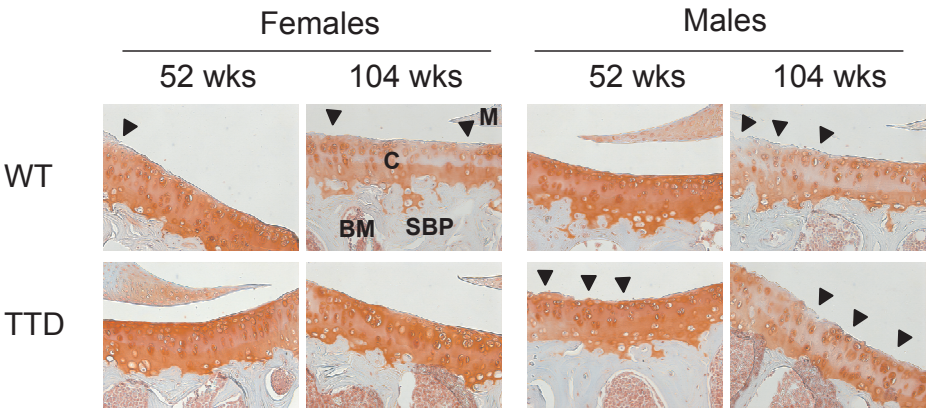

Chapter 5, Figure 5. Representative examples of cartilage damage at the lateral tibial plateau in female and male WT and TTD mice, aged 52 and 104 weeks. Cartilage damage (arrowheads) in 104-week-old female TTD mice was only sporadically observed, contrary to the other groups of 104-week-old mice. In addition, Safranin O depletion indicating proteoglycan loss was observed in all 104-week-old mice, except for the TTD females. Magnification x200. C= cartilage, SBP= subchondral bone plate, M= meniscus, BM= bone marrow.

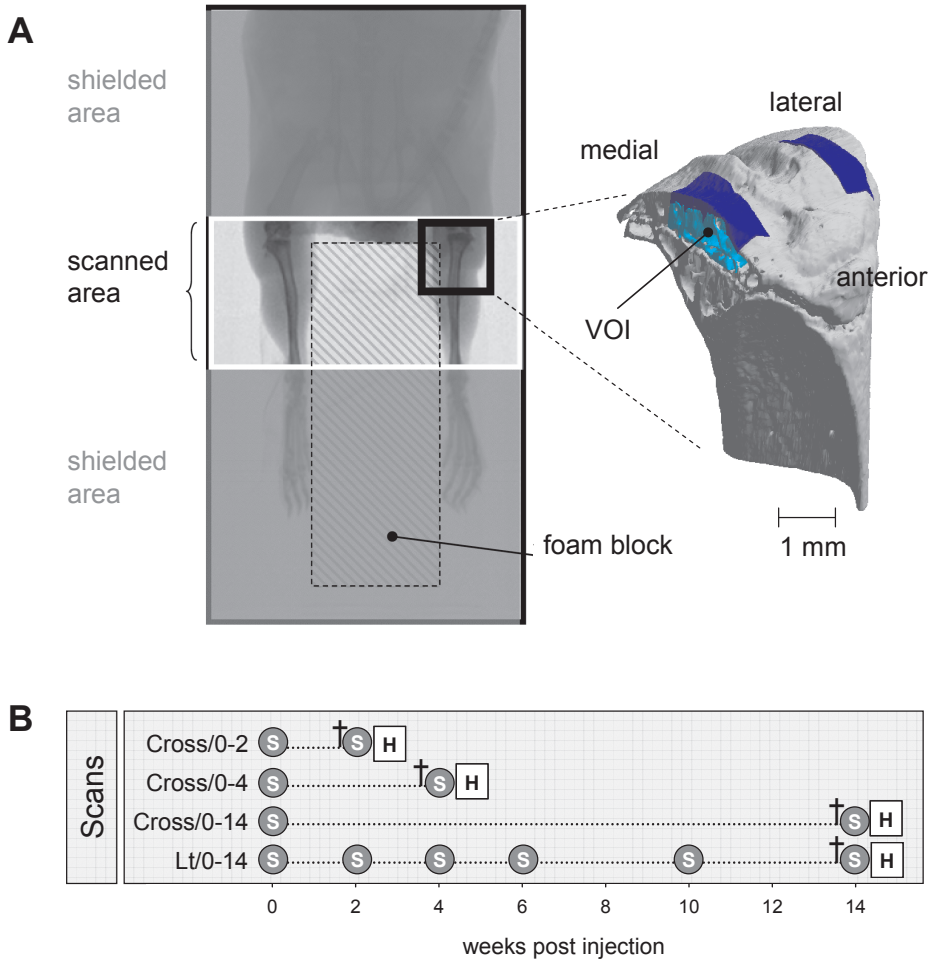

Chapter 6, Figure 1. Schematic overview of the scanning procedure. A, After anesthetization, a foam block was placed between the animals' hind legs with soft adhesive tape, to prevent any soft tissue from entering the scanned area. The tail of the animal was bended out of view dorso-cranially. After a fast scout scan using low radiation dose for orientation, the X-ray beam was focused on the proximal tibia for the actual scan, leaving all areas outside shielded from radiation. On the right a 3D model of the proximal tibia is shown, with two volumes of interest (VOI) indicated in blue: one on the medial and one on the lateral side, which were chosen for analysis. These VOIs included the subchondral bone plate (dark blue) and subchondral trabeculae (light blue). B, time points at which animals of each group were scanned is indicated by 'S'. The first scan (at T=0 weeks) was performed just before the first of the two intra-articular injections, the last scan (at T=14 weeks) was performed immediately after sacrifice (indicated by †). After sacrifice, hind limbs of mice were processed for *ex vivo* scanning and histology ('H'). Cross= cross sectional group, Lt= longitudinal group.

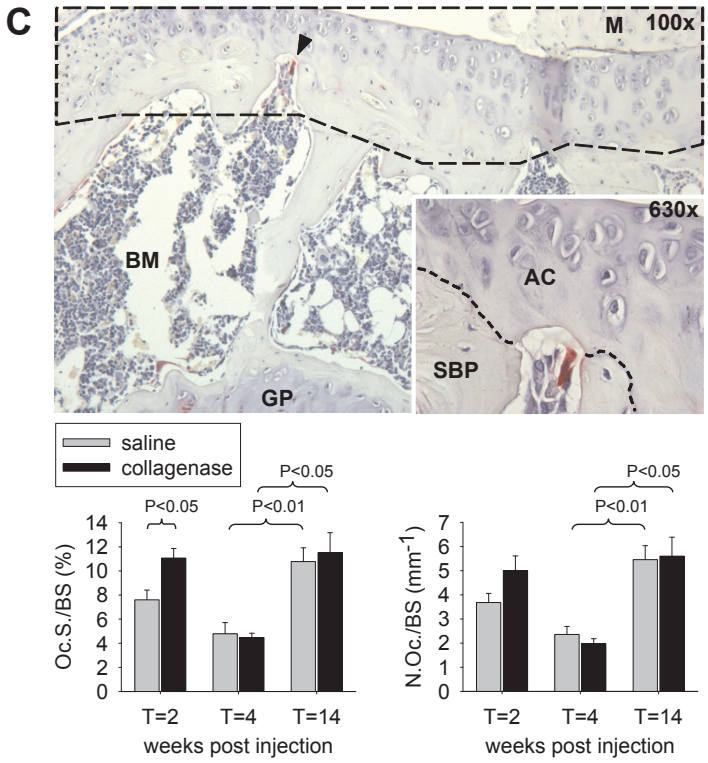

Chapter 6, Figure 2. C, Microphotograph of tibial subchondral bone plate area (dotted area was examined). A TRAP positive osteoclast indicated by the arrow head is shown enlarged in the inset. M= meniscus, AC= articular cartilage, SBP= subchondral bone plate, BM= bone marrow, GP= growth plate (top), quantification of osteoclast activity in the dotted area after collagenase or saline injection (bottom). Osteoclast surface per bone surface (left) and number of osteoclasts per bone surface (right) were determined. For T=2 and T=4, *n*=4 for each bar, for T=14, *n*=8 (group Lt/0-14). All bar graphs show averages ± SEM, $p<0.05$ was considered significant.

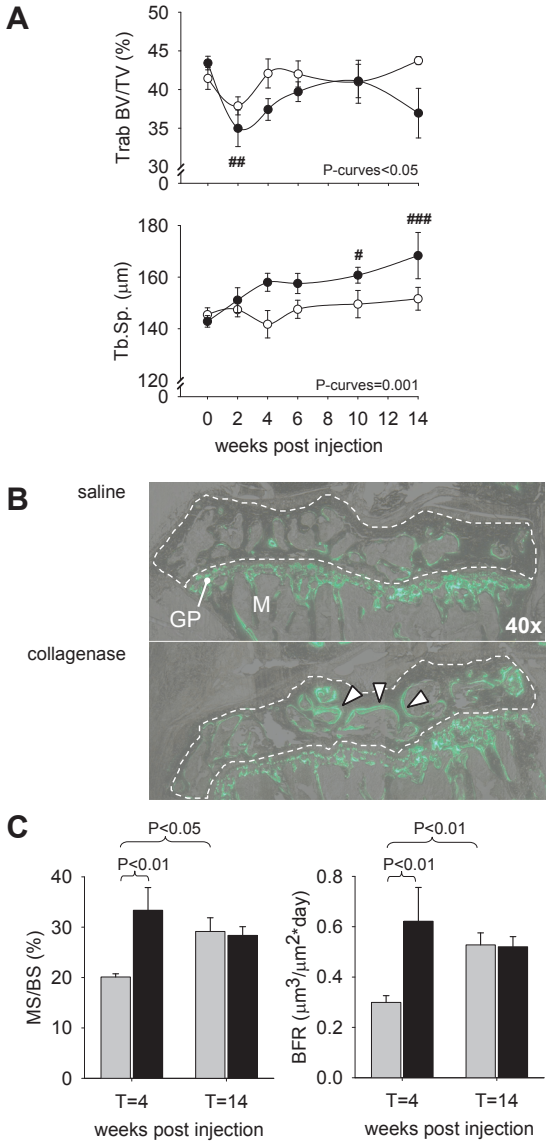

Chapter 6, Figure 3. A, Temporal changes in the subchondral trabecular bone of collagenase injected knee joints and contralateral control knee joints. Bone volume fraction (top) and trabecular spacing (bottom). Shown are averages ± SEM, # $p<0.05$ vs. T=0 (within treatment). Although no differences were found at each individual time point, the ANOVA test ('P-curves') indicated that the curves are significantly different for both morphometric parameters. B, merged bright field and fluorescent microphotographs of the proximal tibia of a control knee joint and a collagenase injected knee joint at T=4 weeks post injection, with calcein labeling in green and the epiphysis delineated by the white dotted line. In the collagenase injected joint increased osteoblast activity is visible by the larger distance between the two labels (white arrowheads). GP= growth plate, M= metaphysis. C, quantification of osteoblast activity, in mineralizing surface (MS/BS, left) and bone formation rate (BFR, right). For T=4, n=4 for each bar, for T=14, n=8 (group Cross/0-14). Shown are averages ± SEM, $p<0.05$ was considered significant.

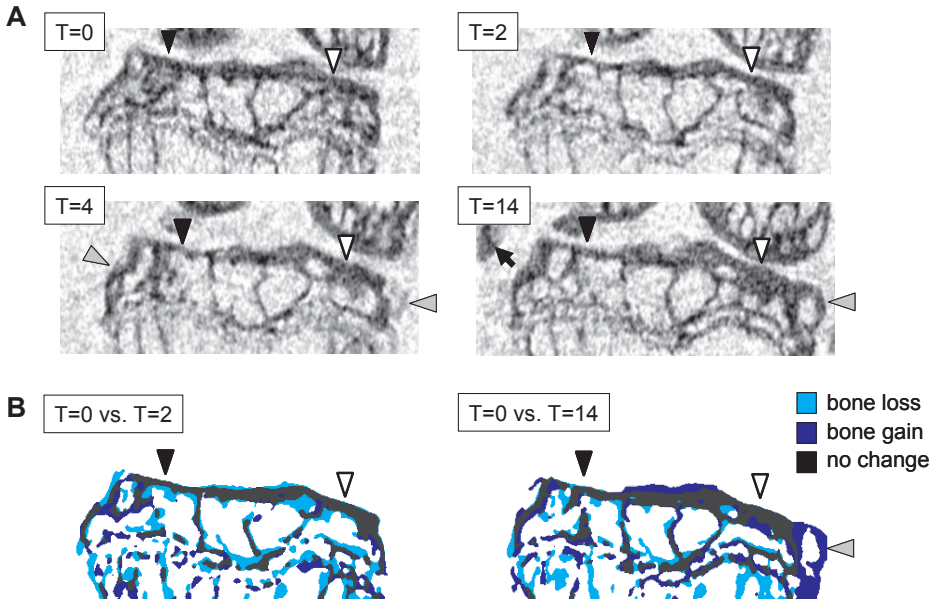

Chapter 6, Figure 4. Visualization of subchondral bone changes within the proximal tibia of a single mouse (group Lt/0-14) at T=0, 2, 4 and 14 weeks post injection. A, At the beginning of follow-up (T=2), initial thinning of the subchondral bone plate was followed by thickening (T=4, T=14) at both the lateral (black arrowheads) and medial (white arrowheads) sides. Notice the development of mineralized osteophytes in this animal (grey arrowheads) at the medial and lateral sides of the tibial plateau from 4 weeks post injection onwards. In some cases ectopic calcifications were observed in the collateral ligaments, for example in week 14 post injection (black arrow). B, Segmented overlaps of the images shown in A, highlighting differences between T=0 vs. T=2 and T=0 vs. T=14. Changes in bone architecture are indicated by colour coding.

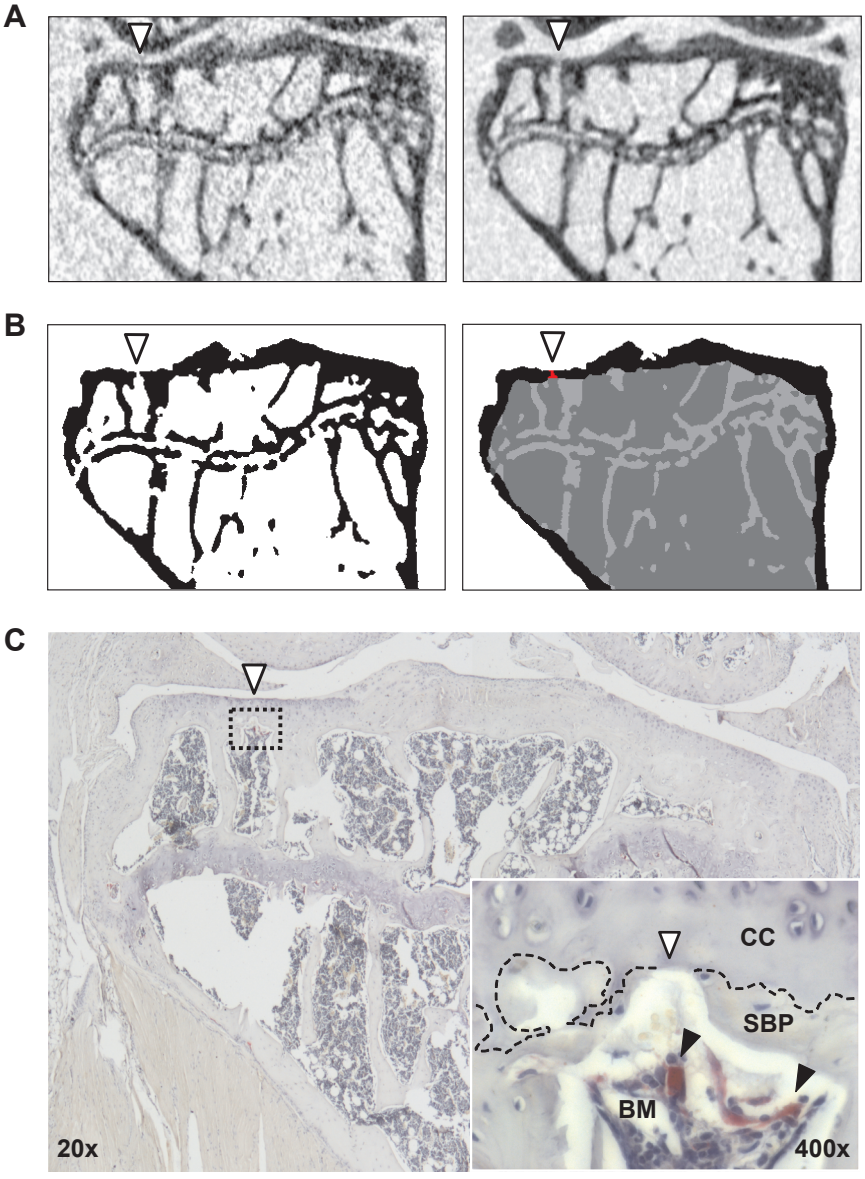

Chapter 6, Figure 5. Example of a subchondral bone plate perforation that pierces the tibial plateau in a collagenase injected knee joint. All images were derived from the exact same anatomical location of the same animal, with the white arrowhead indicating the location of the subchondral bone plate perforation. A, Perforations are visible in *in vivo* obtained grey-scale images (left) as well in scans obtained with the *ex vivo* scan protocol which had a higher signal-to-noise ratio (right). B, In the segmented images (left) each anatomical component (cortex, trabeculae, plate perforation) was labeled with a different gray tone (right, plate perforation indicated in red). C, The accompanying histological section (dotted area enlarged as inset) confirmed the perforation to be present. TRAP stained osteoclasts (inset, black arrowheads) were observed in close vicinity of the perforation. CC= calcified cartilage, SBP= subchondral bone plate, BM= bone marrow.

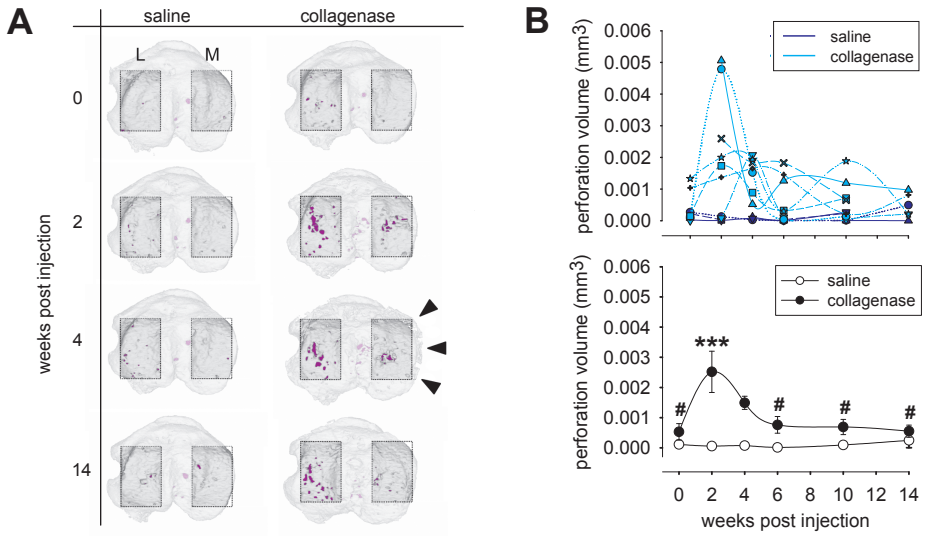

Chapter 6, Figure 6. Formation of subchondral bone plate perforations in time. A, 3D top views of the tibial plateau at T=0, 2, 4 and 14 with subchondral bone perforations (purple) superimposed. Regions of interest (bright dotted areas) from which quantitative data was derived are indicated on the lateral (L) and medial (M) sides. Mineralization of an osteophyte at T=4 is indicated by arrowheads. B, Quantification of medial perforation volume in individual mice (top) belonging to group Lt/0-14. Some scans which had low quality due to movement artifacts were omitted, but it is clear that collagenase injected joints show larger and more dynamic temporal changes in subchondral plate porosity compared to contralateral control joints. At the bottom averages ± SEM are shown: $p<0.05$ was considered significant. # $p<0.05$ vs. T=2 (within treatment), * $p<0.05$ between treatments.

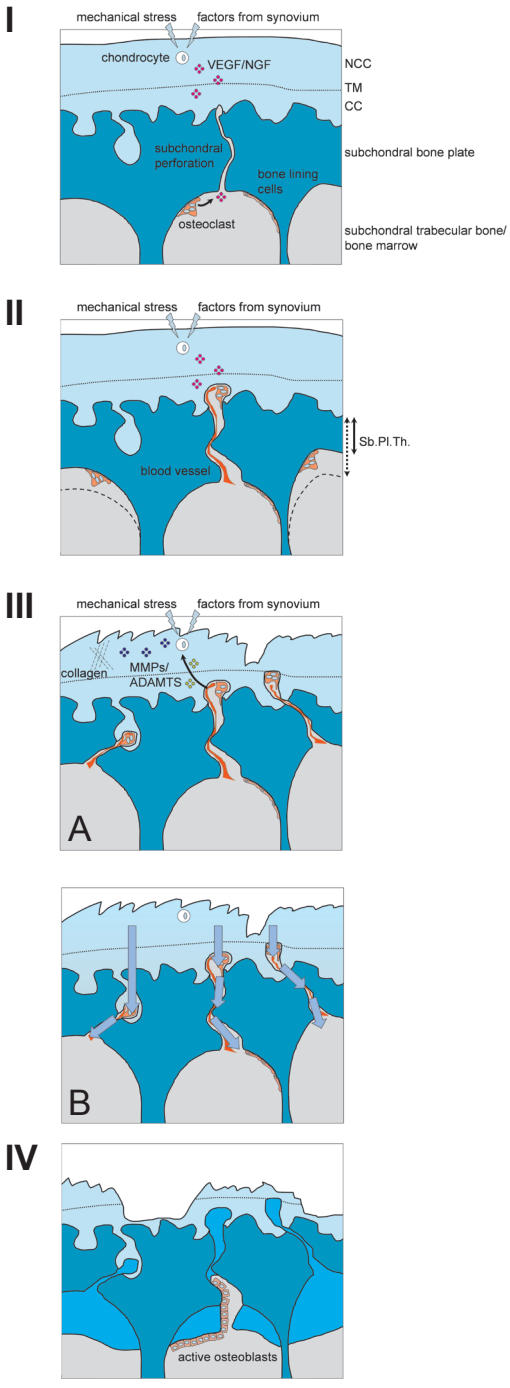

Phase I: occurence of the earliest changes, where an instability-inducing stimulus (in our case the chemical or surgical destabilization of the knee joint, or in aging-related osteoarthritis perhaps degeneration of the joint musculature) causes increased mechanical stress on the articular chondrocytes. These cells then start to produce angiogenic factors such as VEGF and/or NGF. Via normally present subchondral bone plate perforations, these growth factors reach osteoclasts residing in the subchondral bone.

Phase II: the osteoclasts follow the chemotactic gradient towards the chondrocytes, creating subchondral bone plate perforations in the process and decreasing subchondral bone plate thickness (Sb.Pl.Th.). In addition, newly formed blood vessels start to grow inside the plate perforations.

Phase III: with time progressing, more vessel-containing subchondral perforations are formed and enhanced crosstalk between subchondral bone and articular cartilage commences: bone-derived factors (depicted green) stimulate chondrocytes to produce matrix metalloproteinases and/or 'a disintegrin and metalloproteinase with a thrombospondin type 1 motif' (MMPs/ADAMTS, depicted blue) which destroy the collageneous structure of the cartilage extracellular matrix. Consequential, the first visual damage starts to appear (Phase IIIa). In addition, since the destruction of the cartilage matrix causes loss of the water-retaining GAGs, the articular cartilage loses fluid through the plate perforations with each mechanical compression (Phase IIIb, blue arrows). Without sufficient amounts of fluid the cartilage can no longer aptly withstand mechanical pressure, and is further degraded.

Phase IV: in the last phase, active osteoblasts, stimulated by the increased osteoclast activity and/or (growth) factors derived from the damaged cartilage, start to fill the bone plate perforations with newly formed, but poorly organized woven bone, and cause subchondral bone plate sclerosis in end-stage disease.

Chapter 7, Figure 1. Hypothetical model of changes in cartilage and subchondral bone that may contribute to initiation and progression of osteoarthritis. VEGF= vascular endothelial growth factor, NGF= nerve growth factor, NCC= non-calcified cartilage, TM= tidemark, CC= calcified cartilage.

Publication of this thesis was financially supported by:

The departments of Orthopaedics and Internal Medicine,
Erasmus MC University Medical Centre, Rotterdam, The Netherlands.

Nederlandse Vereniging voor Calcium- en Botstofwisseling (NVCB).